Electronic Supplementary Material (ESI) for Chemical Communications.

Electronic Supporting Information

Photochromic Switching Behaviour of Donor-Acceptor Stenhouse Adducts in Organic Solvents

Neil Mallo, Patrick T. Brown, Hasti Iranmanesh, Thomas S. C. MacDonald,

Matthew J. Teusner, Jason B. Harper, Graham E. Ball, Jonathon E. Beves

Table of Contents

Table of Figures

1 General Experimental

1.1 General Experimental

Reagents and solvents were purchased from Sigma-Aldrich, Merck, Chem Supply or Alfa Aeser, and used without purification. NMR spectroscopy was performed using a Bruker Avance III 400, an Avance III 500, or an Avance III 600 in CD_3CN, $CDCl_3$, C_6D_6, DMSO-d_6, D_2O, CD_3OD, or toluene-d_8, purchased from Cambridge Isotope Laboratories, Inc. All chemical shifts were calibrated against residual solvent signals. All coupling constants (*J*) are reported in Hertz. Signals in the NMR spectra are reported as broad (br), singlet (s), doublets (d), triplets (t), quartets (q), quintets (qu), sextets (sx), septets (sept), or unclear multiplets (m). NMR spectra were processed with MestReNova 10.0.2 software. UV-vis experiments were performed on an Agilent Cary 60 Bio UV-Visible Spectrophotometer equipped with a Cary Single Cell Peltier Accessory or an Agilent Cary 8454 UV-Vis Diode Array System equipped with an Agilent PCB 1500 Water Peltier System. ESI mass spectra were recorded on a Thermo-scientific LCQ Fleet Ion Trap Mass Spectrometer.

2 Summary of the compounds prepared in this study

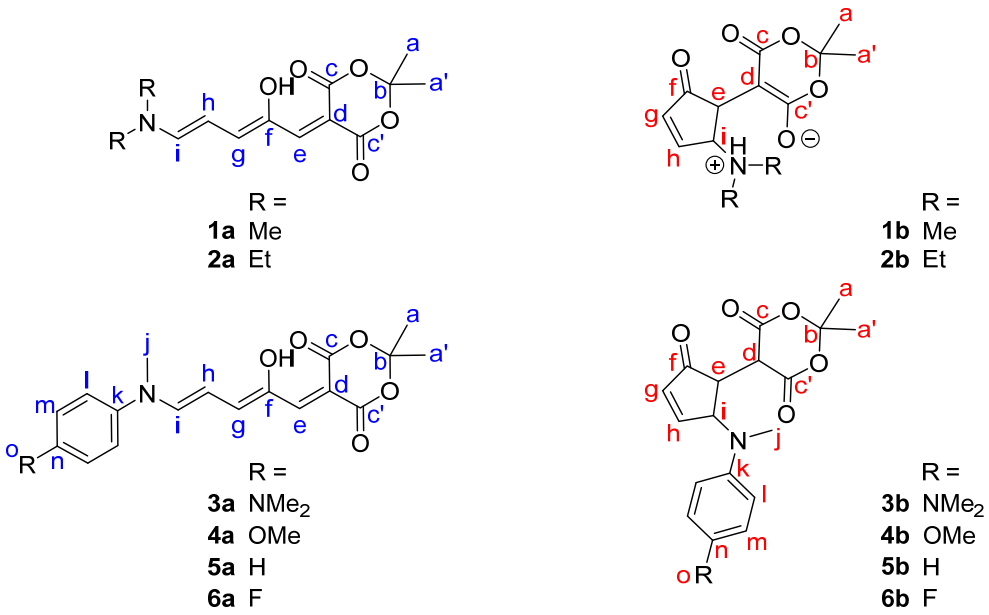

Figure S1. Structures of the donor-acceptor Stenhouse adducts prepared in this study.

In the case of the most electron withdrawing groups we attempted (R=NO_2) synthesis of the DASA was unsuccessful, suggesting there is a limit to the electron withdrawing nature of the substituent which can be tolerated. These complexes were isolated in mainly in the linear form on precipiation from THF. Upon dissolving the isolated solids in MeCN, CHCl3, benzene or other solvents, the samples were found to equilibrate to the mixtures of linear:cyclic as shown in Table S8.

3 Synthetic route and synthesis of precursor compounds

3.1 Synthetic route

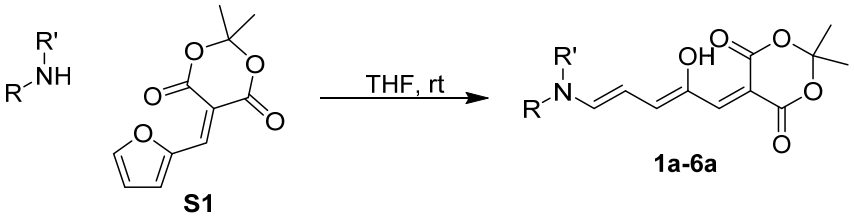

Scheme S1. General synthesis of compounds **1a-6a**

3.2 Synthesis of precursor S1

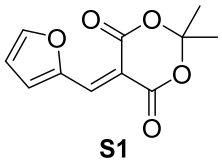

Compound **S1** was prepared according to a reported procedure. Spectral properties matched previously reported values.[1]

3.3 Synthesis of precursor S2

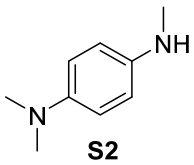

Compound **S2** was prepared according to a reported procedure. Spectral properties matched previously reported values.[2]

4 Synthesis and characterization of compound 1a/1b

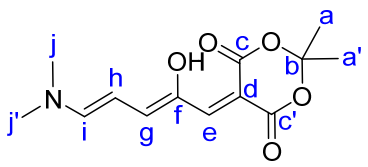

1a

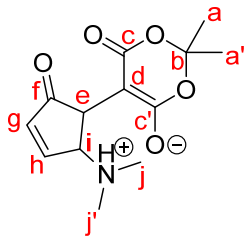

1b

4.1 Synthesis of 1a/1b

40% Dimethylamine in water (98 µL, 1.0 mmol) was added to a solution of **S1** (220 mg, 1.0 mmol) in THF (1 mL) and stirred for 2 hrs. The reaction was concentrated under a stream of N_2 and diethyl ether (5 mL) was added. The mixture was cooled to -20 °C for 20 minutes to yield a red precipitate which was collected and washed with diethyl ether to afford **1a** as a red powder. Yield: 112 mg (35%). **1a** (50 mg) was dissolved in toluene (20 mL) and the solution was irradiated with white light overnight. A grey-white solid precipitated, which was dried to afford **1b** as a grey-white powder. Yield: 42 mg (84%).

1a ^{1}H NMR (500 MHz, CD_3CN) δ 11.43 (s, 1H, H^{OH}), 7.62 (d, J = 11.5 Hz, 1H, H^{i}), 7.00 (d, J = 12.8 Hz, 1H, H^{g}), 6.75 (s, 1H, H^{e}), 6.08 (d, J = 12.9 Hz, 1H, H^{h}), 3.31 (s, 3H, H^{j}), 3.16 (s, 3H, $H^{j'}$), 1.63 (s, 6H, $H^{a/a'}$).

^{13}C{^{1}H} NMR (126 MHz, CD_3CN) δ 163.16 (C^{i}), 154.20 (C^{g}), 144.91 (C^{f}), 134.52 (C^{e}), 104.91 (C^{h}), 103.38 (C^{b}), 87.83 (C^{d}), 47.44 (C^{j}), 39.32 ($C^{j'}$), 26.53 ($C^{a/a'}$),

UV-vis ($CHCl_3$): λ_{max}/nm 540.

1b ^{1}H NMR (500 MHz, CD_3CN) δ 7.52 (dd, J = 6.1, 2.0 Hz, 1H, H^{h}), 6.18 (d, J = 5.9 Hz, 1H, H^{g}), 3.99 (s, 1H, H^{i}), 2.38 (s, 6H, $H^{j/j'}$), 1.55 (s, 6H, $H^{a/a'}$).

^{13}C{^{1}H} NMR (126 MHz, CD_3CN) δ 72.83 (C^{i}), 45.04 (C^{e}), 42.18 ($C^{j/j'}$), 26.14 ($C^{a/a'}$).

(+)-ESI MS found *m/z* 268.00 (calc. [$C_{13}H_{17}NO_5$ (M) + H^+] *m/z* 268.11).

4.2 ^{1}H NMR spectrum of 1a/1b in CD_3CN

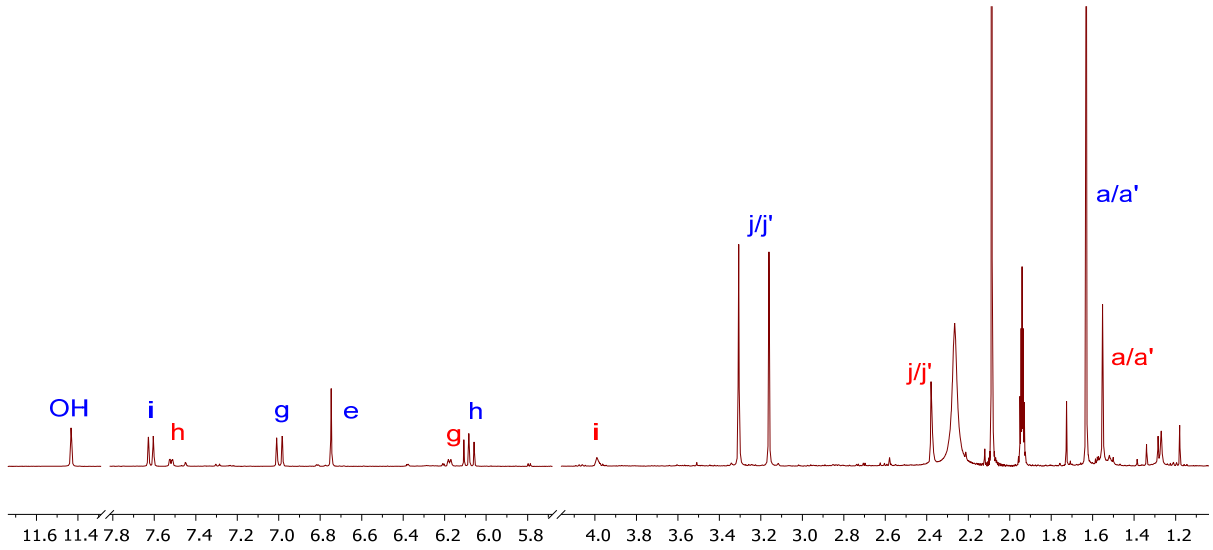

Figure S2. ^{1}H NMR (500 MHz, CD_3CN, 298 K) spectrum of **1a** (blue) and **1b** (red). NB: the signal for H^{e} of **1b** is either too weak to be observed, or obscured by the $H^{j/j'}$ peak of **1a.**

4.3 $^{13}C\{^{1}H\}$ NMR spectrum of 1a/1b in CD_3CN

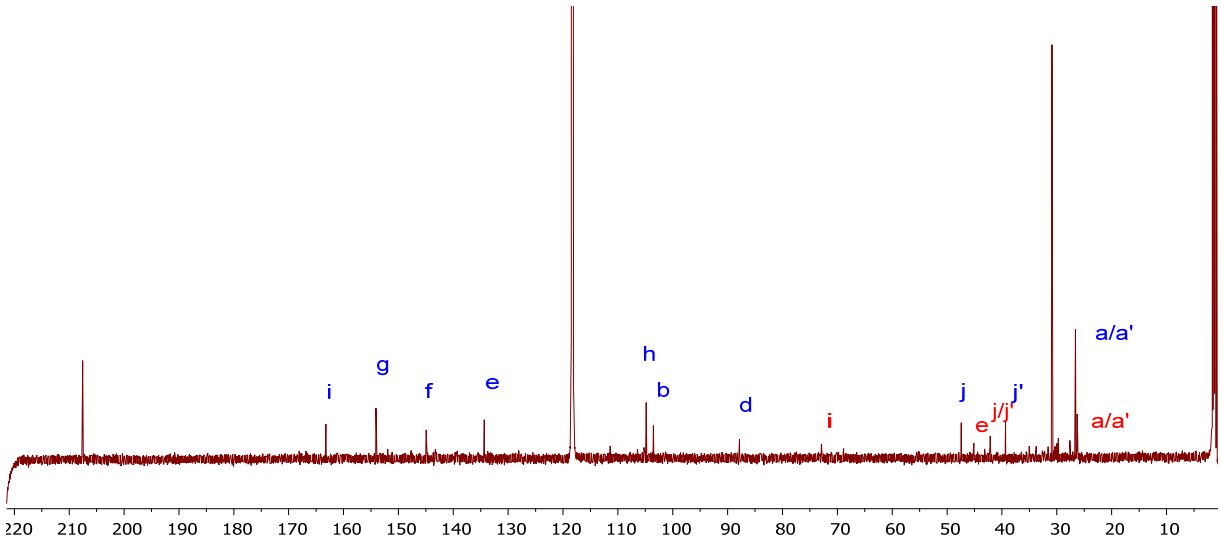

Figure S3. ^{13}C NMR (126 MHz, CD_3CN, 298 K) spectrum of **1a** (blue) and **1b** (red). NB: Most of the signals for **1b** were too weak to be observed in both the ^{13}C and HSQC spectra and so were unable to be assigned.

5 Synthesis and characterization of compound 2a/2b

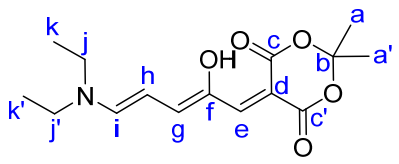

2a

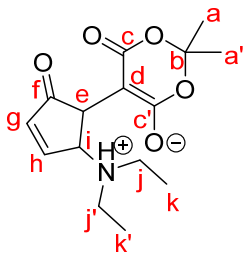

2b

5.1 Synthesis of 2a/2b

Compound **2a/2b** was prepared according to a reported procedure. Spectral properties matched previously reported values.[3]

6 Synthesis and characterization of compound 3a/3b

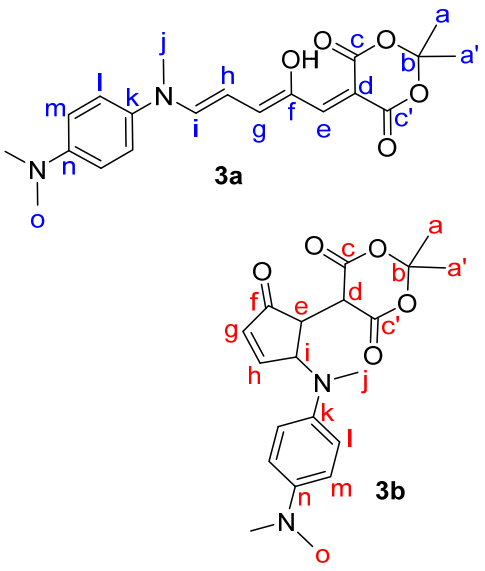

6.1 Synthesis of 3a/3b

S2 (150 mg, 1.0 mmol) was added to a solution of **S1** (220 mg, 1.0 mmol) in THF (4 mL) and triethylamine (1 drop) and stirred overnight. The mixture was cooled to -20 °C for 20 minutes to yield a dark blue precipitate which was collected and washed with diethyl ether to afford **3a** as a dark blue powder. Yield: 184 mg (49%). Crystals of **3a** suitable for single crystal X-ray diffraction were obtained by diffusing diethyl ether into a chloroform solution of **3**.

3a ^{1}H NMR (500 MHz, CD_3CN) δ 11.39 (s, 1H, H^{OH}), 7.78 (d, J = 11.6 Hz, 1H, H^{i}), 7.20 (d, J = 8.8 Hz, 2H, H^{l}), 7.03 (d, J = 12.6 Hz, 1H, H^{g}), 6.92 (s, 1H, H^{e}), 6.77 (d, J = 8.3 Hz, 2H, H^{m}), 6.24 (dd, J = 12.3 Hz, 1H, H^{h}), 3.53 (s, 3H, H^{j}), 2.96 (s, 6H, H^{o}), 1.65 (s, 6H, $H^{a/a'}$).

^{13}C{^{1}H} NMR (151 MHz, CD_3CN) δ 167.97 (C^{c}), 157.42 (C^{i}), 152.50 (C^{g}), 150.85 (C^{n}), 145.98 (C^{f}), 137.96 (C^{e}), 135.69 (C^{k}), 123.26 (C^{l}), 113.41 (C^{m}), 105.83 (C^{h}), 103.90 (C^{b}), 90.59 (C^{d}) 40.61 (C^{o}), 39.54 (C^{j}), 26.70 ($C^{a/a'}$).

UV-vis ($CHCl_3$): λ_{max}/nm 574.

3b ^{1}H NMR (500 MHz, CD_3CN) δ 7.81 (d, J = 4.2 Hz, 1H, H^{h}), 6.89 (d, J = 8.8 Hz, 2H, H^{m}), 6.76 (d, J = 9.0 Hz, 2H, H^{l}), 6.32 (dd, J = 6.0, 2.0 Hz, 1H, H^{g}), 5.14 (d, 1H, H^{i}), 4.00 (s, 1H, H^{d}), 3.43 (dd, J = 4.2, 1.9 Hz, 1H, H^{e}), 2.82 (s, 6H, H^{o}), 2.74 (s, 3H, H^{j}), 1.69 (s, 3H, H^{a}), 1.69 (s, 3H, $H^{a'}$).

^{13}C{^{1}H} NMR (151 MHz, CD_3CN) δ 204.10 (C^{f}), 165.94 (C^{c}), 164.84 (C^{h}), 134.57 (C^{g}), 118.82 (C^{m}), 115.63 (C^{l}), 106.62 (C^{b}) 66.98 (C^{i}), 46.87 (C^{e}), 45.36 (C^{d}), 41.74 (C^{o}), 34.69 (C^{j}), 28.33 ($C^{a/a'}$).

(+)-ESI MS Found *m/z* 373.08 (calc. [$C_{20}H_{24}N_2O_5$ (M) + H^+] *m/z* 373.18).

6.2 ^{1}H NMR spectrum of 3a/3b in CD_3CN

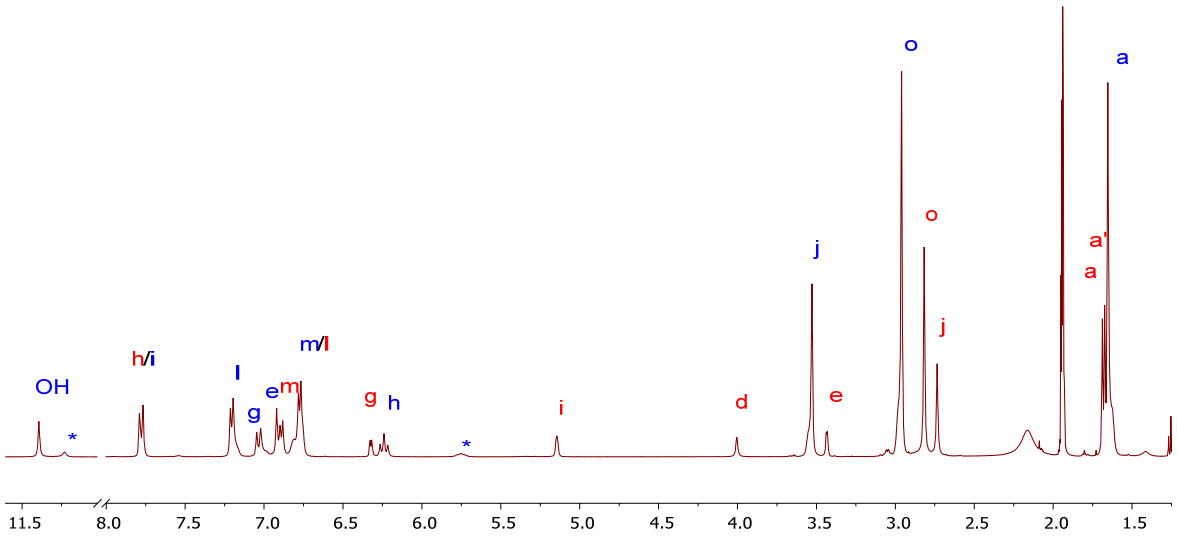

Figure S4. ^{1}H NMR (500 MHz, CD_3CN, 298 K) spectrum of **3a** (blue) and **3b** (red). NB: Signal H^h of the cyclic form is obscured by the peak H^i of the linear form. Signal H^l of the cyclic form is a shoulder on peak H^l of the linear form. Peaks labelled with blue asterisks (*) correspond to the conformer **3a'**; see p. 33 for details.

6.3 ^{13}C{^{1}H} NMR spectrum of 3a/3b in CD_3CN

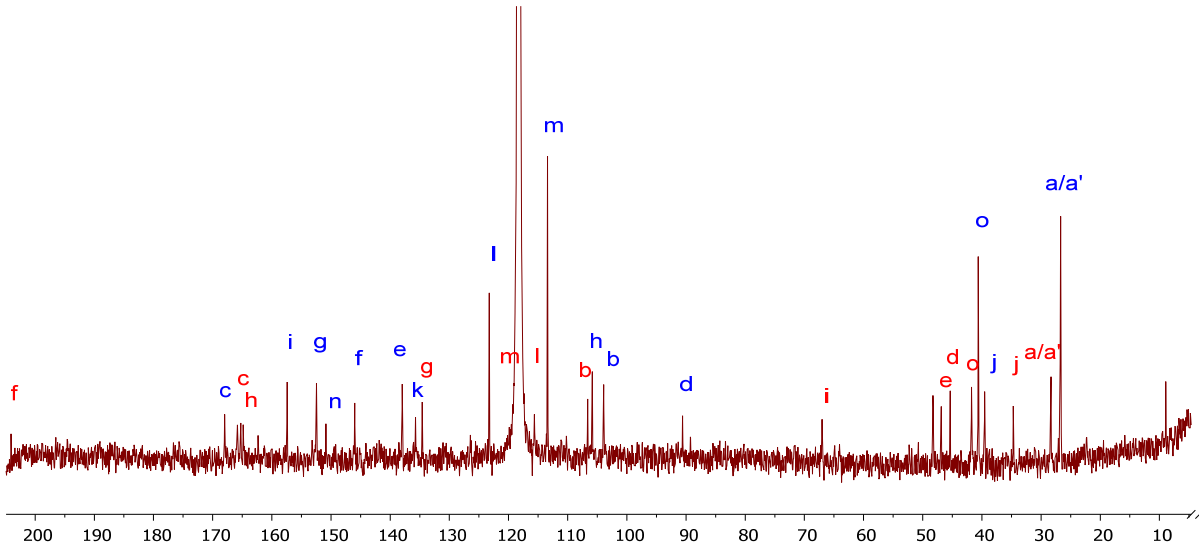

Figure S5. ^{13}C{^{1}H} NMR (151 MHz, CD_3CN, 298 K) spectrum of **3a** (blue) and **3b** (red). NB: The aromatic signals from **3b** were too weak to be observed in the ^{13}C{^{1}H} NMR spectrum and were assigned by signals in the HMBC.

7 Synthesis and characterization of compound 4a/4b

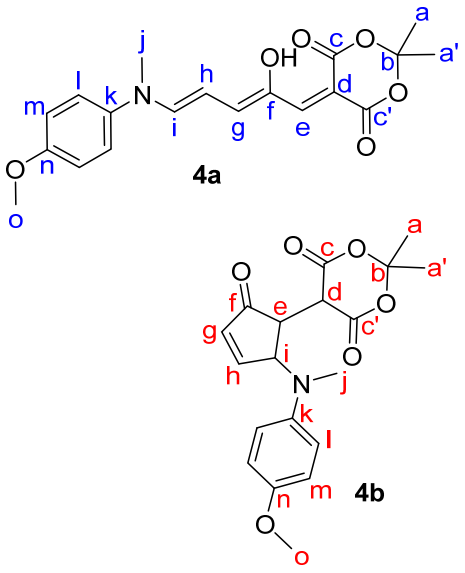

7.1 Synthesis of 4a/4b

N-Methyl-*N*-(4-methoxyphenyl) (137 mg, 1.0 mmol) was added to a solution of **S1** (220 mg, 1.0 mmol) in THF (1 mL) and stirred overnight. The reaction was concentrated under a stream of N_2 and diethyl ether (5 mL) was added. The mixture was cooled to -20 °C for 20 minutes to yield a dark purple precipitate which was collected and washed with diethyl ether to afford **4a** as a dark purple powder**.** Yield: 289 mg (81%). Crystals of **4a** and **4b** suitable for single crystal X-ray diffraction were obtained by diffusing diethyl ether into an acetonitrile solution of **4a** and **4b**.

4a ^{1}H NMR (500 MHz, CD_3CN) δ 11.32 (s, 1H, H^{OH}), 7.77 – 7.76 (m, 1H, H^i), 7.29 (d, J = 9.0 Hz, 2H, H^m), 7.07 – 6.95 (m, 4H, H^l, H^g, H^e), 6.26 – 6.17 (m, 1H, H^h), 3.82 (s, 3H, H^o), 3.52 (s, 3H, H^j), 1.66 (s, 6H, $H^{a/a'}$).

^{13}C{^{1}H} NMR (151 MHz, CD_3CN) δ 55.36 (C^o), 25.81 ($C^{a/a'}$).

UV-vis ($CHCl_3$): λ_{max}/nm 563.

4b ^{1}H NMR (500 MHz, CD_3CN) δ, 7.75 (dd, J = 6.0, 2.0 Hz, 1H, H^h), 6.88 (d, J = 9.5 Hz, 2H, H^l), 6.84 (d, J = 9.3 Hz, 2H, H^m), 6.35 (dd, J = 5.9, 2.1 Hz, 1H, H^g), 5.23 (d, J = 2.1 Hz, 1H, H^i), 4.12 (d, J = 2.0 Hz, 1H, H^d), 3.71 (s, 3H, H^o), 3.45 (dd, J = 4.2, 2.0 Hz, 1H, H^e), 2.74 (s, 3H, H^j), 1.71 (s, 3H, H^a), 1.67 (s, 3H, $H^{a'}$).

^{13}C{^{1}H} NMR (151 MHz, CD_3CN) δ 203.01 (C^f), 165.05 (C^c), 164.85 ($C^{c'}$), 163.89 (C^h), 153.08 (C^n), 143.77 (C^k), 133.74 (C^g), 116.86 (C^m), 114.58 (C^l), 105.73 (C^b), 65.34 (C^i), 55.11 (C^o), 47.52 (C^e), 44.43 (C^d), 33.25 (C^j), 27.36 ($C^{a'}$), 25.91 ($C^{a'}$).

(+)-ESI MS Found *m/z* 360.00 (calc. [$C_{19}H_{21}NO_6$ (M) + H^+] *m/z* 360.14).

7.2 ^{1}H NMR spectrum of 4a/4b in CD_3CN

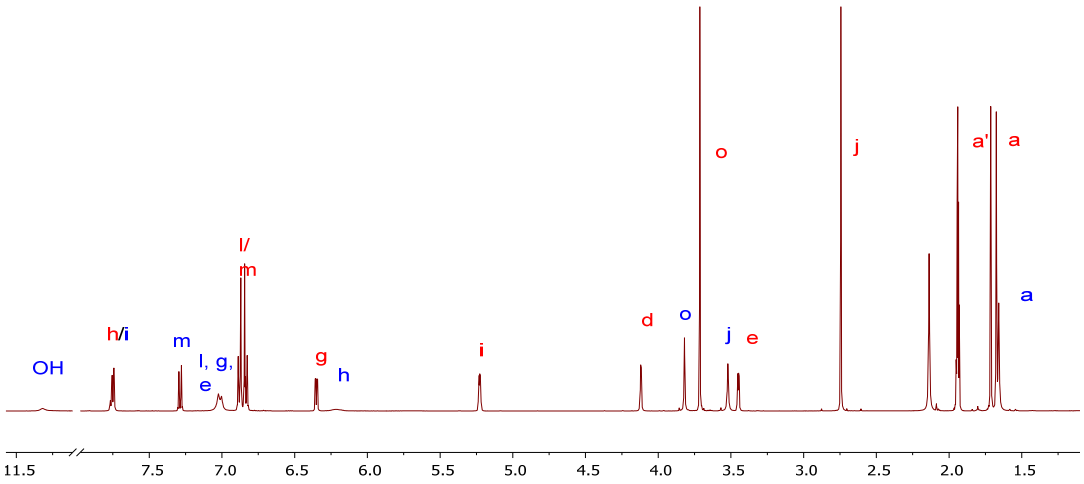

Figure S6. ^{1}H NMR (500 MHz, CD_3CN, 298 K) spectrum of **4a** (blue) and **4b** (red).

7.3 $^{13}C\{^{1}H\}$ NMR spectrum of 4a/4b in CD_3CN

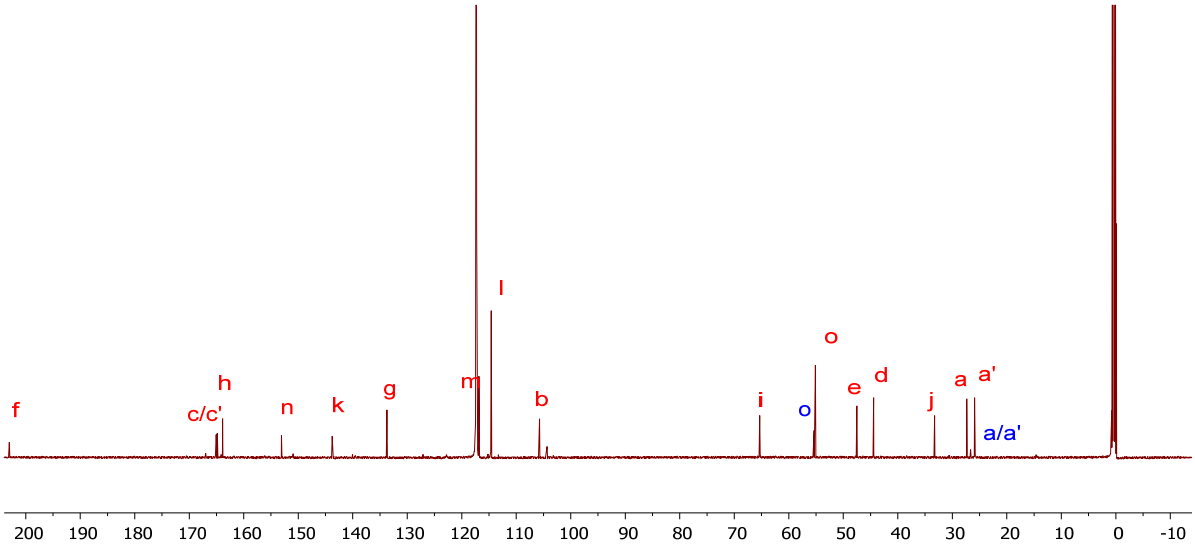

Figure S7. $^{13}C\{^{1}H\}$ NMR (151 MHz, CD_3CN, 298 K) spectrum of **4a** (blue) and **4b** (red). NB: Most of the signals for **4a** were too weak to be observed in both the ^{13}C and HSQC spectra and so were unable to be assigned.

8 Synthesis and characterization of compound 5a/5b

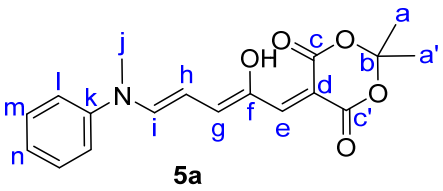

5a

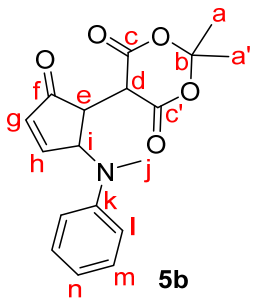

5b

8.1 Synthesis of 5a/5b

N-Methylaniline (98 µL, 1.0 mmol) was added to a solution of **S1** (220 mg, 1.0 mmol) in THF (1 mL) and stirred for 2 hrs. The reaction was concentrated under a stream of N_2 and diethyl ether (5 mL) was added. The mixture was cooled to -20 °C for 20 minutes to yield a green precipitate which was collected and washed with ether to afford **5a** as a green powder. Yield: 112 mg (35%). Crystals of **5a** suitable for single crystal X-ray diffraction were obtained by diffusing diethyl ether into an acetonitrile solution of **5**.

5a ^{1}H NMR (500 MHz, CD_3CN) δ 11.26 (s, 1H, H^{OH}), δ 7.80 (d, J = 12.1 Hz, 1H, H^{i}), 7.48 (dd, J = 7.8 Hz, 2H, H^{m}), 7.39 – 7.29 (m, 3H, H^{l}, H^{n}), 7.11 (s, 1H, H^{e}), 7.01 (d, J = 11.4 Hz, 1H, H^{g}), 6.24 – 6.11 (m, 1H, H^{h}), 3.54 (s, 3H, H^{j}), 1.67 (s, 6H, $H^{a/a'}$).

UV-vis ($CHCl_3$): λ_{max}/nm 561.

5b ^{1}H NMR (500 MHz, CD_3CN) δ 7.71 (dd, J = 5.9, 2.1 Hz, 1H, H^{h}), 7.23 (t, J = 7.0 Hz, 2H, H^{m}), 6.85 (d, J = 8.6 Hz, 2H, H^{l}), 6.74 (t, J = 7.2 Hz, 1H, H^{n}), 6.39 (dd, J = 5.9, 2.1 Hz, 1H, H^{g}), 5.42 (d, J = 4.3 Hz, 1H, H^{i}), 4.25 (d, J = 2.1 Hz, 1H, H^{d}), 3.47 (dd, J = 4.2, 2.1 Hz, 1H, H^{e}), 2.80 (s, 3H, H^{j}), 1.73 (s, 3H, H^{a}), 1.68 (s, 3H, $H^{a'}$).

$^{13}C\{^1H\}$ NMR (151 MHz, CD_3CN) δ 202.81 (C^{f}), 165.07 (C^{c}), 164.82 ($C^{c'}$), 163.75 (C^{h}), 149.50 (C^{k}), 133.90 (C^{g}), 129.32 (C^{m}), 117.85 (C^{n}), 113.57 (C^{l}), 105.81 (C^{b}), 63.19 (C^{i}), 48.06 (C^{e}), 44.45 (C^{d}), 32.28 (C^{j}), 27.38 (C^{a}), 25.92 ($C^{a'}$).

(+)-ESI MS found *m/z* 330.08 (calc. [$C_{18}H_{19}NO_5$ (M) + H^+] *m/z* 330.13).

8.2 ^{1}H NMR spectrum of 5a/5b in CD_3CN

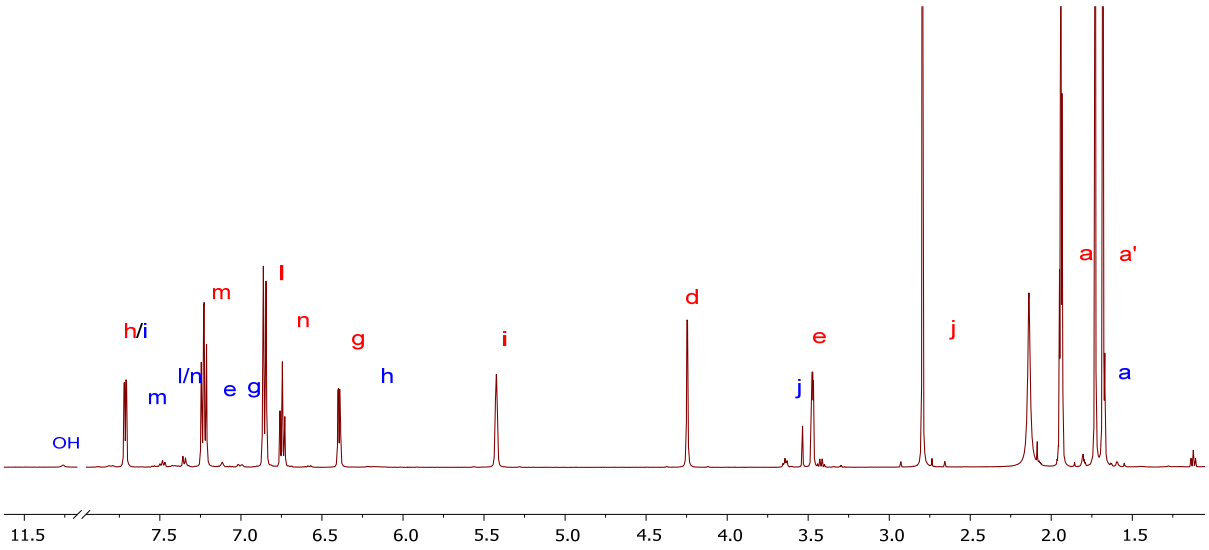

Figure S8. ^{1}H NMR (500 MHz, CD_3CN, 298 K) spectrum of **5a** (blue) and **5b** (red).

8.3 ^{13}C{^{1}H} NMR spectrum of 5a/5b in CD_3CN

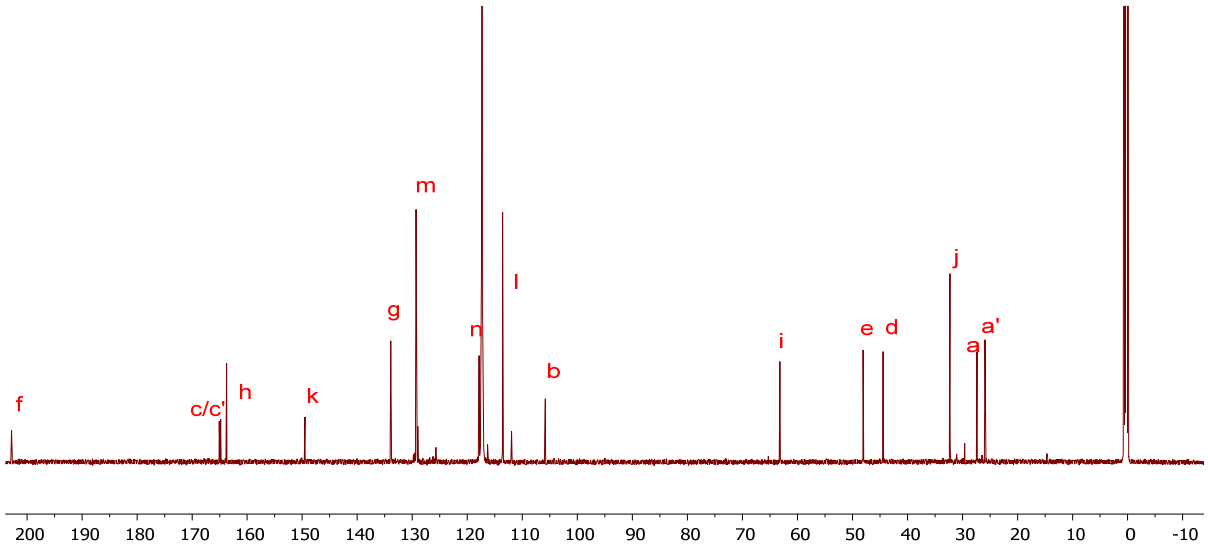

Figure S9. ^{13}C{^{1}H} NMR (151 MHz, CD_3CN, 298 K) spectrum of **5b** (red) NB: Signals for **5a** were too weak to be observed.

9 Synthesis and characterization of compound 6a/6b

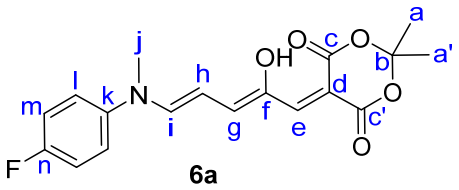

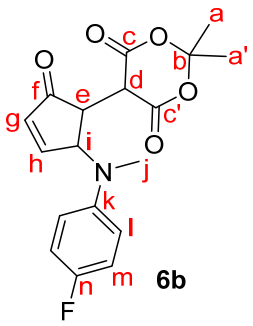

9.1 Synthesis of 6a/6b

4-Fluoro-*N*-methylaniline (125 µL, 1.0 mmol) was added to a solution of **S1** (220 mg, 1.0 mmol) in THF (1 mL) and DABCO (1 mg) and stirred for 3 days. Diethyl ether (3 mL) was added and the solution was cooled to -20 °C overnight. A pink precipitate formed which was collected and washed with diethyl ether to afford **6a** and **6b** as a pink powder. Yield: 83 mg (24%). Crystals of **6b** suitable for single crystal X-ray diffraction were obtained by diffusing diethyl ether into a chloroform/methanol solution of **6**.

6a ^{1}H NMR (500 MHz, CD_3CN) δ 11.25 (s, 1H, H^{OH}), 7.38 – 7.33 (m, 2H, H^{l}), 7.22 (dd, J = 8.3 Hz, 2H, H^{m}), 7.13 (s, 1H, H^{e}), 3.50 (s, 3H, H^{j}), 1.67 (s, 6H, $H^{a/a'}$).

UV-vis ($CHCl_3$): λ_{max}/nm 557.

6b ^{1}H NMR (500 MHz, CD_3CN) δ 7.71 (dd, J = 4.3, 1.4 Hz, 1H, H^{h}), 6.99 (dd, J = 55.1, 9.3 Hz, 2H, H^{m}), 6.88 – 6.84 (m, 2H, H^{l}), 6.39 (dd, J = 4.1, 1.8 Hz, 1H, H^{g}), 5.31 (s, 1H, H^{i}), 4.22 (s, 1H, H^{d}), 3.47 – 3.43 (m, 1H, H^{e}), 2.77 (s, 3H, H^{j}), 1.74 (s, 3H, H^{a}), 1.68 (s, 3H, $H^{a'}$).

^{13}C{^{1}H} NMR (151 MHz, CD_3CN) δ 203.77 (C^{f}), 166.08 (C^{c}), 165.79 ($C^{c'}$), 164.53 (C^{h}), 155.83 (d, J = 234.8 Hz, C^{n}), 147.32 (C^{k}), 134.95 (C^{g}), 116.58 (d, J = 2.6 Hz, C^{l}), 116.43 (d, J = 17.4 Hz, C^{m}), 106.81 (C^{b}), 65.34 (C^{i}), 48.78 (C^{e}), 45.47 (C^{d}), 33.79 (C^{j}), 28.37 (C^{a}), 26.95 ($C^{a'}$).

(+)-ESI MS found *m/z* 348.12 (calc. [$C_{18}H_{18}FNO_5$ (M) + H^+] *m/z* 348.12).

9.2 ^{1}H NMR spectrum of 6a/6b in CD_3CN

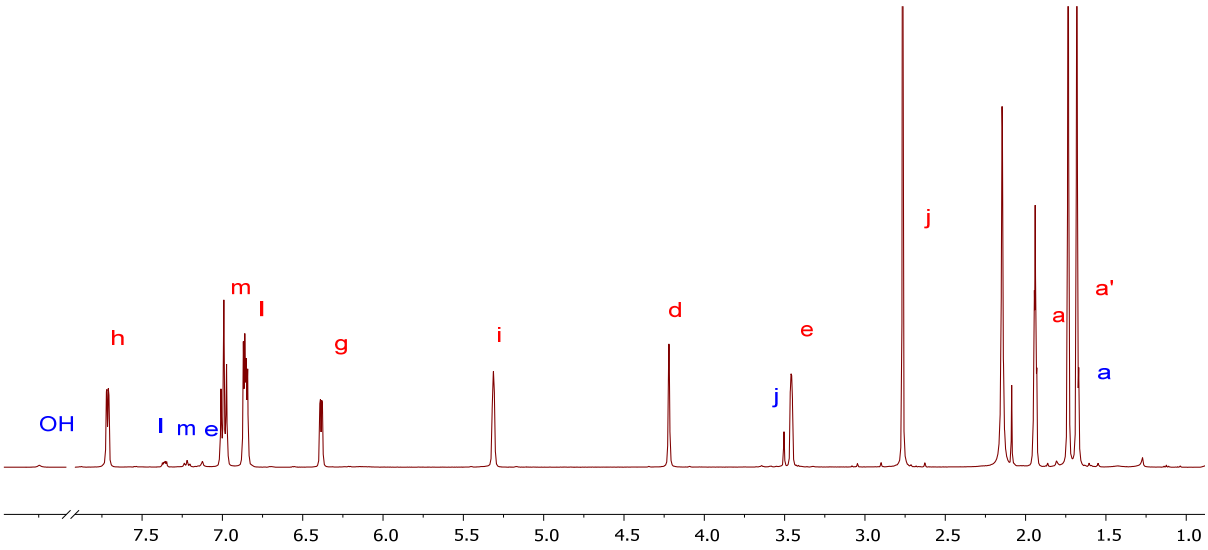

Figure S10. ^{1}H NMR (500 MHz, CD_3CN, 298 K) spectrum of **6a** (blue) and **6b** (red). NB: The peaks for H^g, H^h and H^i of **6a** were too weak to be observed or were overlapping with larger signals.

9.3 $^{13}C\{^{1}H\}$ NMR spectrum of 6a/6b in CD_3CN

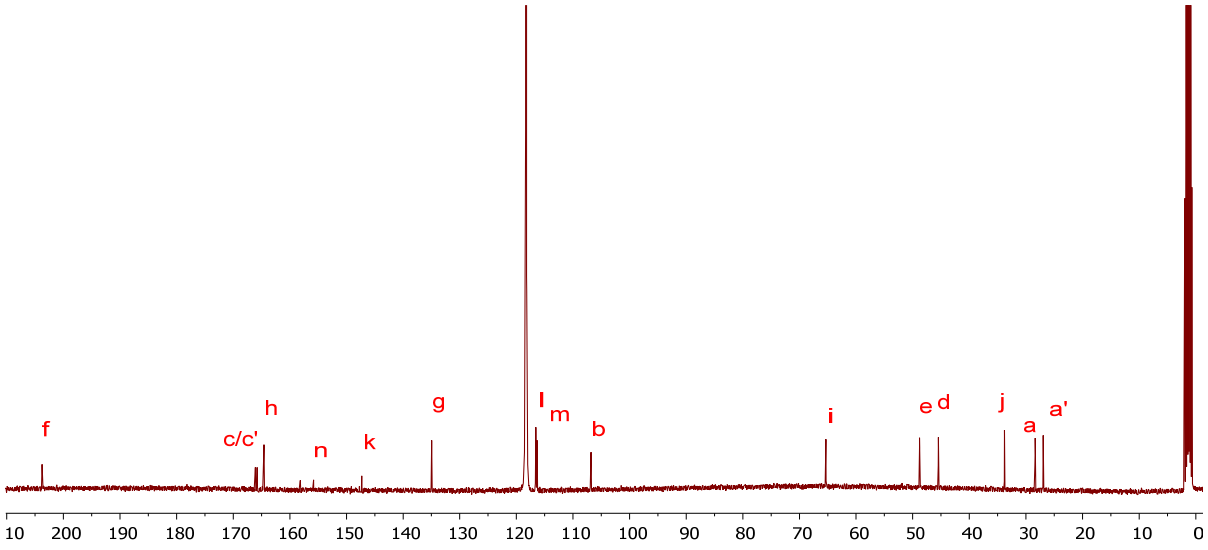

Figure S11. $^{13}C\{^{1}H\}$ NMR (151 MHz, CD_3CN, 298 K) spectrum of **6b** (red). NB: **6a** signals too weak to be observed.

10 Comparison of ^{1}H NMR spectra of compounds 3-6

10.1 ^{1}H NMR spectra of 3-6 in CD_3CN

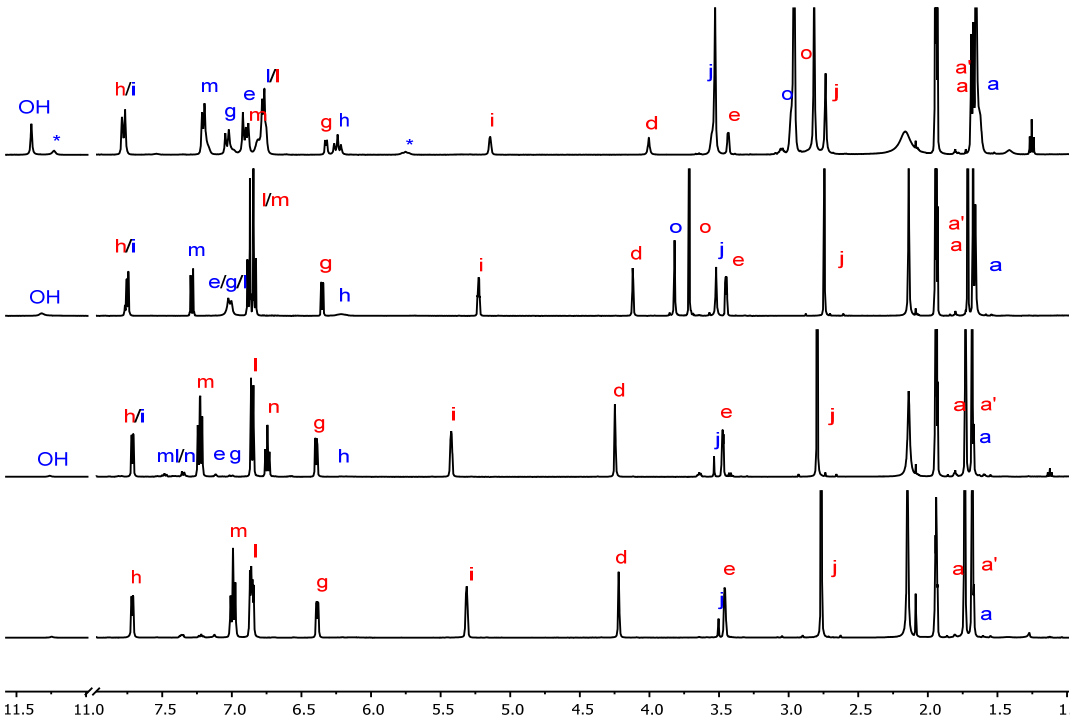

Figure S12. Stacked ^{1}H NMR (500 MHz, CD_3CN, 298 K) spectra of compounds **3-6** (top to bottom). The samples were stored in the dark for 4 h before analysis. ^{1}H NMR analysis was repeated after an additional 24 h stored in the dark to ensure the two isomers are in equilibrium. The linear isomer is labelled with blue labels; the cyclic isomer is labeled with red labels. Signals labelled with * in compound **3** are caused by another conformer, see VT-NMR of compound **3a** on page 33. The change in donor has a large effect on the ratio linear:cyclic, where electron donating substituents favour the linear isomer.

10.2 ^{1}H NMR spectra of 3-6 in $CDCl_3$

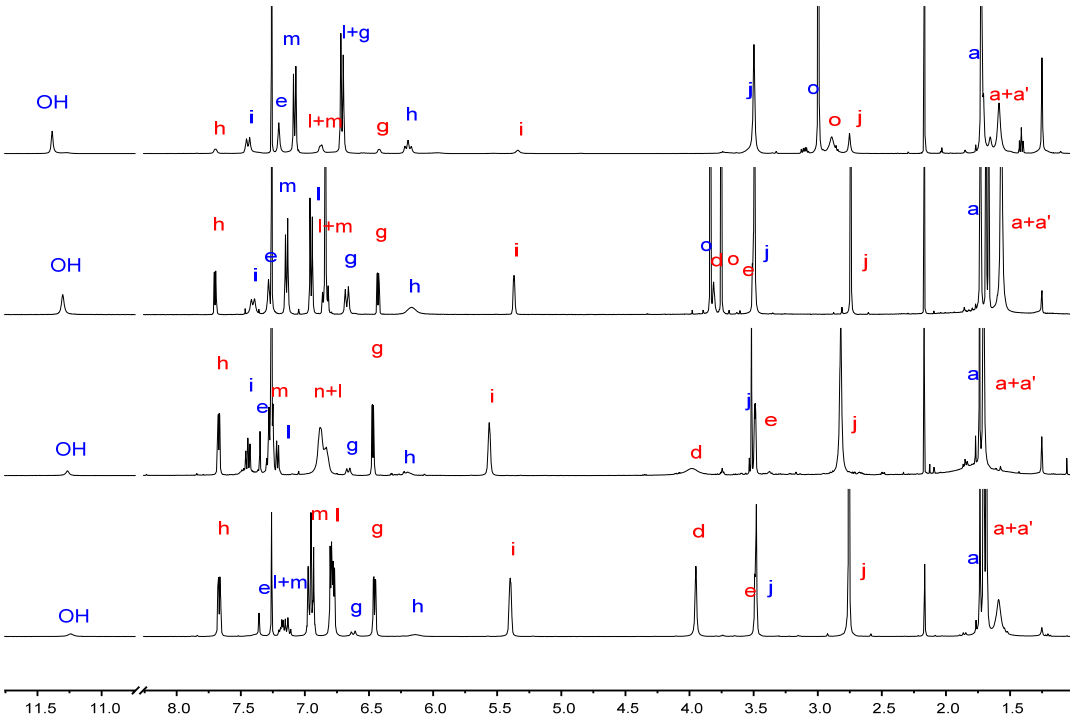

Figure S13. Stacked ^{1}H NMR (500 MHz, $CDCl_3$, 298 K) spectra of compounds **3-6** (top to bottom). The samples were stored in the dark for 5 h before analysis. ^{1}H NMR analysis was repeated after an additional 24 h stored in the dark to ensure the two isomers are in equilibrium. The linear isomer is labeled with blue labels, the cyclic isomer is labeled with red labels. The change in donor has a large effect on the ratio linear:cyclic, where electron donating substituents favour the linear isomer.

10.3 ^{1}H NMR spectra of 3-6 in C_6D_6

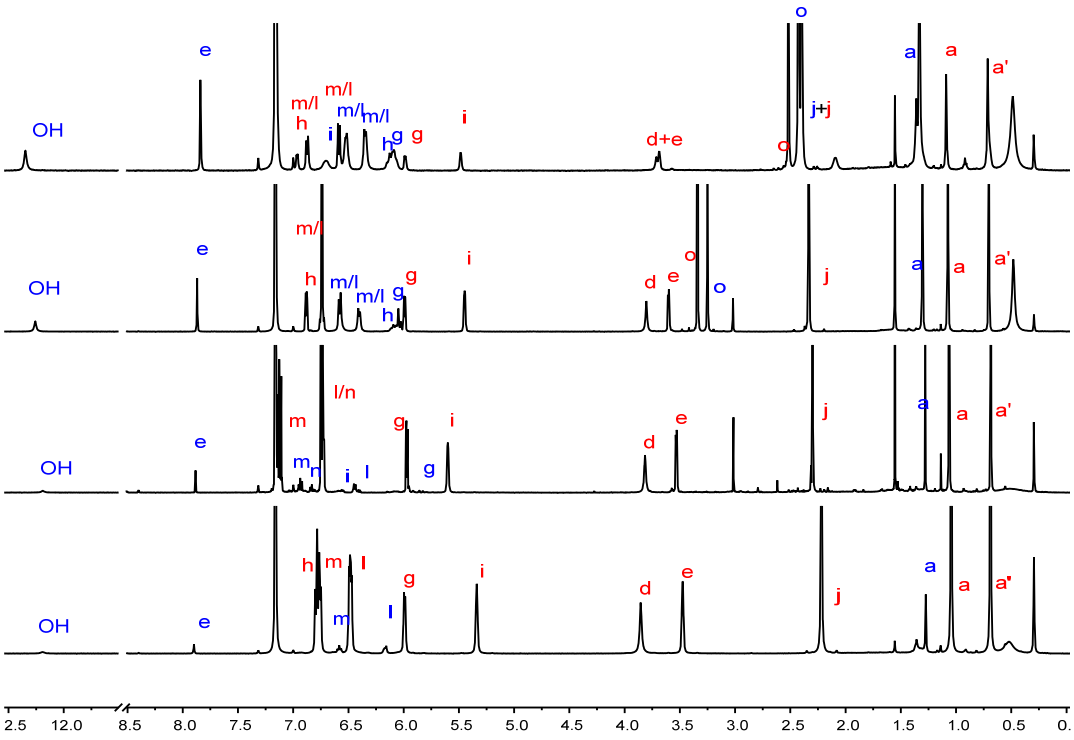

Figure S14. Stacked ^{1}H NMR (500 MHz, C_6D_6, 298 K) spectra of compounds **3-6** (top to bottom). The samples were stored in the dark for 4 h (**3**) to 5 days (**5**) before analysis. ^{1}H NMR analysis was repeated after an additional 24 h stored in the dark to ensure the two isomers are in equilibrium. The linear isomer is labeled with blue labels, the cyclic isomer is labeled with red labels. The change in donor has a large effect on the ratio linear:cyclic, where electron donating substituents favour the linear isomer.

11 2D NMR assignment of solution state cyclic structure

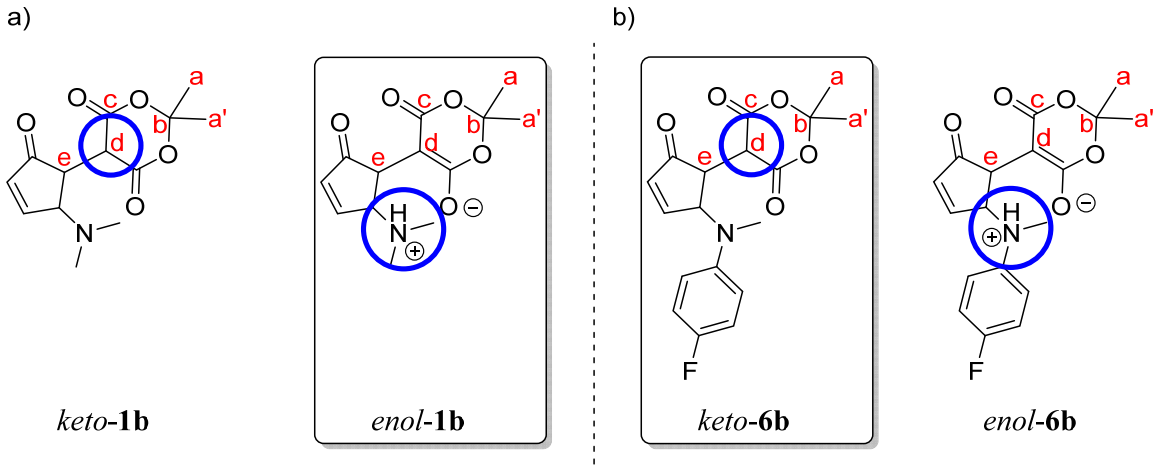

Figure S15. a) Previous work[1] has shown that aliphatic DASA compounds such as **1b** exist in the zwitterionic *enol* tautomer in solution. b) HSQC and HMBC NMR correlation experiments show that the aromatic DASA compounds such as **6b** reported in this work exist in the neutral *keto* form.

Previous work by Helmy *et al.*[1] has reported that DASA compounds with aliphatic donor functionalities exist as zwitterionic *enol* tautomers, as shown in Figure S15a. However, 2D NMR characterization (CD_3CN or DMSO-d_6) revealed that in solution the aryl derivatives exist in their neutral *keto* tautomer, as depicted in Figure S15b. The HSQC NMR spectra of these compounds show that all proton signals are coupled to carbons (Figure S16, Figure S18, Figure S20). In addition, cross-peaks in the HMBC NMR spectra show long multiple bond coupling between proton H^d and carbons $C^{c/c'}$, C^e, C^h and C^i (Figure S17, Figure S19, Figure S21), supporting the assignment and confirming the presence of the *keto* tautomer.

As a reference, compound **1b** was studied in the cyclic form using ^1H, COSY, HSQC and HMBC NMR. Due to the poor solubility of **1b** in CD_3CN, this measurement was performed in DMSO-d_6. As no HSQC cross peak was present for proton H^d, we assign as this signal as NH^+, confirming the molecule exists as a zwitterion in solution. No cross peaks were observed in the HMBC spectrum for proton NH^+ (Figure S23).

11.1 2D NMR spectra of 4b in CD_3CN

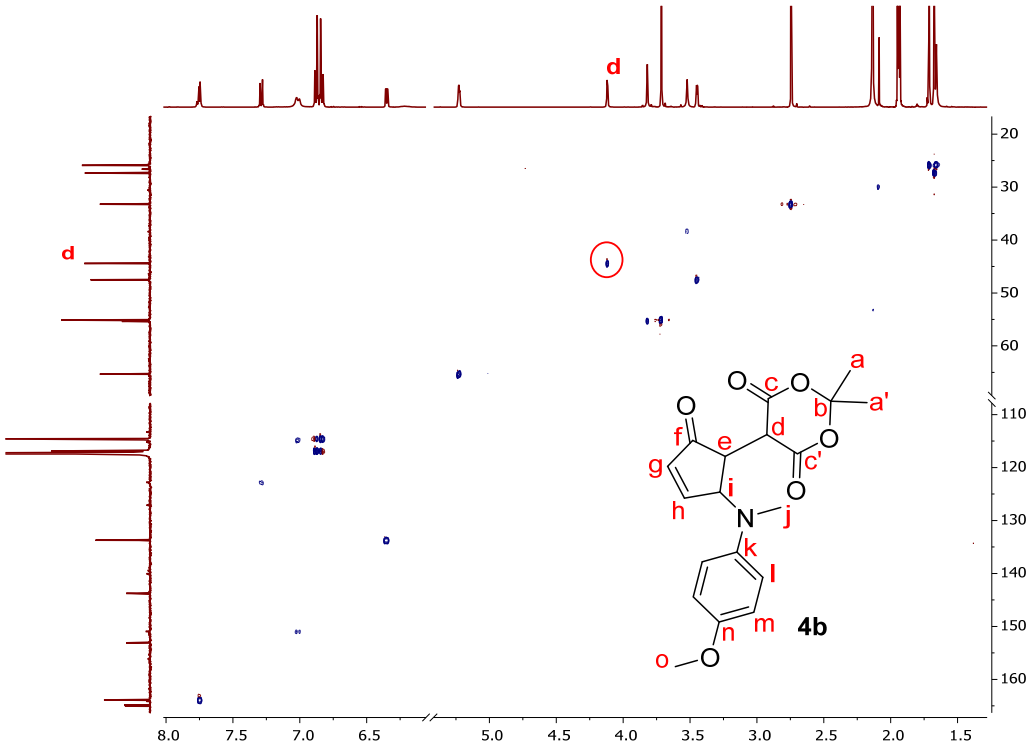

Figure S16. HSQC NMR (500 MHz, CD_3CN, 298 K) spectrum of **4a**/**4b**. All proton peaks couple to carbons, indicating the preference of the *keto* isomer. Circled: the cross-peak of H^d shows that this compound exists in the *keto* tautomeric form.

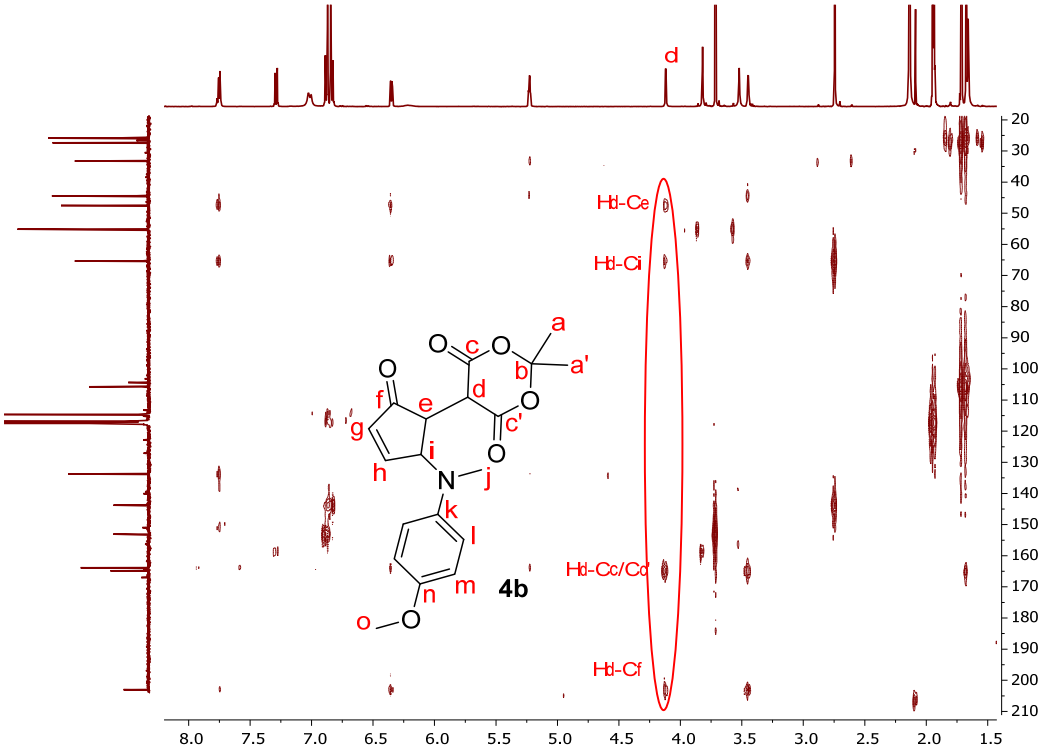

Figure S17. HMBC NMR (500 MHz, CD_3CN, 298 K) spectrum of **4a**/**4b**. The cross-peaks of proton H^d are circled.

11.2 2D NMR spectra of 6b in CD_3CN

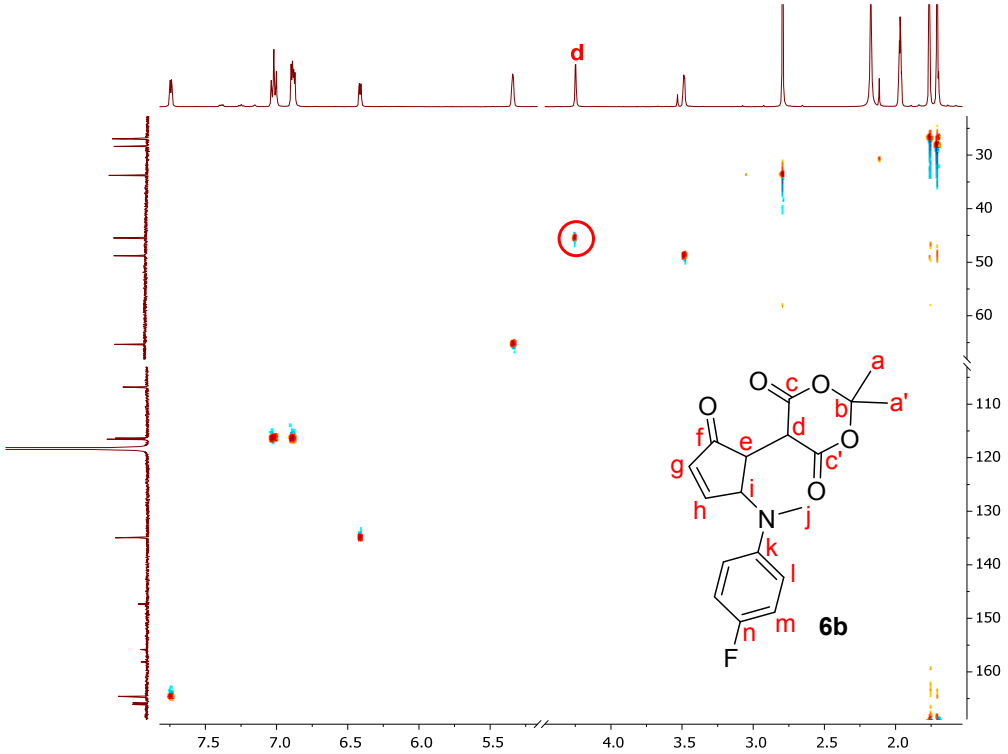

Figure S18. HSQC NMR (500 MHz, CD_3CN, 298 K) spectrum of **6**. All proton peaks couple to carbons, indicating the preference of the *keto* isomer. Circled: the cross-peak of H^d shows that this compound exists in the *keto* tautomeric form.

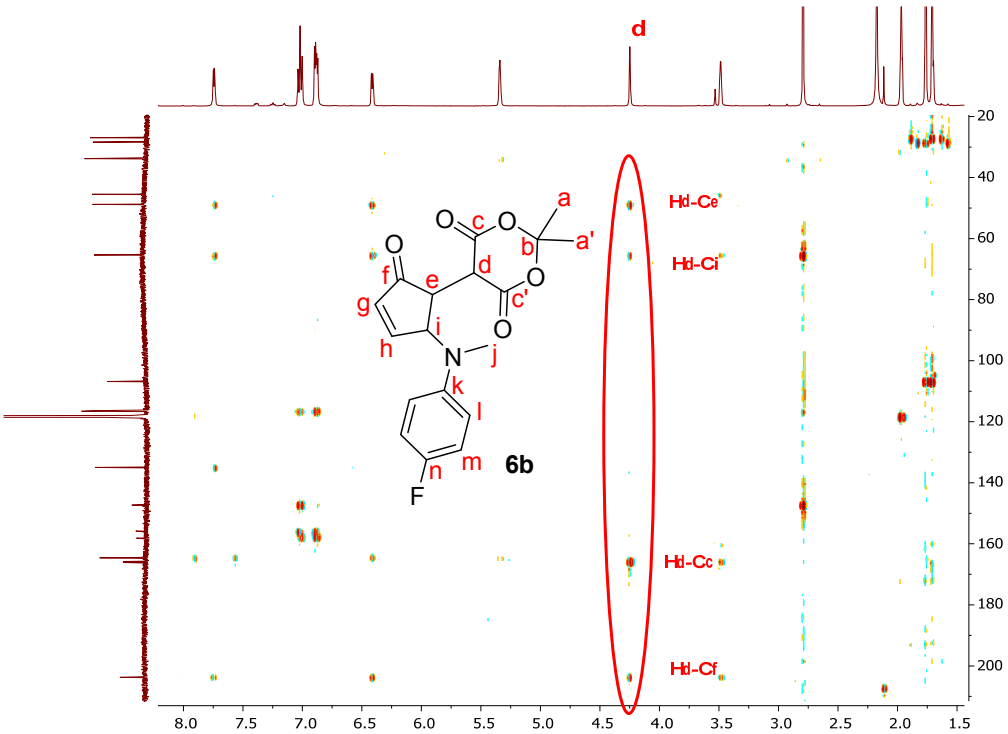

Figure S19. HMBC NMR (500 MHz, CD_3CN, 298 K) spectrum of **6**. The cross-peaks of proton H^d are circled.

11.3 2D NMR spectra of 6b in DMSO-d_6

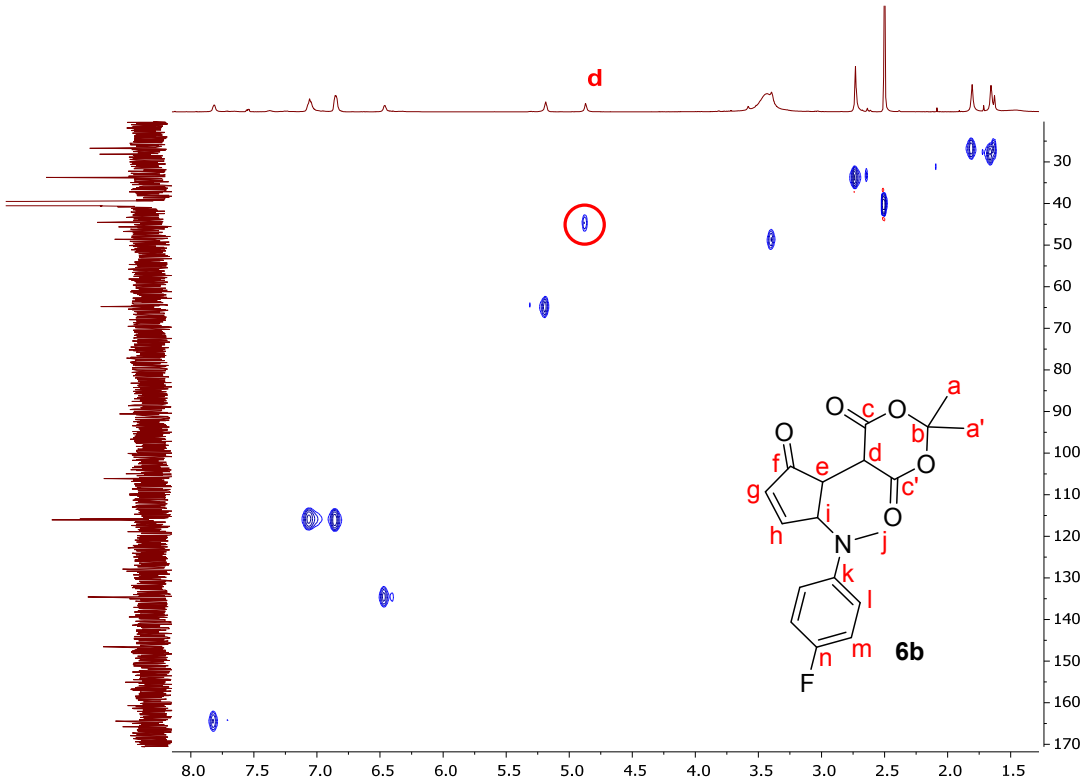

Figure S20. HSQC NMR (500 MHz, DMSO-d_6, 298 K) spectrum of **6**. All proton peaks couple to carbons, indicating the preference of the *keto* isomer.

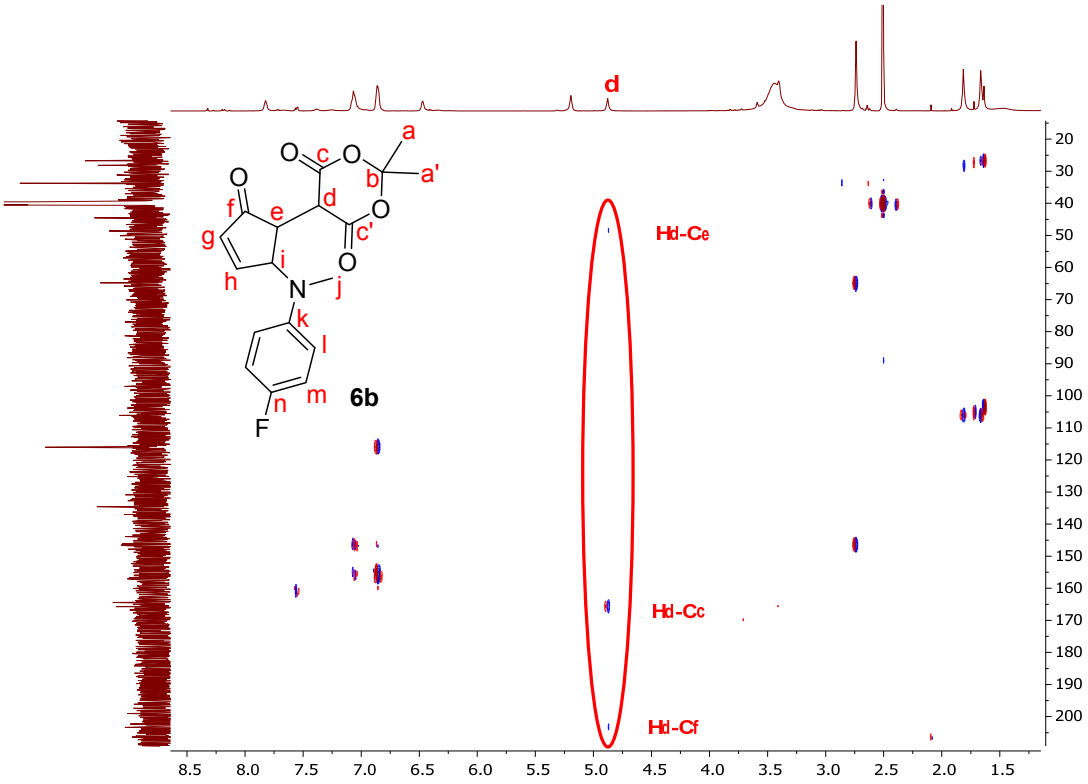

Figure S21. HMBC NMR (500 MHz, DMSO-d_6, 298 K) spectrum of **6**. Highlighted are the cross peaks of proton H^d.

11.4 2D NMR spectra of 1b in DMSO-d_6

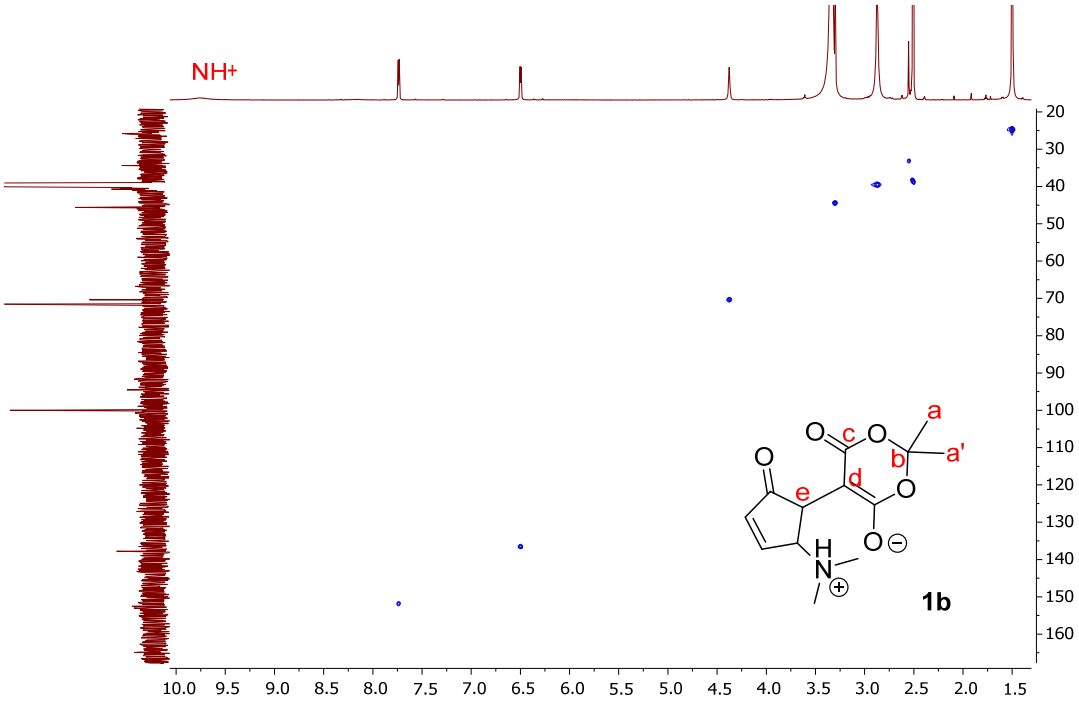

Figure S22. HSQC NMR (500 MHz, DMSO-d_6, 298 K) spectrum of **1b**. The broad peak at δ 9.68 (proton NH^+) does not couple to a carbon, indicating the preference of the *enol* isomer.

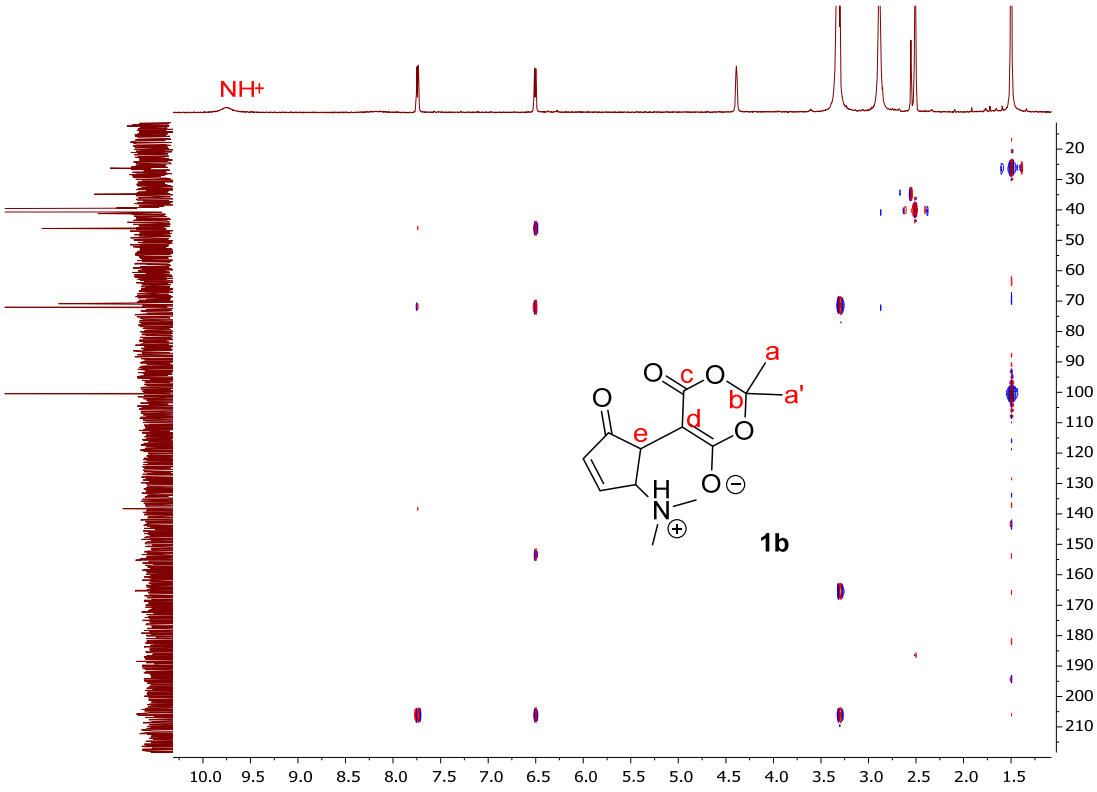

Figure S23. HMBC NMR (500 MHz, DMSO-d_6, 298 K) spectrum of **1b**. No long ranged cross coupling is observed to the NH^+, indicating the presence of the *enol* isomer.

12 VT-NMR of compound 3a in CD_3CN

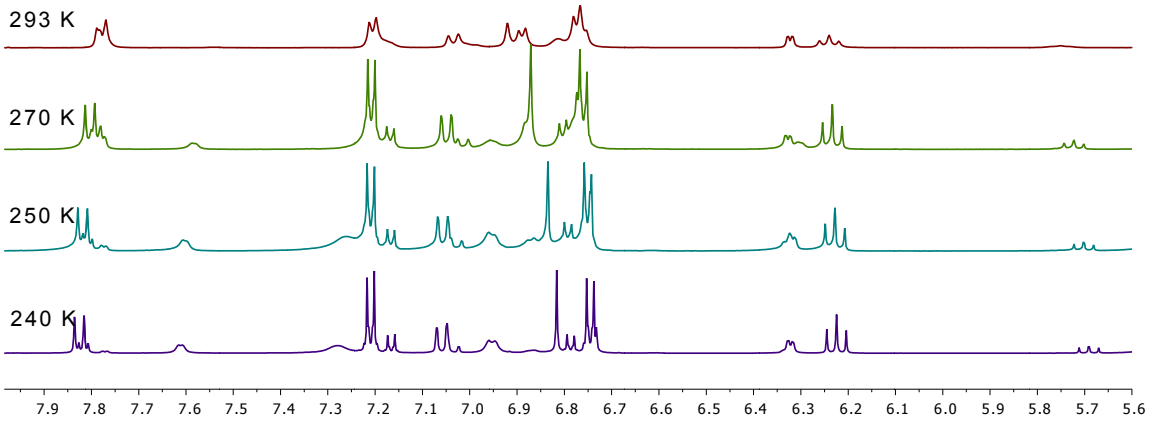

Figure S24. Variable temperature ^{1}H NMR (600 MHz, CD_3CN, 293 K – 240 K) spectra of **3a**.

The ^{1}H peaks of the linear DASA compound **3a** are broadened at 298 K, indicating exchange with some other chemical species on the NMR timescale (Figure S24, 293 K). Cooling to 240 K (Figure S24) resolved the peaks into two separate systems, present in a ratio of approximately 4:1 (the cyclic form also appears to split, but these peaks are still broadened at 240 K). The two components of **3a** were fully characterized using 2D correlation experiments (COSY, ^{13}C HSQC, ^{13}C HMBC, ^{15}N HMBC). Through-space dipolar correlations were then obtained from a NOESY experiment, and used to establish the identity of the two components as conformers resulting from restricted C-N bond rotation.

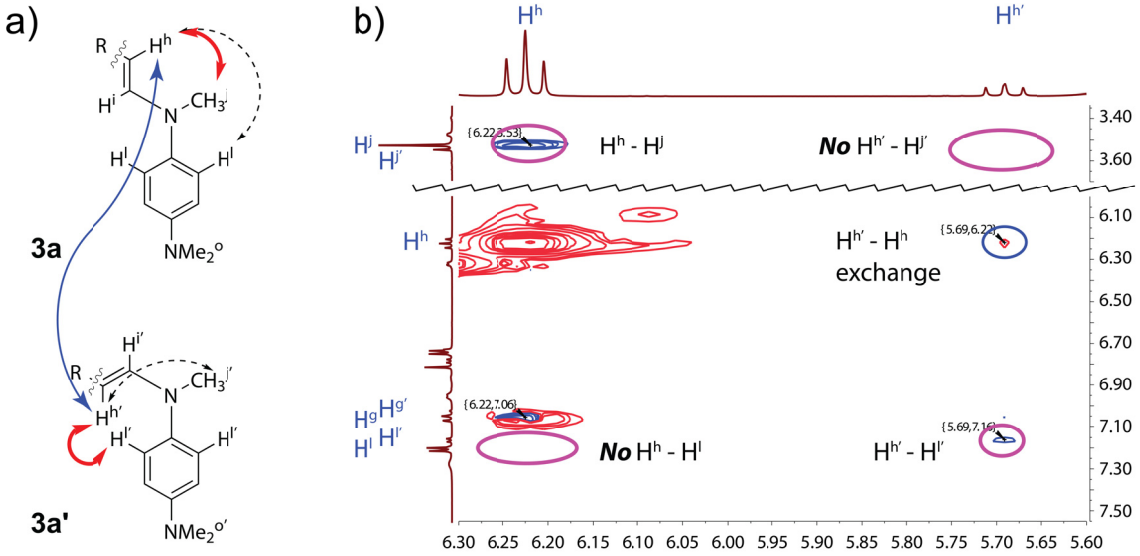

Figure S25. A low-temperature NOESY (600 MHz, CD_3CN, 240 K) experiment was used to identify the two conformers **3a** and **3a'**. a) Solid red arrows show observed NOESY couplings; dashed black arrows show absence of coupling, blue arrow show chemical exchange. b) Expansion of NOESY spectrum. For **3a**, H^h shows dipolar coupling with *N*-methyl protons H^j but not aromatic protons H^l. For **3a'**, $H^{h'}$ shows through-space contact with aromatics $H^{l'}$ but not *N*-methyl protons $H^{j'}$. A H^h-$H^{h'}$ chemical exchange cross peak (opposite phasing) shows that even at 240 K, C-N bond rotation is thermally accessible.

12.1 NMR (^{1}H, ^{13}C, ^{15}N) characterization of linear conformers 3a and 3a'

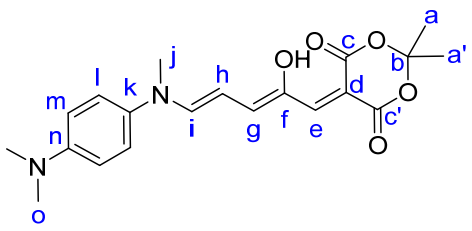

3a

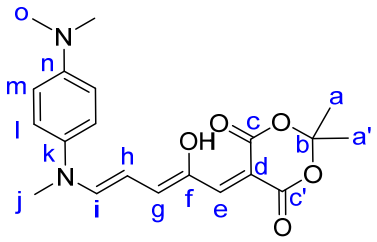

3a'

^{1}H chemical shifts were obtained through 1D ^{1}H experiments. ^{13}C and ^{15}N chemical shifts were obtained from HSQC (^{13}C) and HMBC (^{15}N, ^{13}C) experiments.

3a ^{1}H NMR (600 MHz, CD_3CN, 240 K) δ 11.51 (s, 1H, H^{OH}), 7.83 (d, J = 11.9 Hz, 1H, H^{i}), 7.21 (d, J = 9.1 Hz, 2H, H^{l}), 7.07 (d, J = 1.5 Hz, 1H, H^{g}), 6.82 (s, 1H, H^{e}), 6.75 (d, J = 9.1 Hz, 2H, H^{m}), 6.24 (dd, J = 12.3, 12.3 Hz, 1H, H^{h}), 3.53 (s, 3H, H^{j}), 2.94 (s, 6H, H^{o}), 1.65(s, 6H, H^{a}).

^{13}C NMR (from ^{13}C HSQC and HMBC, 151 MHz, CD_3CN) δ 167.2 (C^{c}), 164.3 ($C^{c'}$), 157.0 (C^{i}), 152.2 (C^{g}), 149.8 (C^{n}), 144.5 (C^{f}), 135.4 (C^{e}), 134.4 (C^{k}), 122.1 (C^{l}), 112.0 (C^{m}), 105.2 (C^{h}), 102.9 (C^{b}), 88.5 (C^{d}), 39.7 (C^{o}), 38.7 (C^{j}), 25.6 (C^{a}).

^{15}N NMR (from ^{15}N HMBC, 60.8 MHz, CD_3CN, 240 K) δ 147.0 (N^{k}), 49.8 (N^{n}).

3a' ^{1}H NMR (600 MHz, CD_3CN, 240 K) δ 11.32 (s, 1H, H^{OH}), 7.82 (d, J = 11.8 Hz, 1H, H^{i}), 7.17 (d, J = 9.0 Hz, 2H, H^{l}), 7.03 (m, 1H, H^{g}), 6.79 (d, J = 9.0 Hz, 2H, H^{m}), 6.73 (s, 1H, H^{e}), 5.69 (dd, J = 13.1, 11.8 Hz, 1H, H^{h}), 3.55 (s, 3H, H^{j}), 2.97 (s, 6H, H^{o}), 1.59 (s, 6H, H^{a}).

^{13}C NMR (from ^{13}C HSQC and HMBC, 151 MHz, CD_3CN) δ 167.1 (C^{c}), 164.4 ($C^{c'}$), 162.8 (C^{i}), 152.3 (C^{g}), 150.5 (C^{n}), 144.0 (C^{f}), 133.4 (C^{e}), 128.9 (C^{k}), 125.4 (C^{l}), 112.0 (C^{m}), 105.3 (C^{h}), 102.7 (C^{b}), 87.3 (C^{d}), 47.4 (C^{j}), 39.7 (C^{o}), 25.5 (C^{a}).

^{15}N NMR (from ^{15}N HMBC, 60.8 MHZ, CD_3CN, 240 K) δ 149.3 (N^{k}), 50.8 (N^{n}).

13 Concentration dependency measured by UV-vis

A series of standard solutions of **3a** were prepared in benzene (6.7×10^{-4}, 1.7×10^{-3}, 3.4×10^{-3}, 5.0×10^{-3} and 6.7×10^{-3} mM). The solutions were allowed to equilibrate in the dark for 5 hours before the UV-vis absorbance of the solutions was measured. Care was taken to ensure the samples where not exposed to light as they were prepared and inserted into the spectrophotometer. The absorbance at λ_{max} was measured for each sample five times over a period of 5 minutes and the average was plotted against concentration.

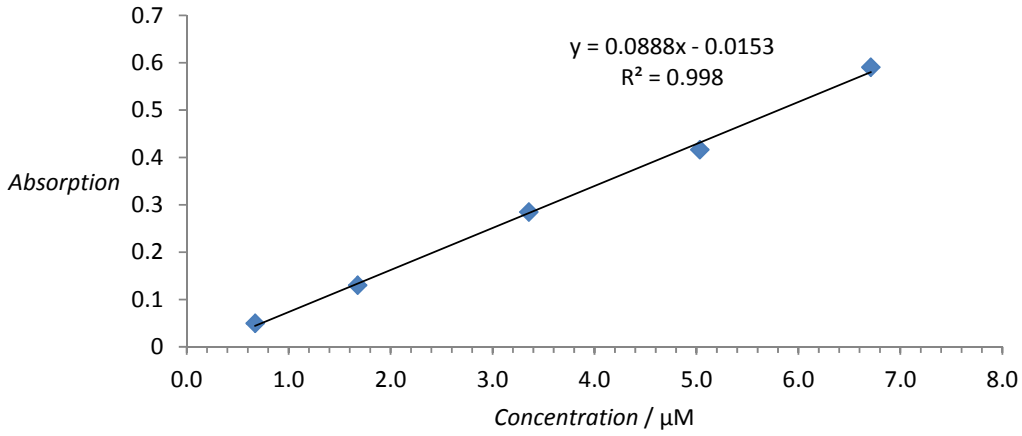

Figure S26. Concentration dependence of absorbance for compound **3a** at 575 nm in benzene at 293 K.

14 Absorption properties of the linear and cyclic compounds measured by UV-vis

The absorption spectra of compounds **3-6** were measured in chloroform, acetonitrile and benzene.

For *in situ* irradiation of UV-vis samples a custom-built setup was used. The cell holder was modified with a slit on one of the side walls to allow for irradiation perpendicular to the direction of measurement. A Luxeon Rebel LED (lime, 567 nm, 313 lm @ 700 mA) was mounted on a heat sink positioned 4 cm away from the cell, and the beam was focused on the cuvette using a Carclo 20.0 mm Fibre Coupling Lens.

As compounds **3-6** exist in mixtures of linear and cyclic isomers in different relative ratios, we present the following data normalized for the maximum absorbance in the visible region.

14.1 Table of absorption maxima in different solvents

Table S1. A comparison of the visible λ_{max} (nm) values for compounds **3a-6a** in CH_3CN, $CHCl_3$ and C_6H_6 (293 K).

	CH_3CN	$CHCl_3$	C_6H_6
3a	561	574	573
4a	553	563	564
5a	551	561	560
6a	550	557	556

14.2 UV-visible absorption in acetonitrile

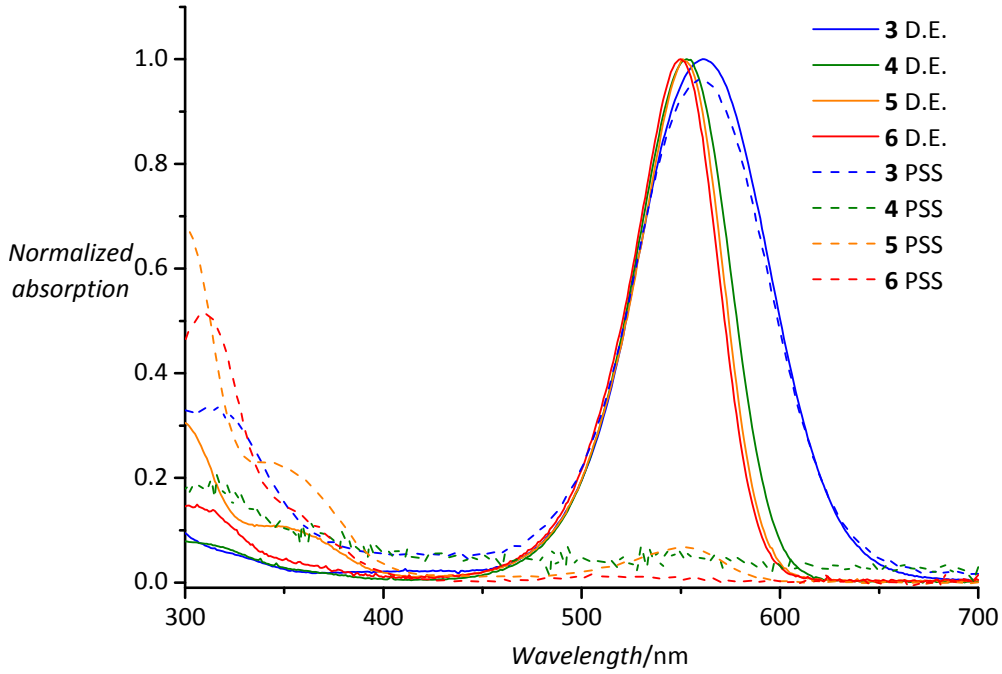

Figure S27. Normalized visible absorption spectra (CH_3CN, 293 K) for **3-6** in dark equilibrium (D.E., equilibrated in the dark for 24 h) and the photostationary state (PSS).

14.3 UV-visible absorption in chloroform

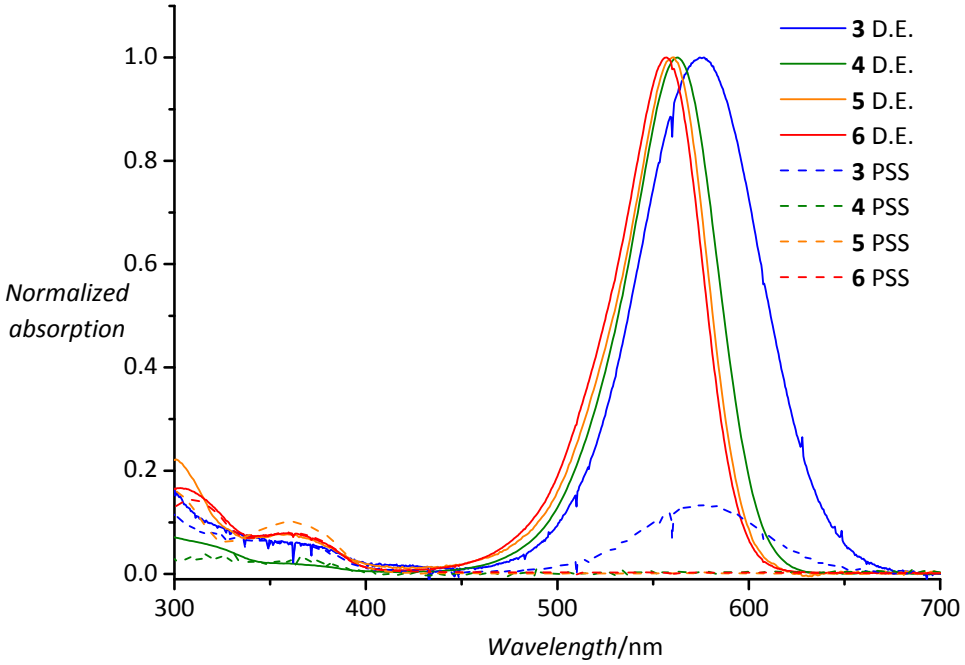

Figure S28. Normalized visible absorption spectra ($CHCl_3$, 293 K) for **3-6** in dark equilibrium (D.E., equilibrated in the dark for 24 h) and the photostationary state (PSS).

14.4 UV-visible absorption in benzene

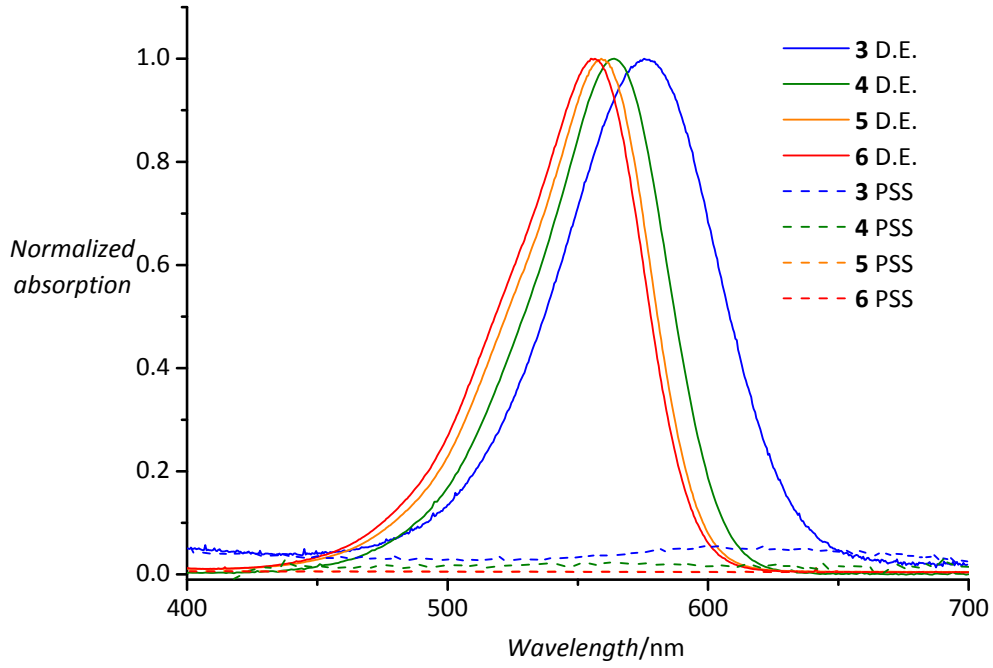

Figure S29. Normalized visible absorption spectra (C_6H_6, 293 K) for **3-6** in dark equilibrium (D.E., equilibrated in the dark for 24 h) and the photostationary state (PSS).

15 Calculation of molar absorptivities of the linear DASA species

As the aromatic DASA compounds prepared exist in equilibrium between the linear and cyclized forms, obtaining values for ε was non-trivial. Solutions of each compound were prepared in deuterated solvents, and both UV-vis and NMR spectra were acquired from the same solution to determine a) the relative populations of the linear and cyclized form, and b) the absolute absorbance of the equilibrated solution. The molar absorptivity for each species was then calculated as:

$$\varepsilon = \frac{A}{x_{linear} c l}$$

where x_{linear} is the proportion of the compound in the photochromic linear state, as determined by NMR.

UV-vis spectra were acquired with a 1.00 mm path length in a quartz cuvette and ^{1}H spectra were acquired using a 600 MHz spectrometer fitted with a cryoprobe. Both NMR and UV-vis spectra were acquired from the same solutions, at concentrations of 0.04 – 2.0 mM.

The linear:cyclic ratios were determined by the relative integrals of the methyl peaks, as these were non-overlapping and could be integrated quantitatively. For compounds **3** and **4** (DASA-NMe_2 and DASA-OMe) this gave three points of comparison for each isomer, while for compound **5** and **6** two signals were used for the comparison.

For all experiments, errors were estimated from the square root of the sum of squares of component errors ($\sigma_{total} = \sqrt{\sum_i \sigma_i^2}$). These were estimated at ±0.05 mg in sample mass and ±3% for each dilution to make the solutions (using gastight syringes and HPLC septa vials).

15.1 Molar absorptivities in CD_3CN

Solutions were prepared in CD_3CN, left to equilibrate for 4 hours, and spectra were acquired. Results are given in Table S2.

Table S2. Molar absorptivities for the aromatic DASA compounds in CD_3CN.

Compound	Percent linear	C [mM]	A [λ_{max}]	ε [$\times 10^3$ M^{-1} cm^{-1}]
3a	65%	0.10	0.524	81±4
4a	26%	0.50	0.909	70±6
5a	3.9%	1.0	0.290	74±10
6a	4.3%	2.0	0.427	50±4

Molar absorptivities of linear DASA compounds **3a-6a** as measured in CD_3CN at 293 K. The absorptivities of the linear forms were calculated from absorption and linear:cyclic values taken from NMR and UV-vis experiments on the same solutions.

15.2 Molar absorptivities in $CDCl_3$

Solutions were prepared in $CDCl_3$, left to equilibrate for 3 hours, and spectra were acquired. Results

are given in Table S3.

Table S3. Molar absorptivities for the aromatic DASA compounds in $CDCl_3$.

Compound	Percent linear	C [mM]	A [λ_{max}]	ε [$\times 10^3$ M^{-1} cm^{-1}]
3a	81%	4.0×10^{-2}	0.300	90±7
4a	53%	0.10	0.505	97±8
5a	20%	0.40	0.840	110±10
6a	17%	0.40	0.571	84±6

Molar absorptivities of linear DASA compounds **3a-6a** as measured in $CDCl_3$ at 293 K. The absorptivities of the linear forms were calculated from absorption and linear:cyclic values taken from NMR and UV-Vis experiments on the same solutions.

16 Photoswitching experiments monitored by UV-vis

16.1 *In situ* photoswitching of 4a/4b in $CHCl_3$

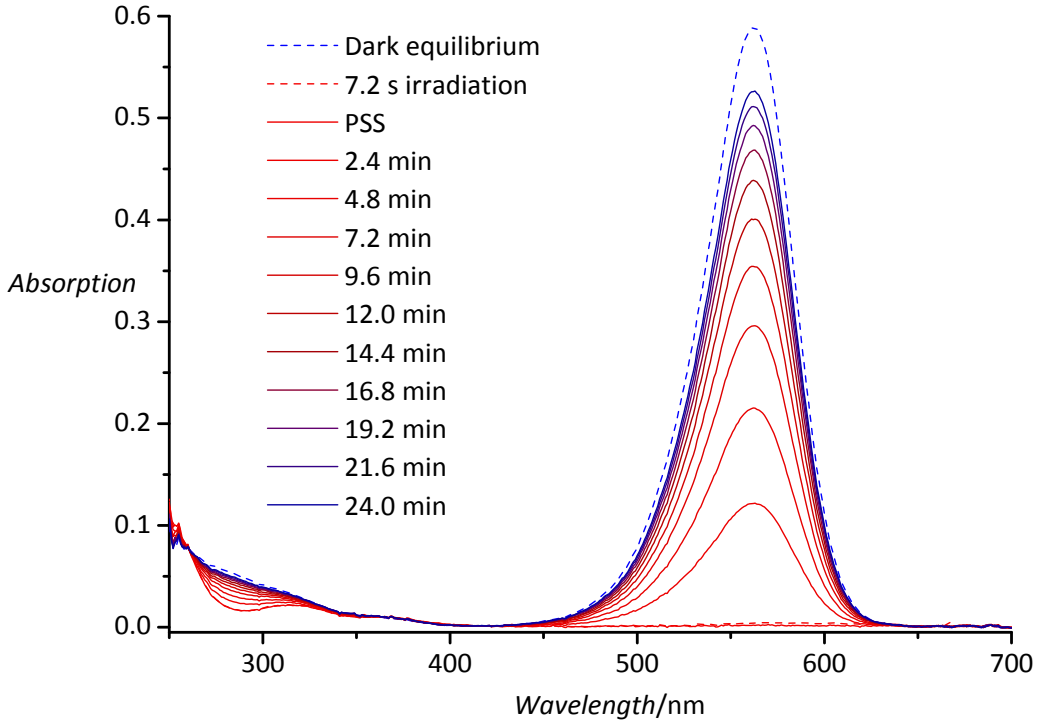

Figure S30. Optical switching (567 nm LED) and thermal relaxation of compound **4a**/**4b** in $CHCl_3$ (298 K), followed by UV-visible spectroscopy.

16.2 Switching in of 3-6 CH_3CN

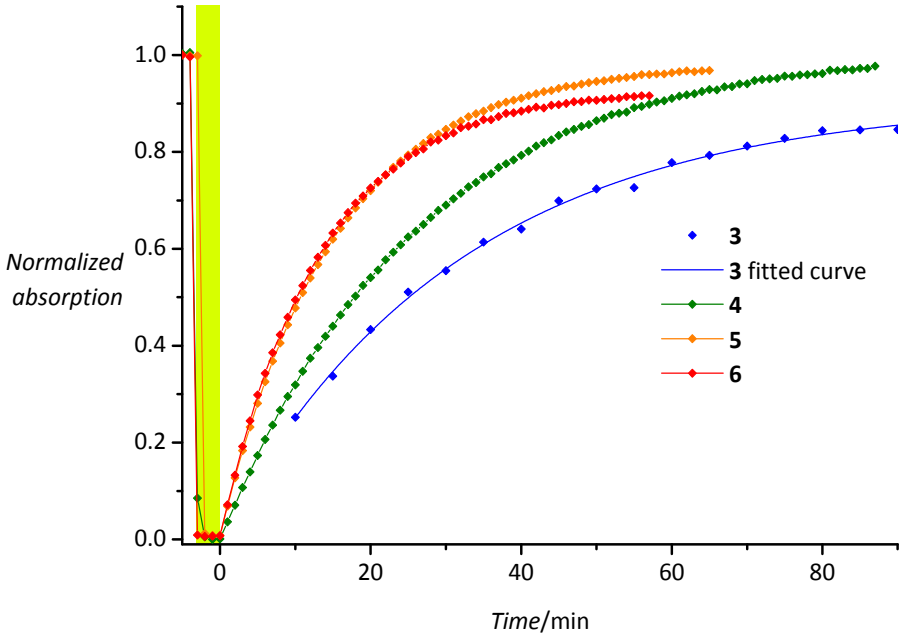

Figure S31. Single cycle of photoswitching and thermal reversion for compounds **3-6** measured in MeCN (293 K) and monitored for each compound at the visible absorption λ_{max}. The lime-coloured block indicates irradiation of the sample (567 nm). Compound **3** only switches approximately 10%, causing significantly more noise in the normalized curve. To lessen the noise, every five points was averaged into one point, through which an exponential curve was fitted to determine the apparent half-life time.

Table S4. Apparent half-life times of compound **3-6**, measured by UV-vis spectroscopy (MeCN, 293 K, see Figure S31).

Compound	$t_{½}$ [min] CH_3CN
3	22.0±0.1
4	18.0±0.1
5	10.5±0.1
6	9.2±0.1

16.3 Switching of compound 4 in $CHCl_3$, CH_3CN and C_6H_6

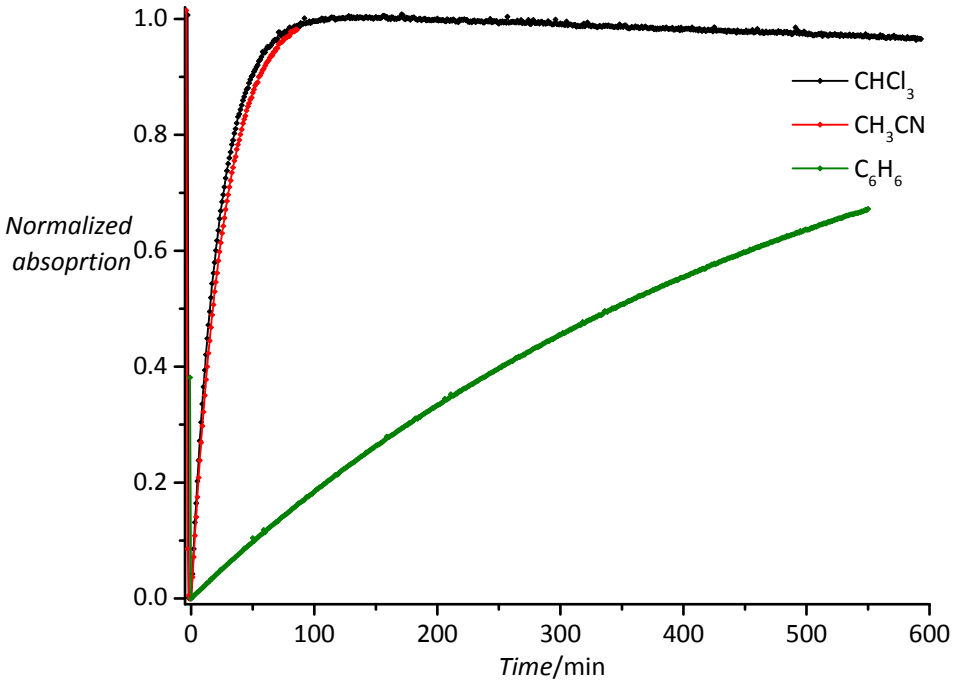

Figure S32. Single cycle of photoswitching and thermal reversion for compound **4** measured in $CHCl_3$, CH_3CN and C_6H_6 at 293 K, monitored at λ_{max} for each solvent. Thermal reversion of **4** in benzene did not reach the dark equilibrium due to the slow kinetics. The data was normalized using the half-life time derived from the data.

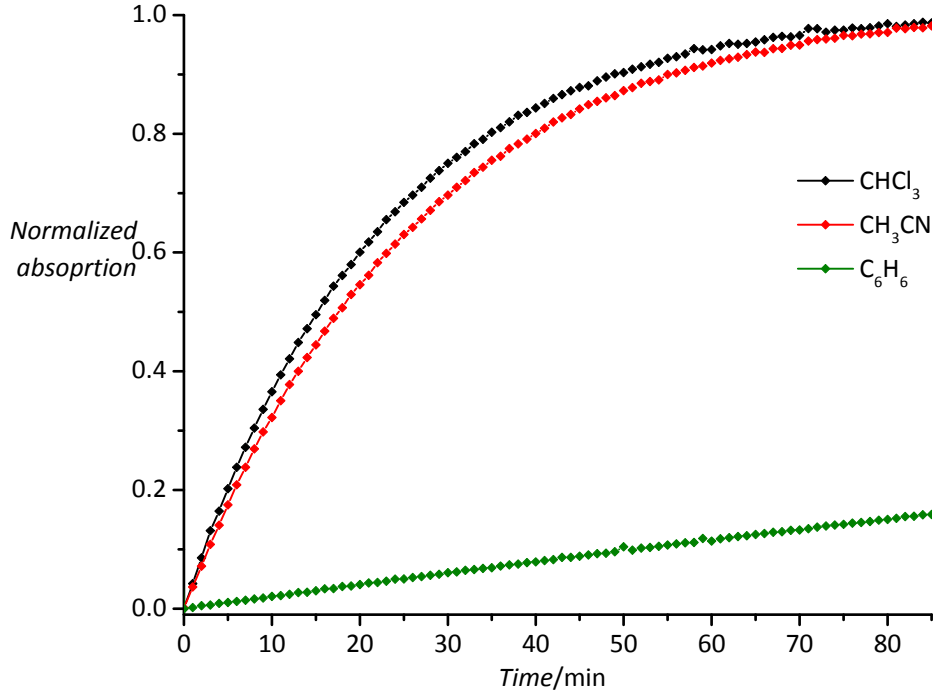

Figure S33. Expansion of Figure S32, showing thermal reversion during the first 60 minutes following cessation of irradiation (567 nm) at t=0.

Table S5. Apparent half-life times of compound **4** in $CHCl_3$, CH_3CN and C_6H_6 (293 K), measured by UV-vis spectroscopy (see Figure S32).

Compound	$t_{½}$ [min] $CHCl_3$	$t_{½}$ [min] CH_3CN	$t_{½}$ [min] C_6H_6
4	15.3±0.1	18.0±0.1	343±0.5

17 Fatigue resistance of 4 in $CHCl_3$ and CH_3CN monitored by UV-vis

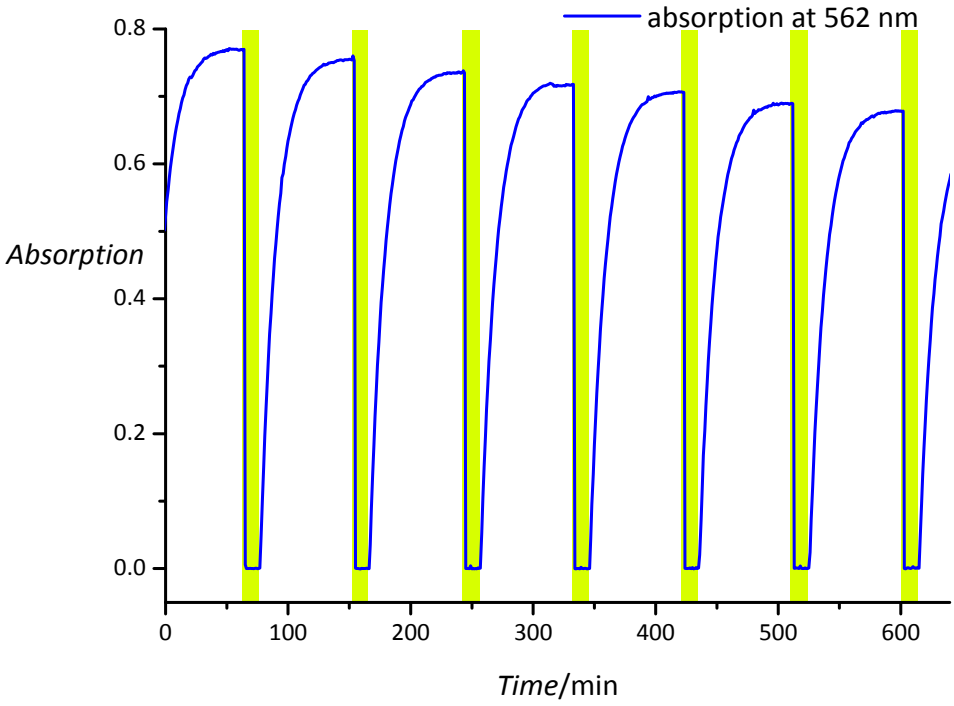

Figure S34. Fatigue resistance of compound **4** in $CHCl_3$ monitored by UV-vis spectroscopy (298 K). The absorption was measured at the absorption maximum of 562 nm. The coloured blocks indicate periods of photo irradiation (567 nm). A 12% decrease in absorption was observed over 9 hours, due to decomposition of the linear isomer.

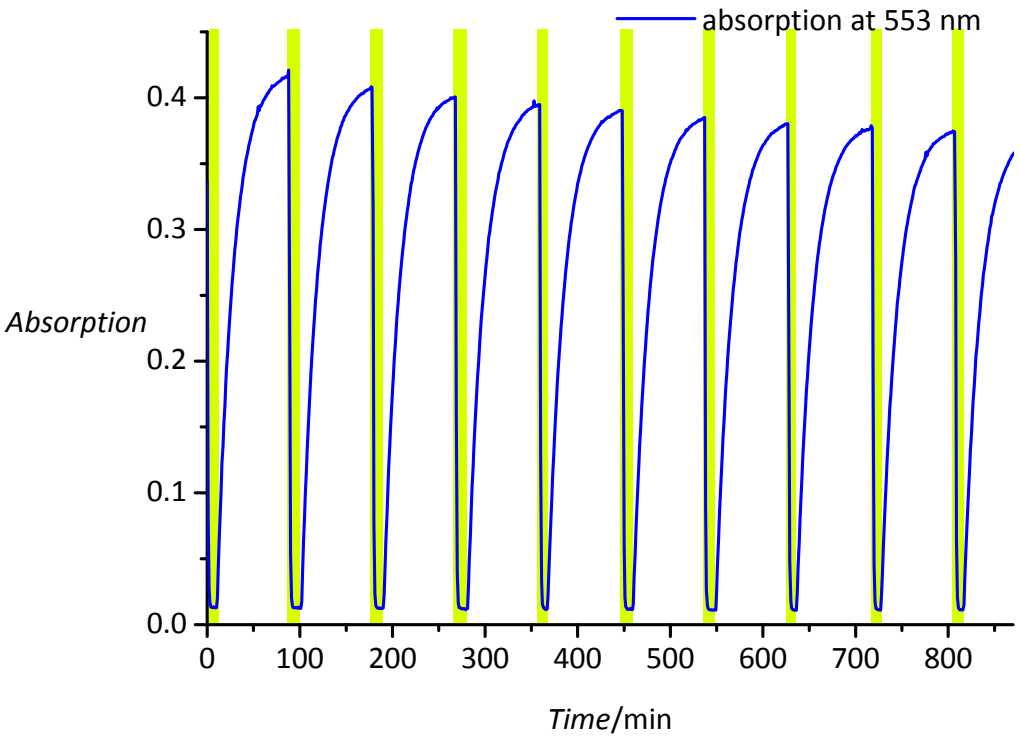

Figure S35. Fatigue resistance of compound **4** in CH_3CN monitored by UV-vis spectroscopy (298 K). The absorption was measured at the absorption maximum of 553 nm. The coloured blocks indicate periods of photo irradiation (567 nm). A 12% decrease in absorption was observed over 12 hours, due to decomposition of the linear isomer.

As in previously reports[4] these compounds were observed to slowly decompose over time when stored in solution

18 *In situ* NMR irradiation experiments

18.1 General

The switching behaviour of compounds **3-6** was studied using *in situ* irradiation during ^{1}H NMR spectroscopy. The compounds were studied in $CDCl_3$, CD_3CN and C_6D_6 at concentrations between 1-4 mM. Solvents were filtered over $MgSO_4$ and $NaHCO_3$ before sample preparation. The samples were placed in 5 mm screw thread sample tubes (New Era NE-HL5-ST-158) and left in the dark to reach thermal equilibrium before spectrum acquisition.

A custom-made setup was used to position one end of an optical fibre in front of an LED light source. Luxeon Rebel LEDs (lime, 567 nm, 313 lm @ 700 mA) were used to irradiate the samples. Light was directed into the NMR samples *via* a 3 meter long, 0.39 NA, Ø1500 µm core multimode optical fibre (Thorlabs FT1500UMT). The last 4 cm was roughened with sand paper (80 grit), as previous reported by Gschwind,[5] and inserted into the solution.

Switching behaviour under light irradiation was observed by performing a series of 8 scan ^{1}H experiments at 60 second intervals. During the first experiments the samples were measured without irradiation to demonstrate the sample is in thermal equilibrium. Subsequently, the samples were irradiated until a photostationary state was obtained. The rate of thermal relaxation was measured after irradiation of the sample ceased.

The relative proportions of the linear and cyclic compounds over time were obtained by integration of all non-overlapping signals, using the MestReNova concentration graph analysis routine. Exponential regression analysis (performed in Origin) was used to fit curves of the form $y = y_0 + Ae^{R_0 t}$ to the time-dependent data, where y = fraction, y_0 = y offset, A = amplitude, R_0 = rate constant and t = time in minutes.

The apparent half-life times ($t_{½}$) were calculated as $t_{½} = \frac{ln\,½}{R_0}$.

Rate constants for both isomerization reactions without irradiation were measured on the same data, and fitted to the kinetic model $A \underset{k_{-1}}{\overset{k_1}{\rightleftharpoons}} B$, where A is the fraction linear and B is the fraction cyclic (Scheme S2).

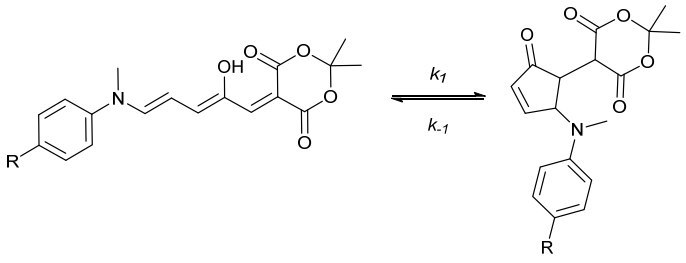

Scheme S2. Kinetic model of thermal isomerization.

To determine the rate constants, the data was fitted with a curve of the form

$y = 1 - \frac{k_1+k_{-1}e^{-(k_1+k_{-1})(t+z)}}{k_1+k_{-1}}$, where y = fraction, k_1 and k_{-1} are rate constants for the conversion in the dark, t = time in minutes, and z = time offset to correct to 100% cyclic.

Equilibrium constant K was determined by $K = \frac{k_1}{k_{-1}}$

18.2 Apparent half-life times and photostationary states in CD_3CN

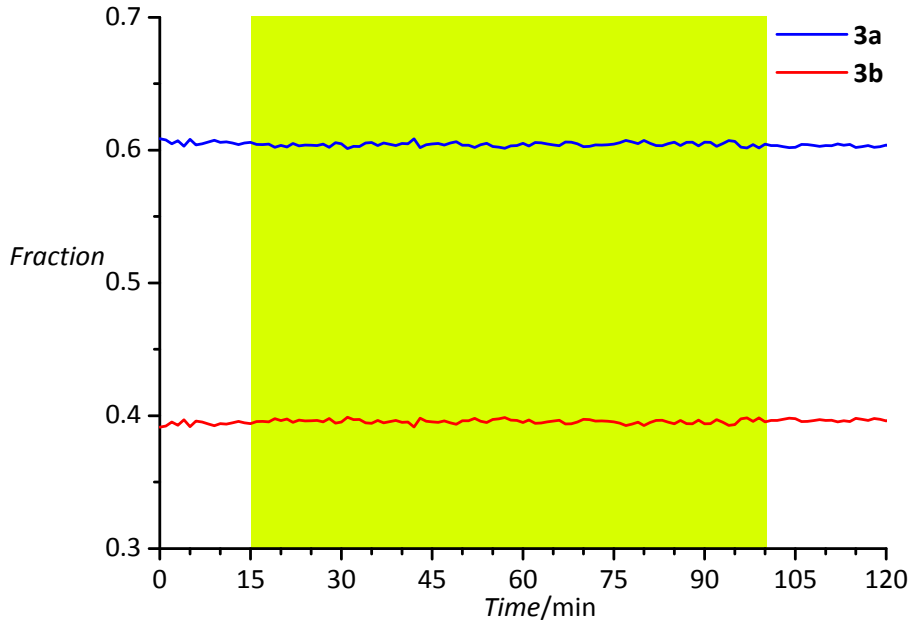

Figure S36. Fraction **3a** and **3b** during the *in situ* photo-switching experiment, measured by ^{1}H NMR (500 MHz, CD_3CN, 298 K) spectroscopy. The lime-coloured block indicates the period of irradiation. No significant change in the ratio linear:cyclic was observed.

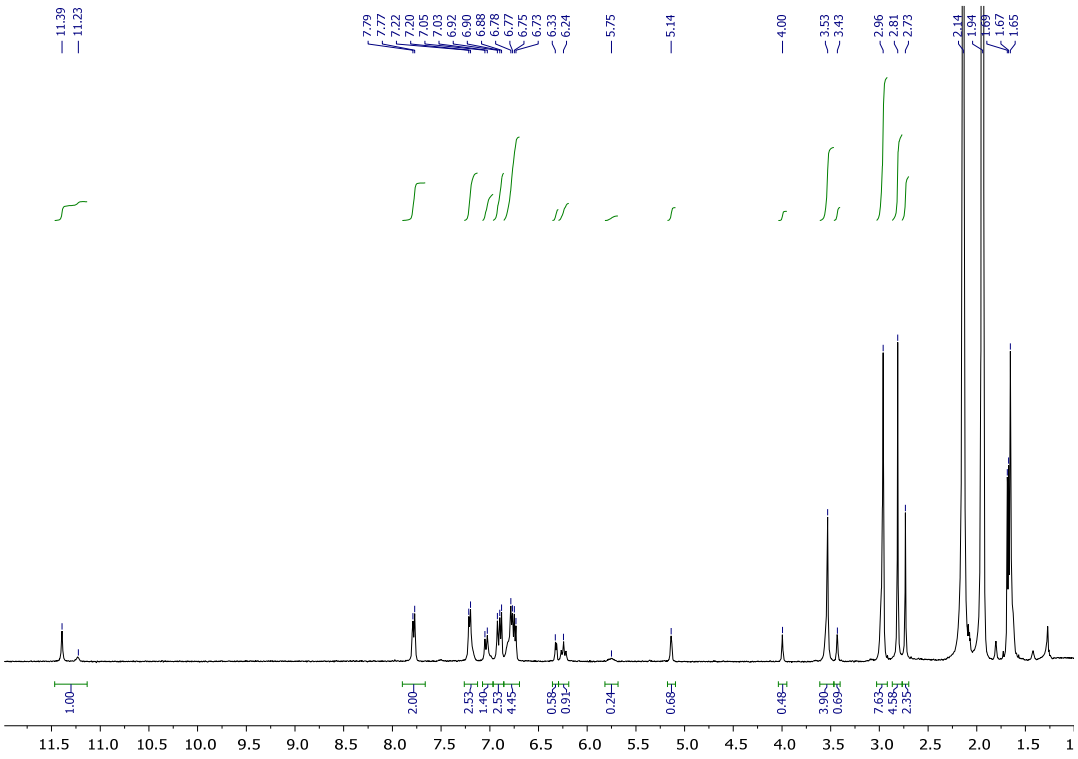

Figure S37. ^{1}H NMR (500 MHz, CD_3CN, 298 K) spectrum of **3a**/**3b** after continuous irradiation for 60 min.

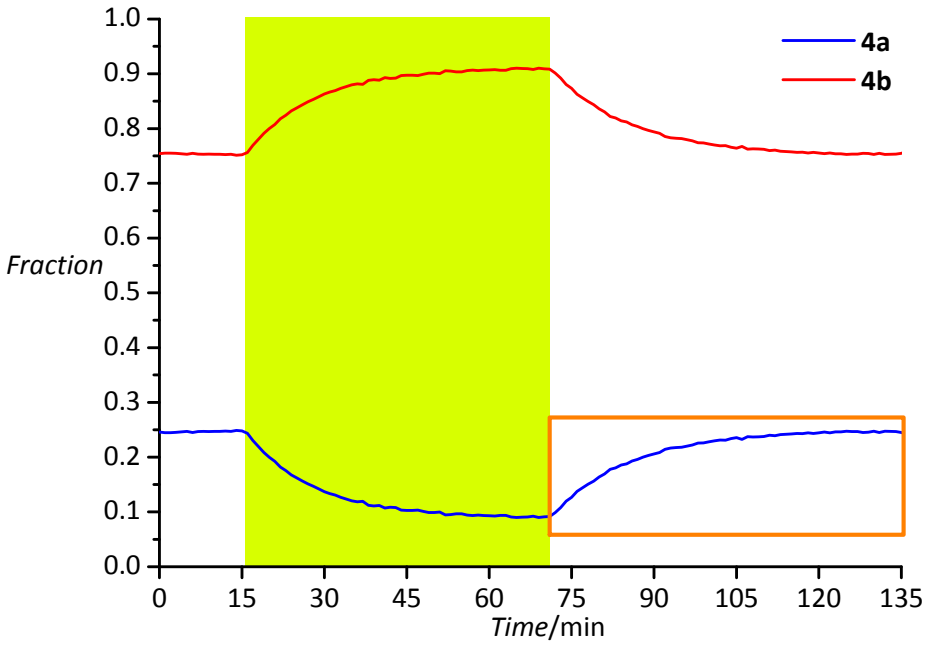

Figure S38. Fraction **4a** and **4b** during the *in situ* photo-switching experiment, measured by ^{1}H NMR (500 MHz, CD_3CN, 298 K) spectroscopy. The lime-coloured block indicates the period of irradiation, the orange box highlights the phase of thermal relaxation used to calculate the apparent half-life time and rate constants.

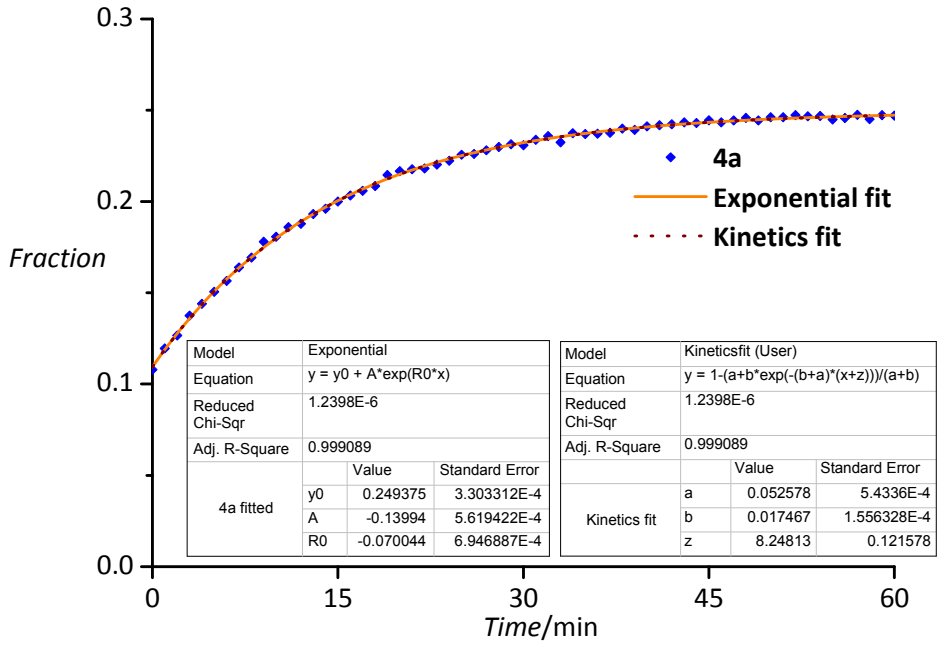

Model	Exponential		
Equation	y = y0 + A*exp(R0*x)		
Reduced Chi-Sqr	1.2398E-6		
Adj. R-Square	0.999089		
		Value	Standard Error
4a fitted	y0	0.249375	3.303312E-4
	A	-0.13994	5.619422E-4
	R0	-0.070044	6.946887E-4

Model	Kineticsfit (User)		
Equation	y = 1-(a+b*exp(-(b+a)*(x+z)))/(a+b)		
Reduced Chi-Sqr	1.2398E-6		
Adj. R-Square	0.999089		
		Value	Standard Error
Kinetics fit	a	0.052578	5.4336E-4
	b	0.017467	1.556328E-4
	z	8.24813	0.121578

Figure S39. Thermal isomerization of **4b** to **4a**, measured by ^{1}H NMR (500 MHz, CD_3CN, 298 K) spectroscopy after reaching the PSS. Exponential curves were fitted to determine the apparent half-life time and rate constants.

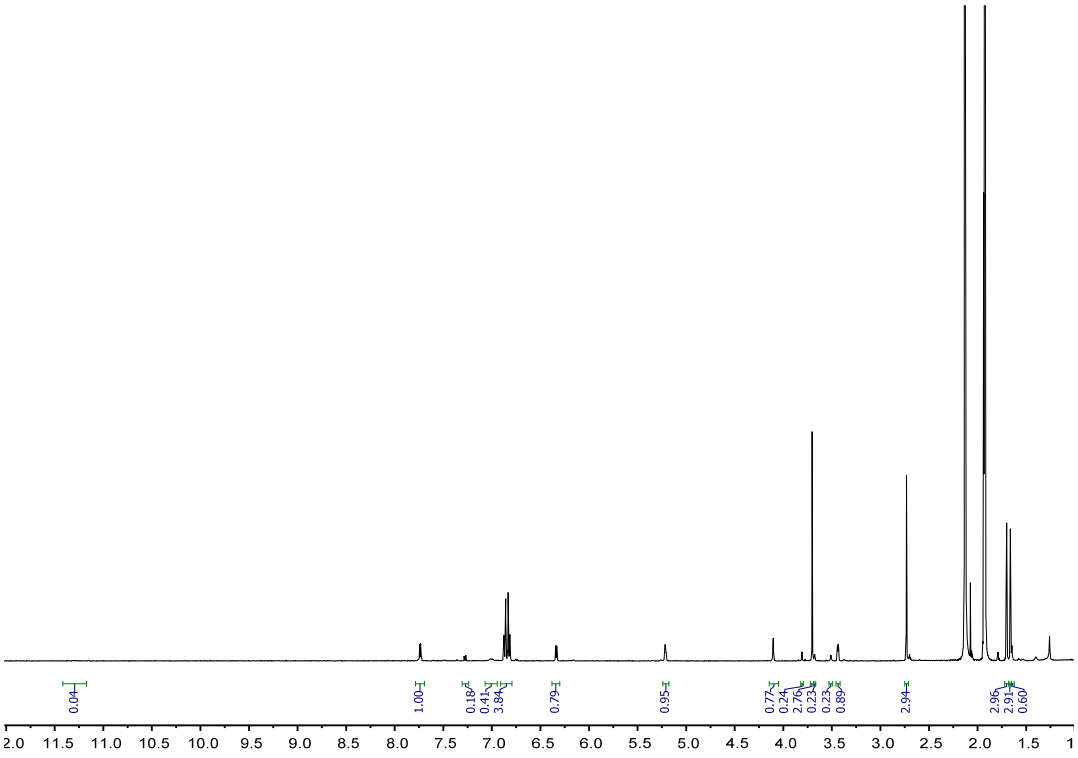

Figure S40. ^{1}H NMR (500 MHz, CD_3CN, 298 K) spectrum of **4a**/**4b** after continuous irradiation for 55 min.

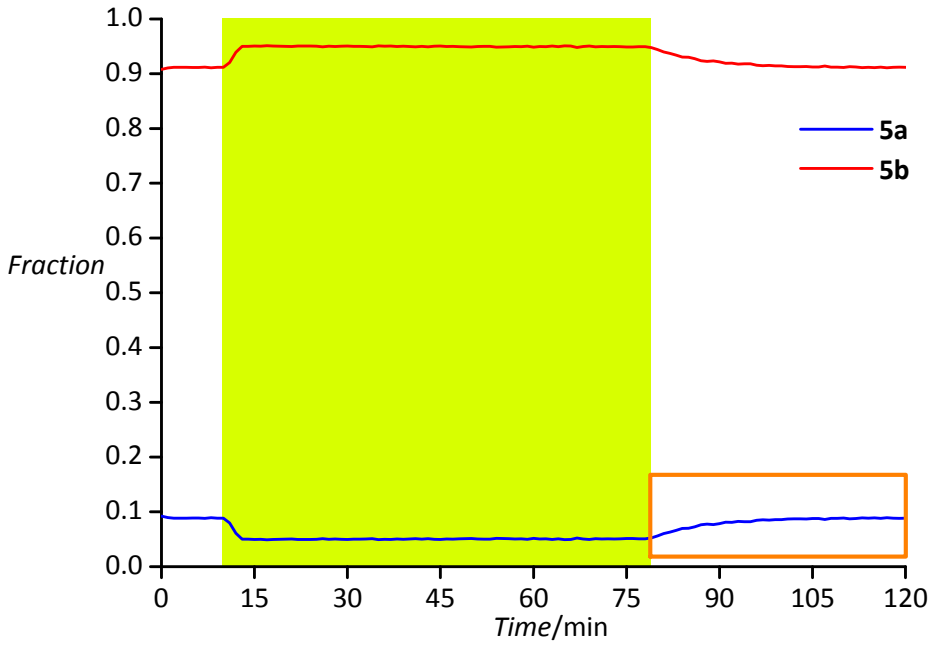

Figure S41. Fraction **5a** and **5b** during the *in situ* photo-switching experiment, measured by ^{1}H NMR (500 MHz, CD_3CN, 298 K) spectroscopy. The lime-coloured block indicates the period of irradiation, the orange box highlights the phase of thermal relaxation used to calculate the apparent half-life time and rate constants.

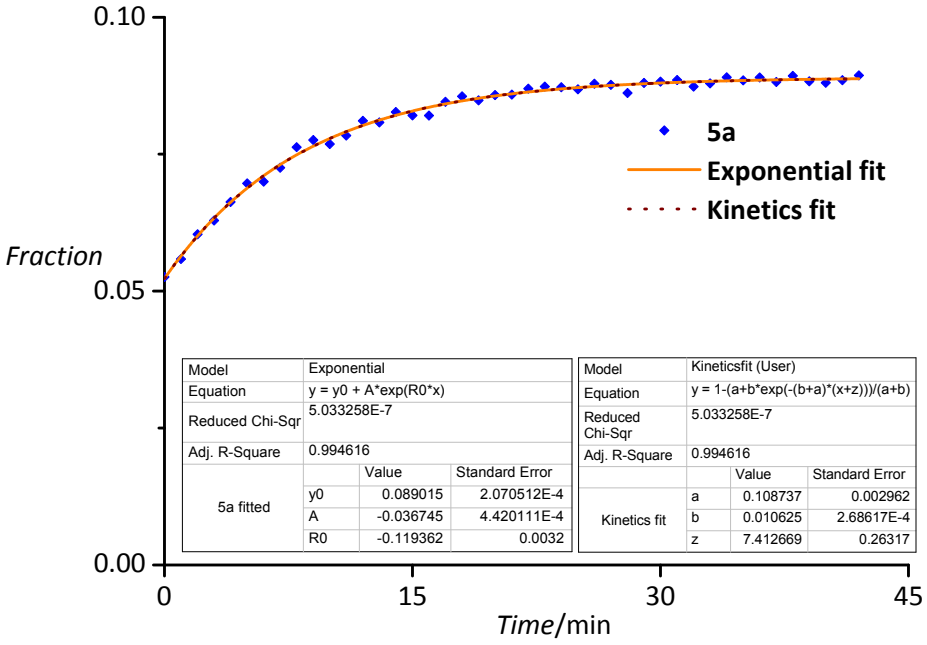

Model	Exponential		
Equation	y = y0 + A*exp(R0*x)		
Reduced Chi-Sqr	5.033258E-7		
Adj. R-Square	0.994616		
		Value	Standard Error
5a fitted	y0	0.089015	2.070512E-4
	A	-0.036745	4.420111E-4
	R0	-0.119362	0.0032

Model	Kineticsfit (User)		
Equation	y = 1-(a+b*exp(-(b+a)*(x+z)))/(a+b)		
Reduced Chi-Sqr	5.033258E-7		
Adj. R-Square	0.994616		
		Value	Standard Error
Kinetics fit	a	0.108737	0.002962
	b	0.010625	2.68617E-4
	z	7.412669	0.26317

Figure S42. Thermal isomerization of **5b** to **5a**, measured by ^{1}H NMR (500 MHz, CD_3CN, 298 K) spectroscopy after reaching the PSS. Exponential curves were fitted to determine the apparent half-life time and rate constants.

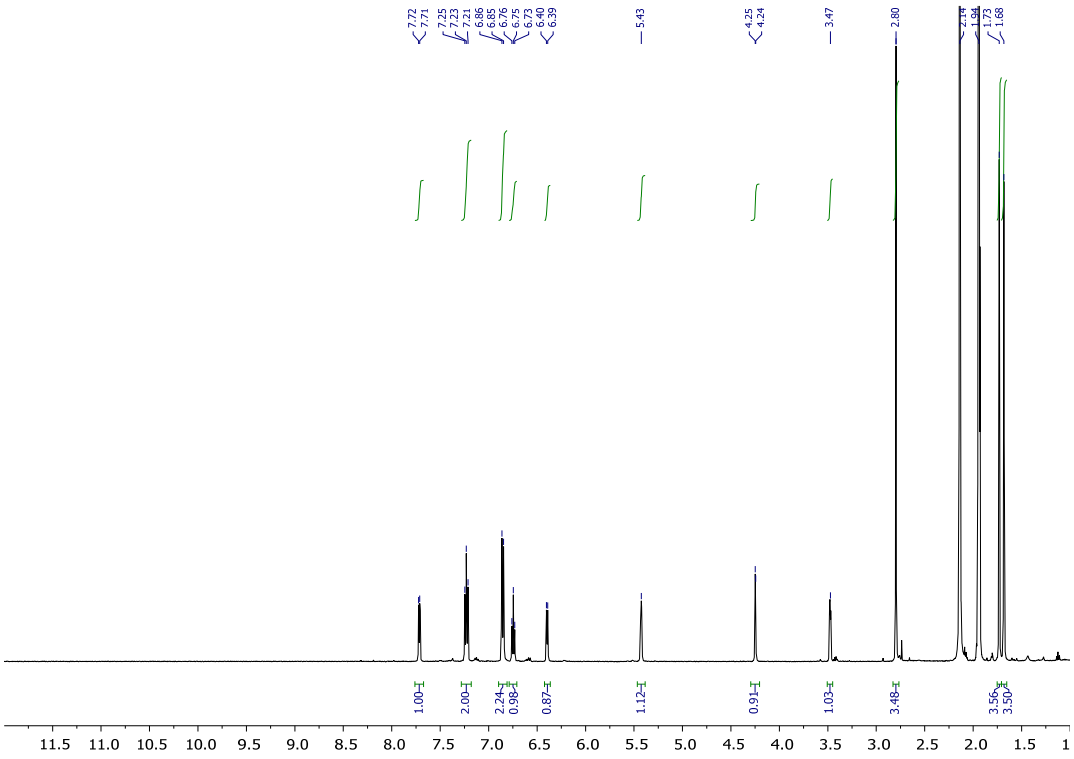

Figure S43. ^{1}H NMR (500 MHz, CD_3CN, 298 K) spectrum of **5a**/**5b** after continuous irradiation for 60 min.

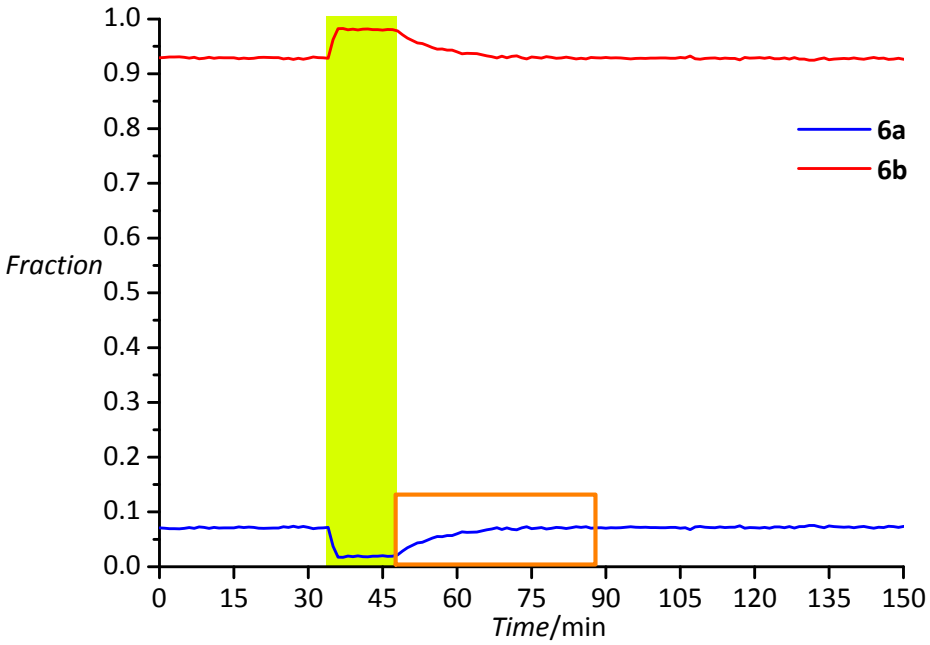

Figure S44. Fraction **6a** and **6b** during the *in situ* photo-switching experiment, measured by ^{1}H NMR (500 MHz, CD_3CN, 298 K) spectroscopy. The lime-coloured block indicates the period of irradiation, the orange box highlights the phase of thermal relaxation used to calculate the apparent half-life time and rate constants.

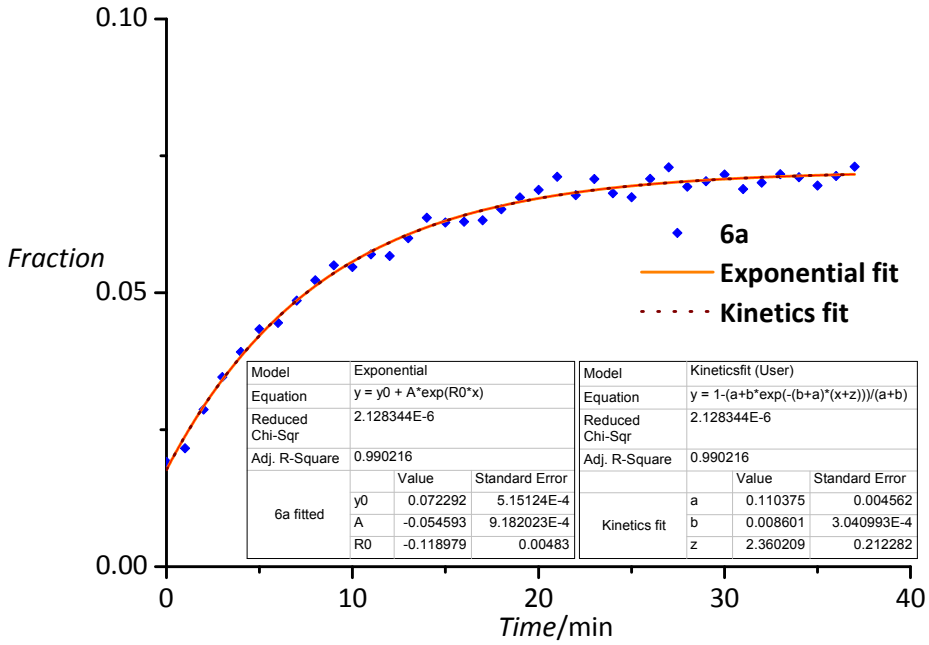

Model	Exponential		
Equation	y = y0 + A*exp(R0*x)		
Reduced Chi-Sqr	2.128344E-6		
Adj. R-Square	0.990216		
		Value	Standard Error
6a fitted	y0	0.072292	5.15124E-4
	A	-0.054593	9.182023E-4
	R0	-0.118979	0.00483

Model	Kineticsfit (User)		
Equation	y = 1-(a+b*exp(-(b+a)*(x+z)))/(a+b)		
Reduced Chi-Sqr	2.128344E-6		
Adj. R-Square	0.990216		
		Value	Standard Error
Kinetics fit	a	0.110375	0.004562
	b	0.008601	3.040993E-4
	z	2.360209	0.212282

Figure S45. Thermal isomerization of **6b** to **6a**, measured by ^{1}H NMR (500 MHz, CD_3CN, 298 K) spectroscopy after reaching the PSS. Exponential curves were fitted to determine the apparent half-life time and rate constants.

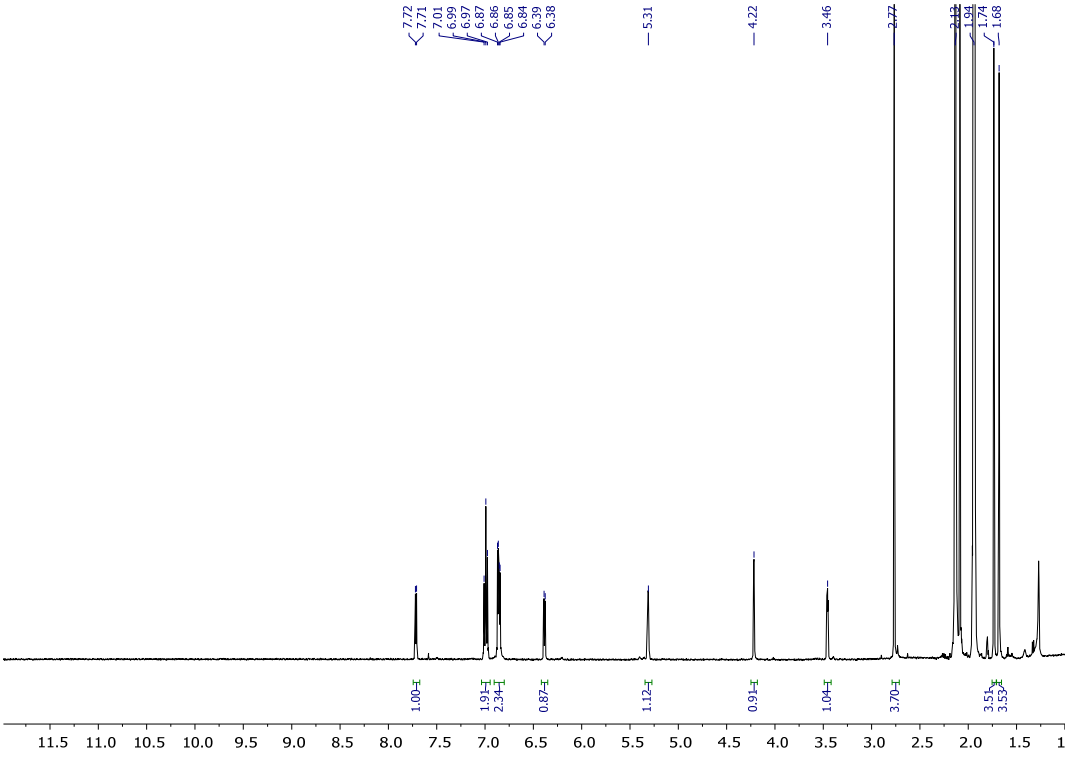

Figure S46. ^{1}H NMR (500 MHz, CD_3CN, 298 K) spectrum of **6a**/**6b** after continuous irradiation for 10 min.

18.3 Apparent half-life times and photostationary states in $CDCl_3$

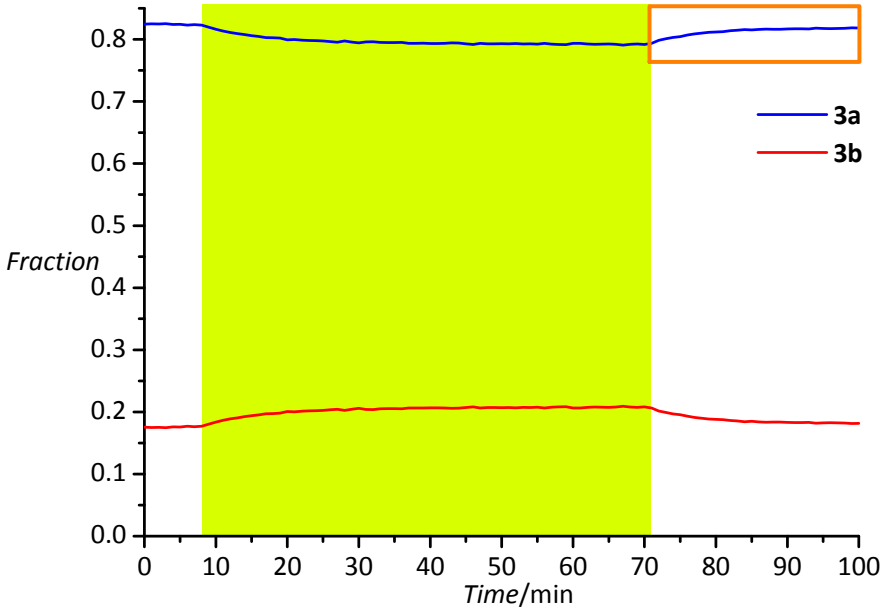

Figure S47. Fraction **3a** and **3b** during the *in situ* photo-switching experiment, measured by ^{1}H NMR (500 MHz, $CDCl_3$, 298 K) spectroscopy. The lime-coloured block indicates the period of irradiation, the orange box highlights the phase of thermal relaxation used to calculate the apparent half-life time and rate constants.

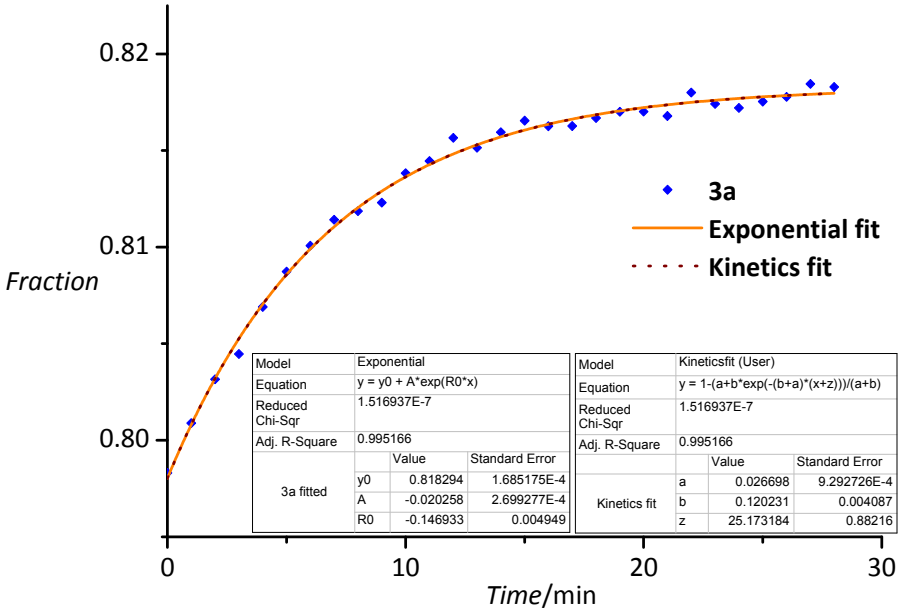

Figure S48. Thermal isomerization of **3b** to **3a**, measured by ^{1}H NMR (500 MHz, $CDCl_3$, 298 K) spectroscopy after reaching the PSS. Exponential curves were fitted to determine the apparent half-life time and rate constants.

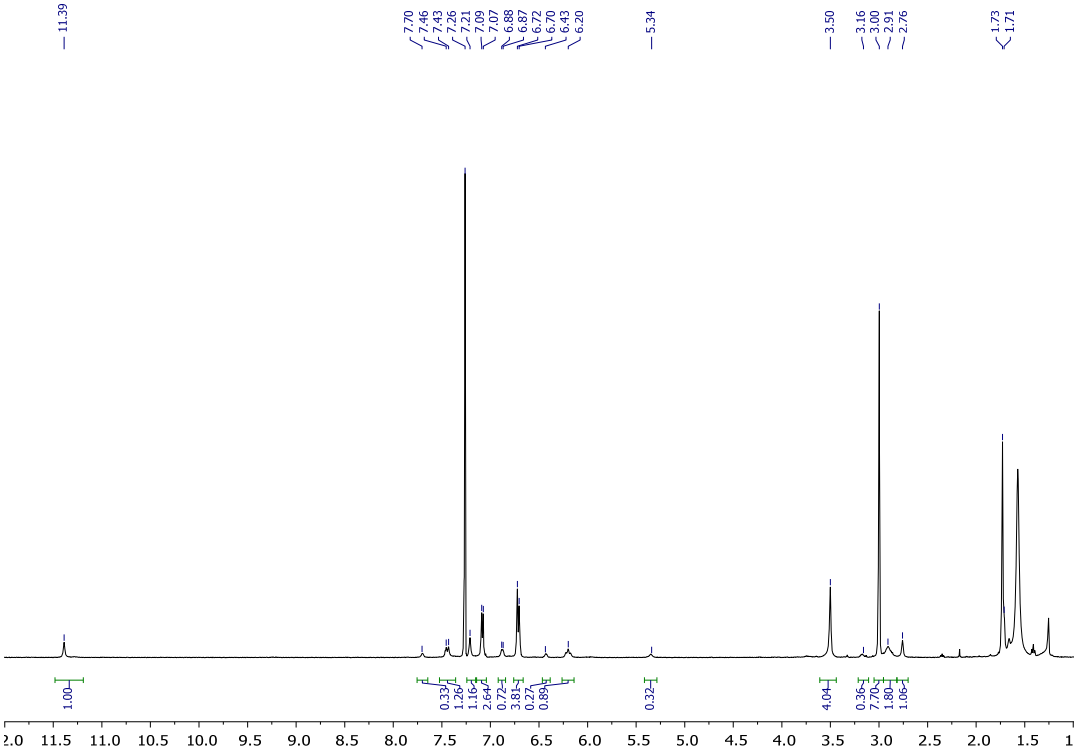

Figure S49. ^{1}H NMR (500 MHz, $CDCl_3$, 298 K) spectrum of compound **3a**/**3b**. The sample was irradiated with 567 nm light until a PSS was obtained (60 min).

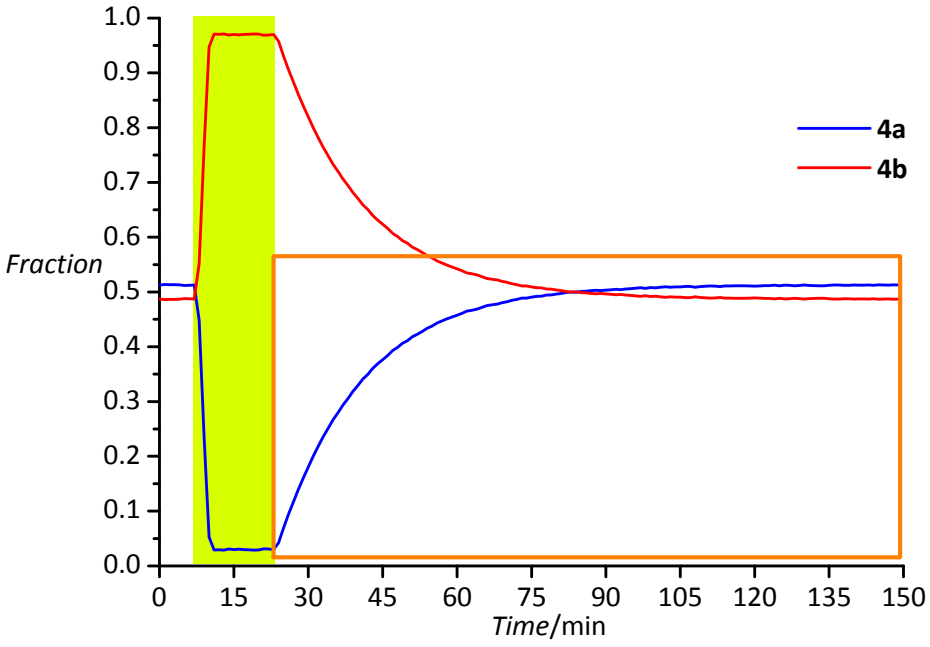

Figure S50. Fraction **4a** and **4b** during the *in situ* photo-switching experiment, measured by ^{1}H NMR (500 MHz, $CDCl_3$, 298 K) spectroscopy. The lime-coloured block indicates the period of irradiation, the orange box highlights the phase of thermal relaxation used to calculate the apparent half-life time and rate constants.

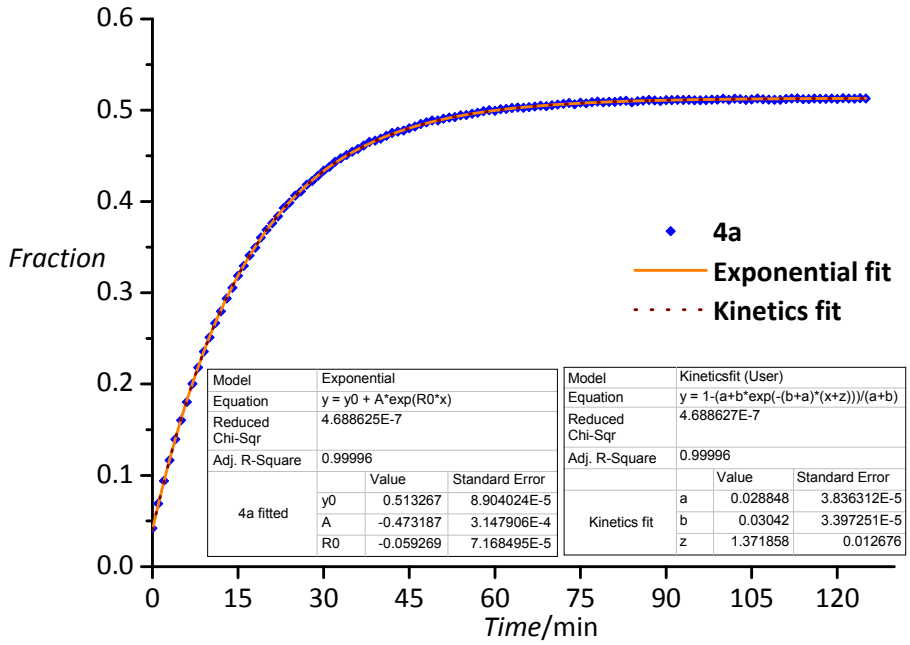

Figure S51. Thermal isomerization of **4b** to **4a**, measured by ^{1}H NMR (500 MHz, $CDCl_3$, 298 K) spectroscopy after reaching the PSS. Exponential curves were fitted to determine the apparent half-life time and rate constants.

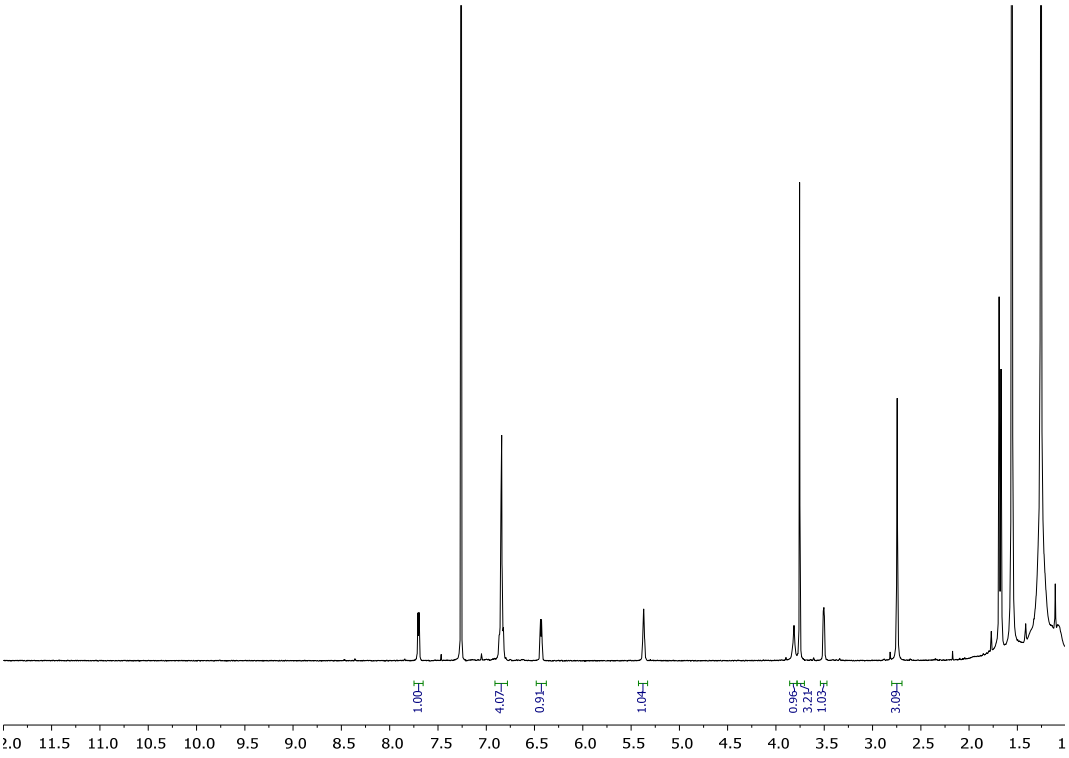

Figure S52. ^{1}H NMR (500 MHz, $CDCl_3$, 298 K) spectrum of compound **4a**/**4b**. The sample was irradiated with 567 nm light until a PSS was obtained (12 min).

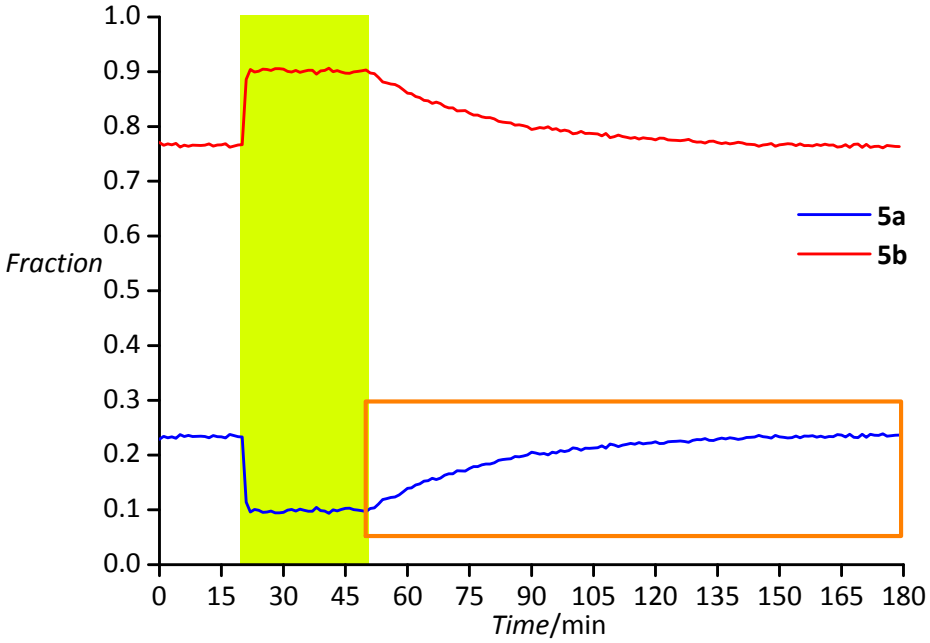

Figure S53. Fraction **5a** and **5b** during the *in -situ* photo-switching experiment, measured by ^{1}H NMR (500 MHz, $CDCl_3$, 298 K) spectroscopy. The lime-coloured block indicates the period of irradiation, the orange box highlights the phase of thermal relaxation used to calculate the apparent half-life time and rate constants.

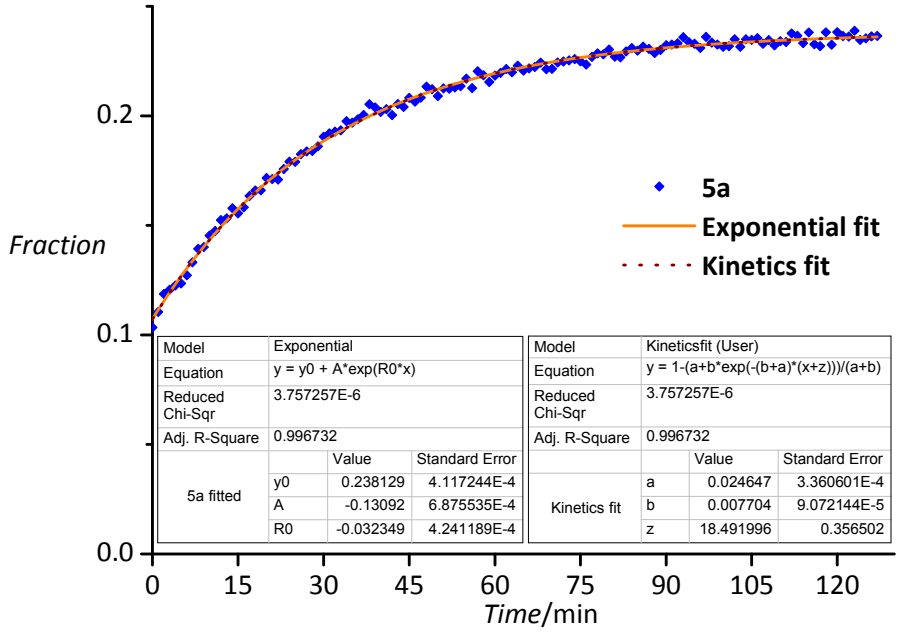

Model	Exponential		
Equation	y = y0 + A*exp(R0*x)		
Reduced Chi-Sqr	3.757257E-6		
Adj. R-Square	0.996732		
		Value	Standard Error
5a fitted	y0	0.238129	4.117244E-4
	A	-0.13092	6.875535E-4
	R0	-0.032349	4.241189E-4

Model	Kineticsfit (User)		
Equation	y = 1-(a+b*exp(-(b+a)*(x+z)))/(a+b)		
Reduced Chi-Sqr	3.757257E-6		
Adj. R-Square	0.996732		
		Value	Standard Error
Kinetics fit	a	0.024647	3.360601E-4
	b	0.007704	9.072144E-5
	z	18.491996	0.356502

Figure S54. Thermal isomerization of **5b** to **5a**, measured by ^{1}H NMR (500 MHz, $CDCl_3$, 298 K) spectroscopy after reaching the PSS. Exponential curves were fitted to determine the apparent half-life time and rate constants.

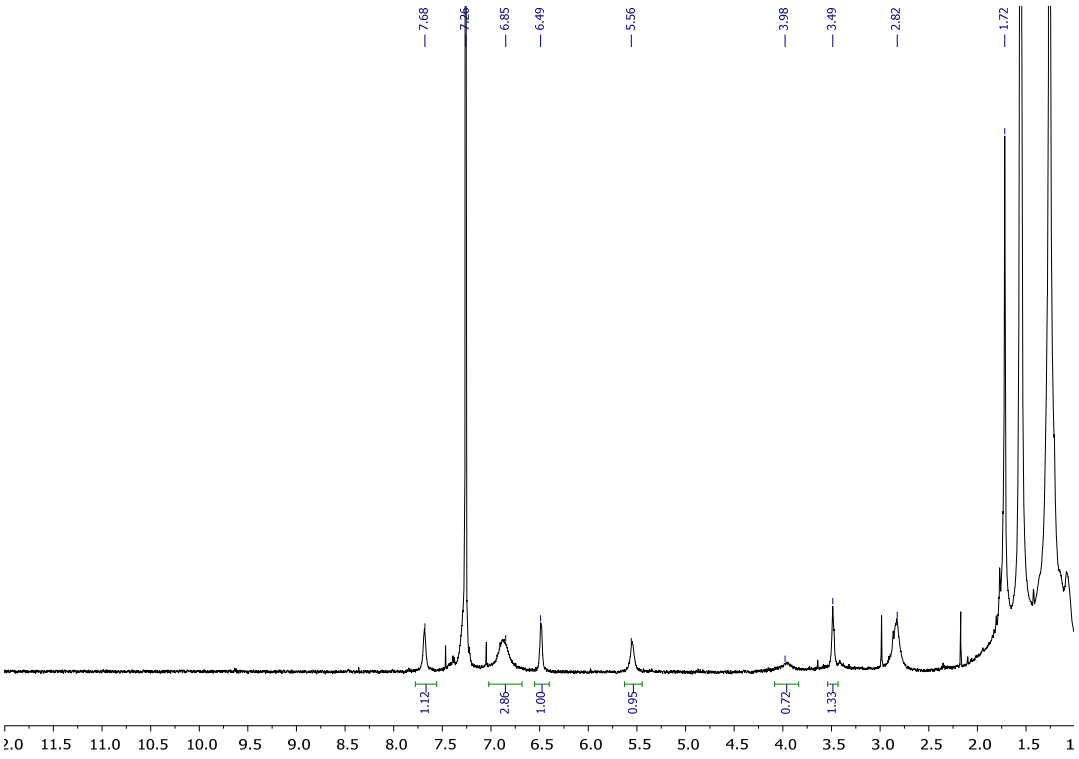

Figure S55. ^{1}H NMR (500 MHz, $CDCl_3$, 298 K) spectrum of compound **5a**/**5b**. The sample was irradiated with 567 nm light until a PSS was obtained (25 min).

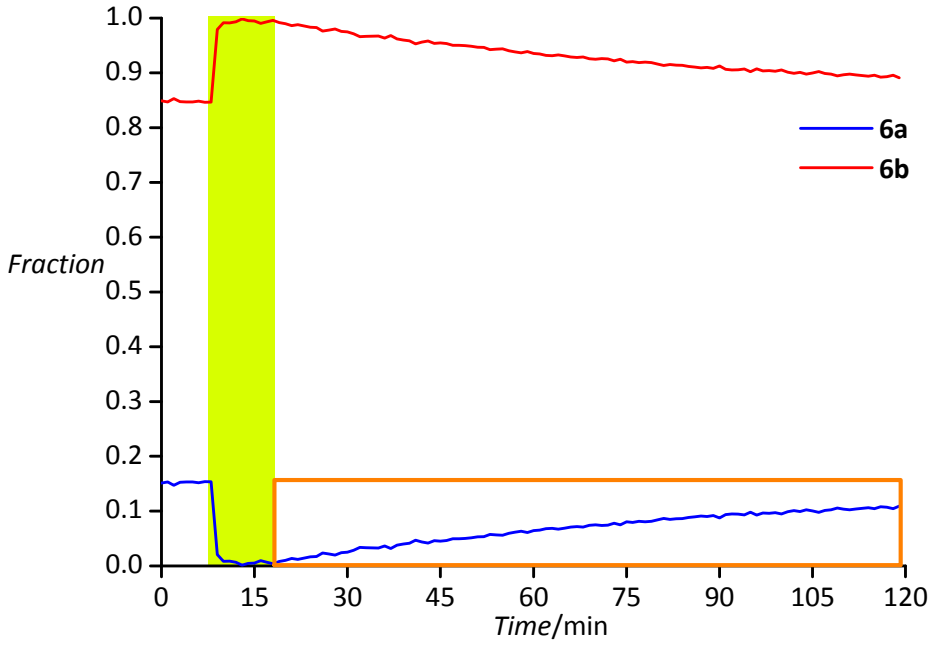

Figure S56. Fraction **6a** and **6b** during the *in situ* photo-switching experiment, measured by ^{1}H NMR (500 MHz, $CDCl_3$, 298 K) spectroscopy. The lime-coloured block indicates the period of irradiation, the orange box highlights the phase of thermal relaxation used to calculate the apparent half-life time and rate constants.

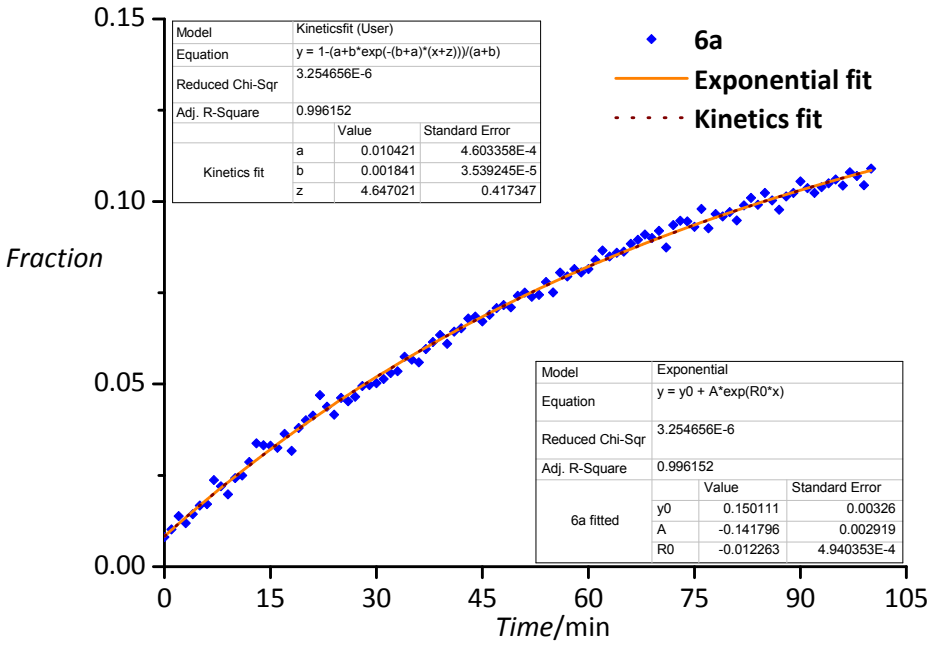

Figure S57. Thermal isomerization of **6b** to **6a**, measured by ^{1}H NMR (500 MHz, $CDCl_3$, 298 K) spectroscopy after reaching the PSS. Exponential curves were fitted to determine the apparent half-life time and rate constants.

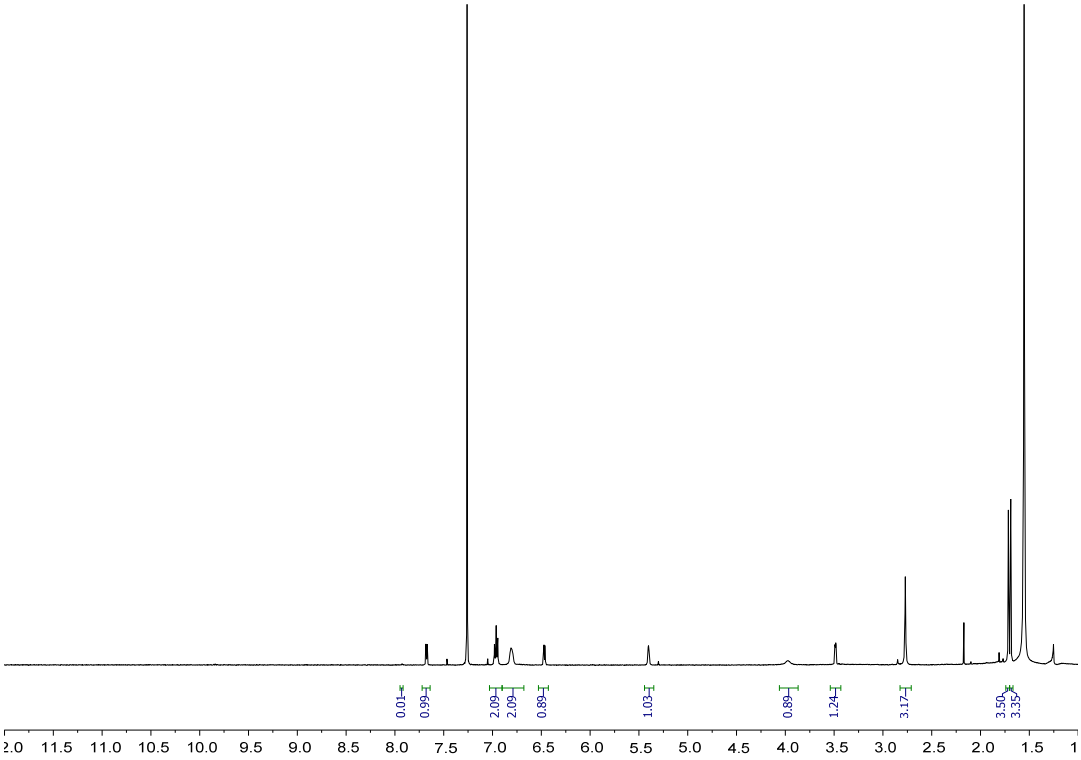

Figure S58. ^{1}H NMR (500 MHz, $CDCl_3$, 298 K) spectrum of compound **6a**/**6b**. The sample was irradiated with 567 nm light until a PSS was obtained (5 min).

18.4 Apparent half-life times and photostationary states in C_6D_6

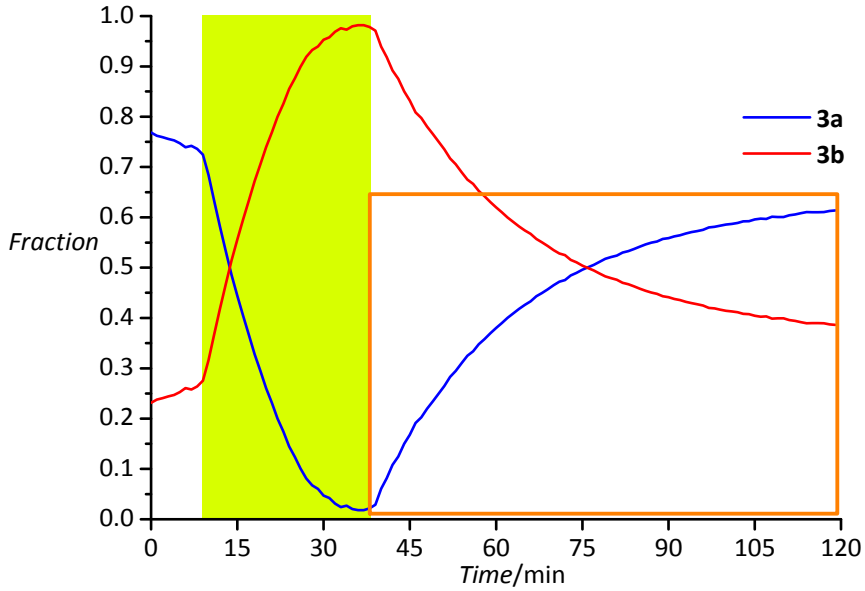

Figure S59. Fraction **3a** and **3b** during the *in situ* photo-switching experiment, measured by ^{1}H NMR (500 MHz, C_6D_6, 298 K) spectroscopy. The lime-coloured block indicates the period of irradiation, the orange box highlights the phase of thermal relaxation used to calculate the apparent half-life time and rate constants. NB: The ratio linear:cyclic was not constant before irradiation, indicating that the sample had not yet reached thermal equilibrium.

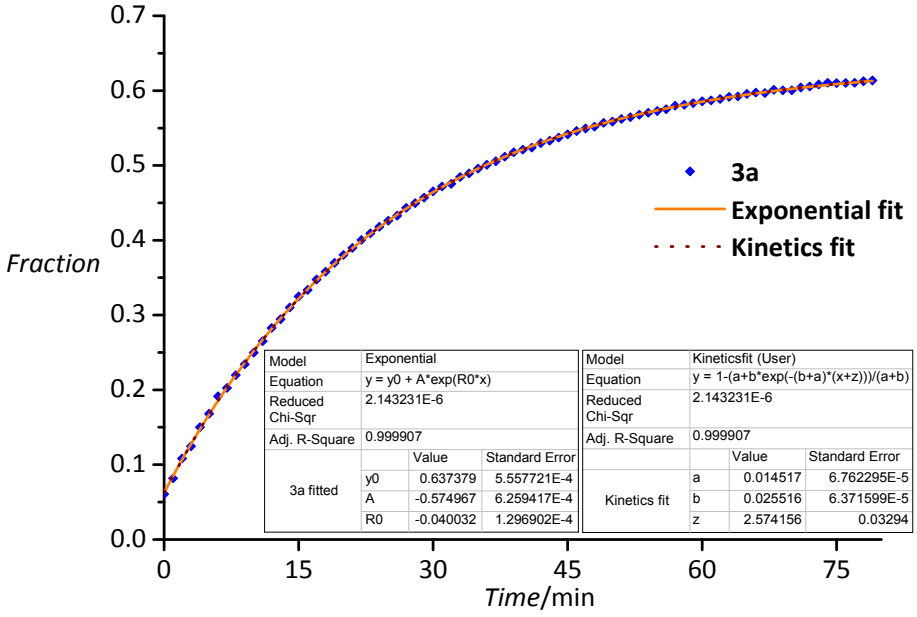

Figure S60. Thermal isomerization of **3b** to **3a**, measured by ^{1}H NMR (500 MHz, C_6D_6, 298 K) spectroscopy after reaching the PSS. Exponential curves were fitted to determine the apparent half-life time and rate constants.

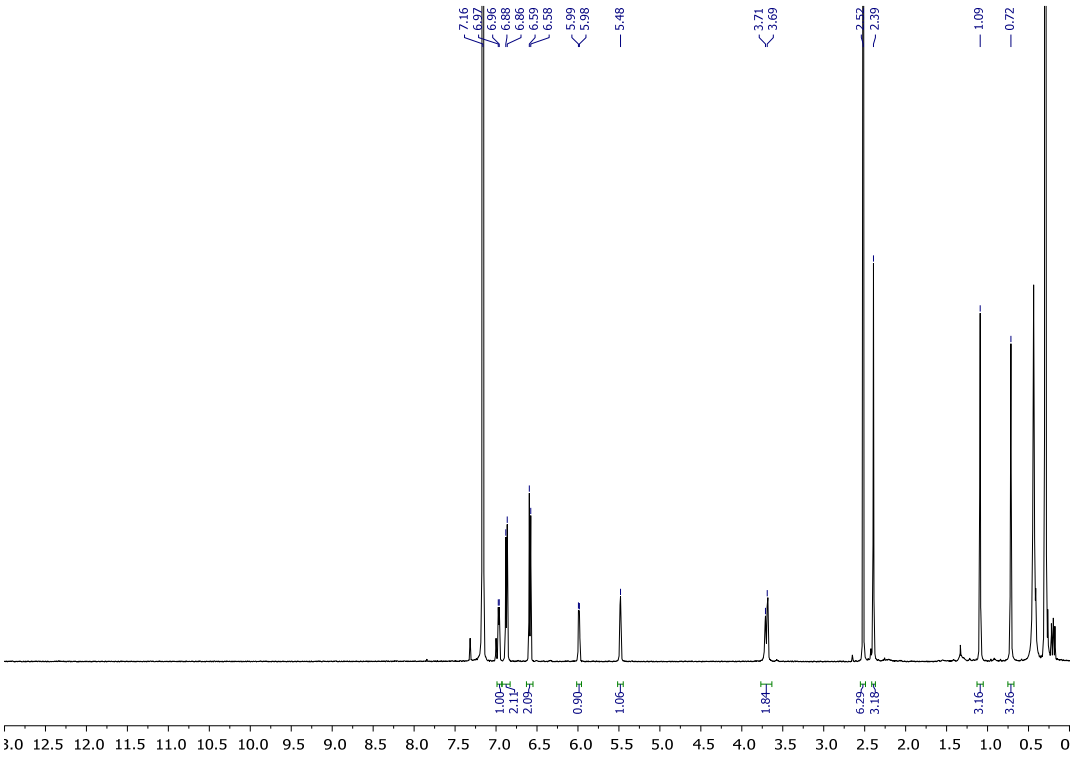

Figure S61. ^{1}H NMR (500 MHz, C_6D_6, 298 K) spectrum of **3a**/**3b** after continuous irradiation for 29 min.

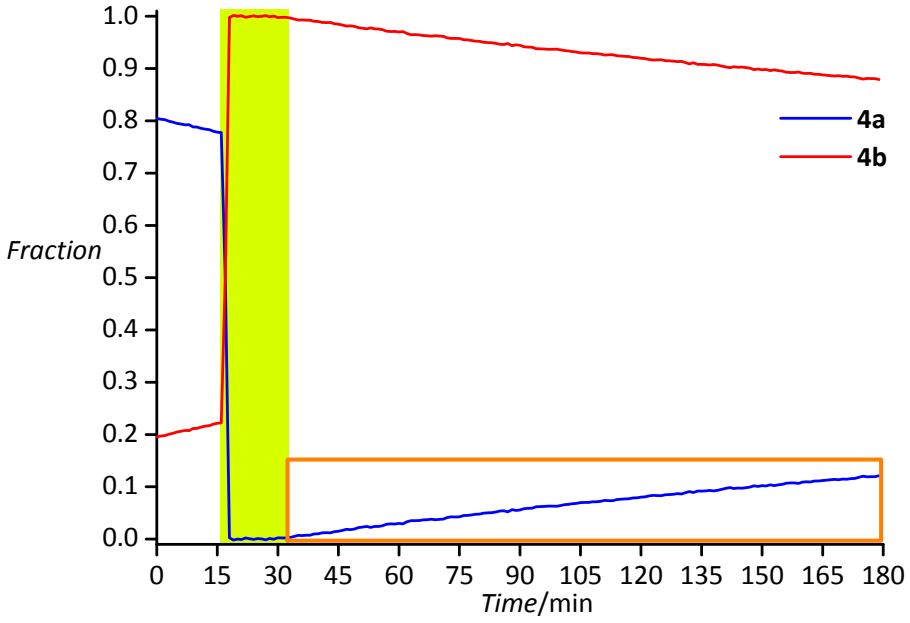

Figure S62. Fraction **4a** and **4b** during the *in situ* photo-switching experiment, measured by ^{1}H NMR (500 MHz, C_6D_6, 298 K) spectroscopy. The lime-coloured block indicates the period of irradiation, the orange box highlights the phase of thermal relaxation used to calculate the apparent half-life time and rate constants. Nb: The ratio linear:cyclic was not constant before irradiation, indicating that the sample had not yet reached thermal equilibrium.

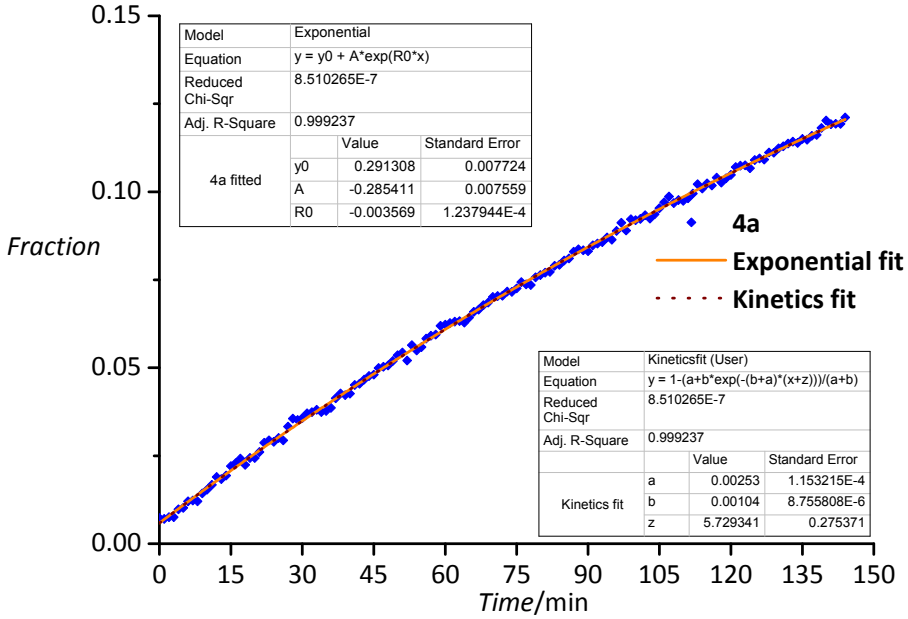

Figure S63. Thermal isomerization of **4b** to **4a**, measured by ^{1}H NMR (500 MHz, C_6D_6, 298 K) spectroscopy after reaching the PSS. Exponential curves were fitted to determine the apparent half-life time and rate constants.

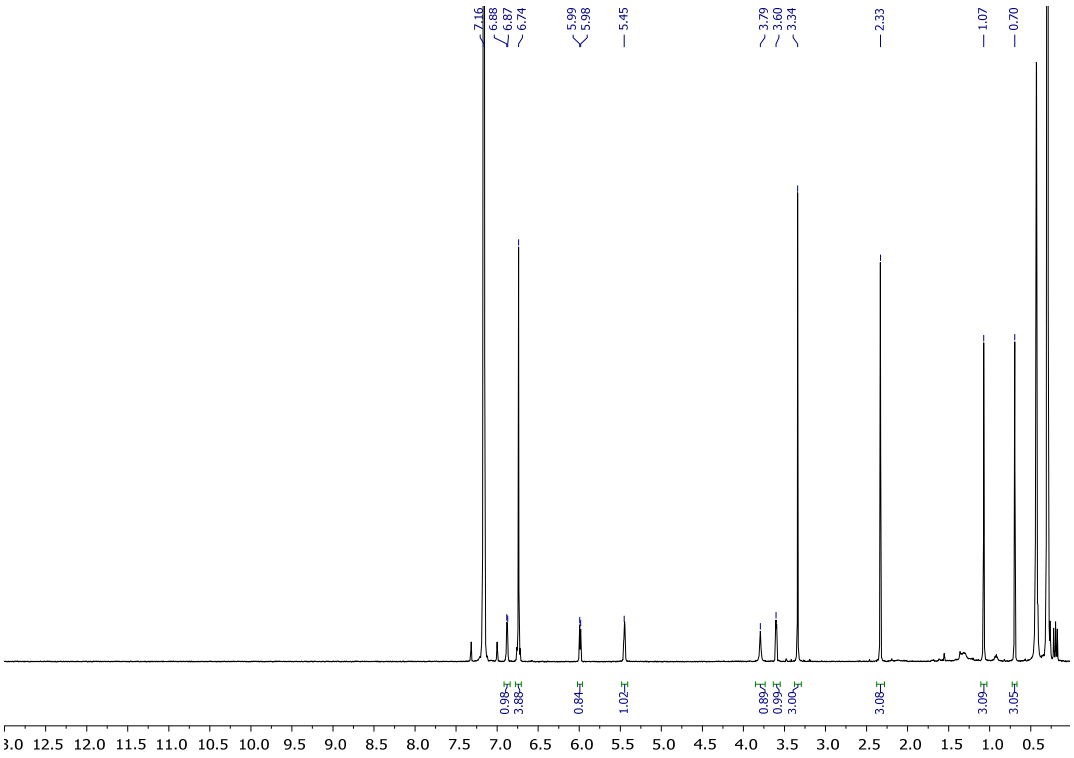

Figure S64. ^{1}H NMR (500 MHz, C_6D_6, 298 K) spectrum of **4a**/**4b** after continuous irradiation for 10 min.

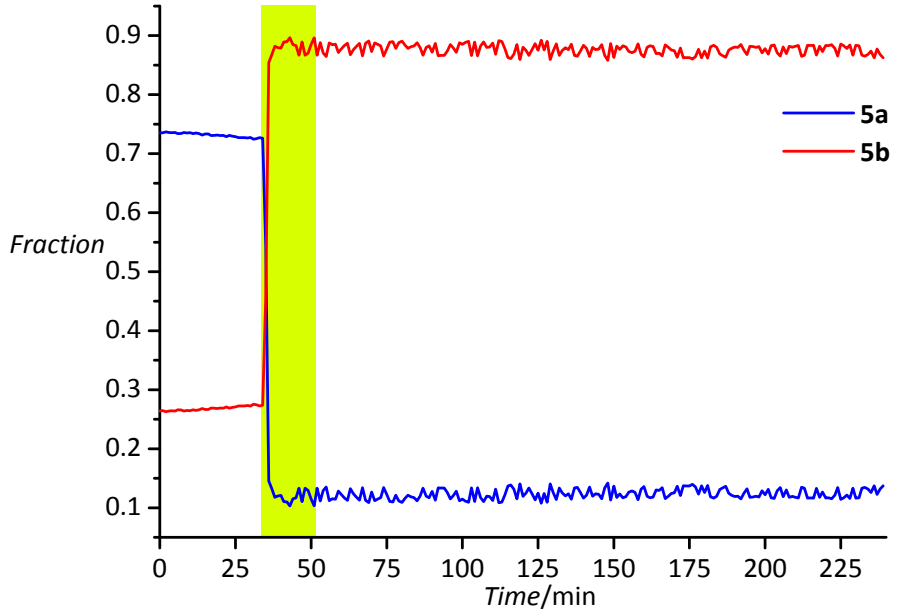

Figure S65. Fraction **5a** and **5b** during the *in situ* photo-switching experiment, measured by ^{1}H NMR (500 MHz, C_6D_6, 298 K) spectroscopy. The lime-coloured block indicates the period of irradiation. After irradiation ceased, no change in the ratio linear:cyclic was observed during the course of the experiment. NB: The ratio linear:cyclic was not constant before irradiation, indicating that the sample had not yet reached thermal equilibrium.

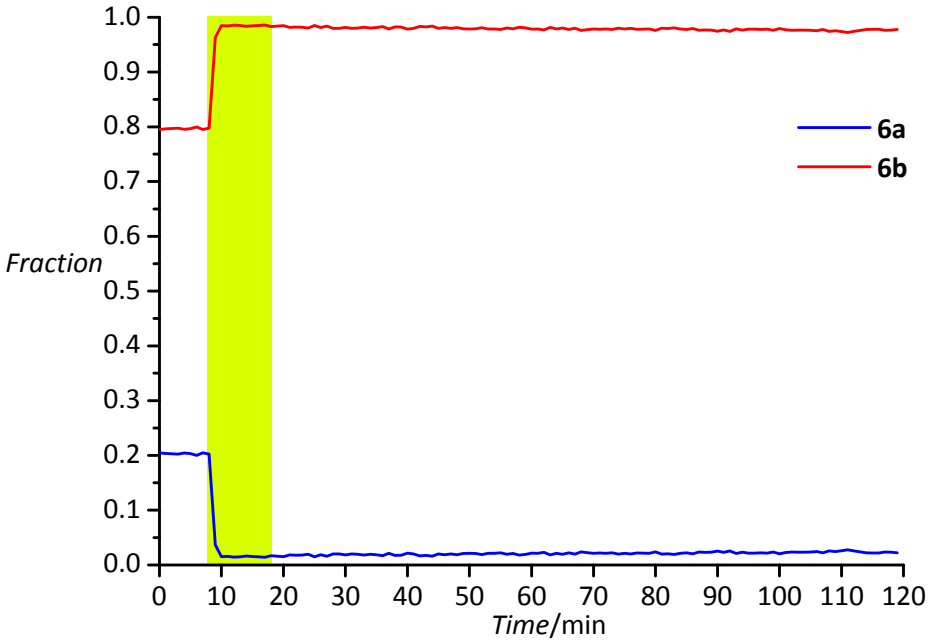

Figure S66. Fraction **6a** and **6b** during the *in situ* photo-switching experiment, measured by ^{1}H NMR (500 MHz, C_6D_6, 298 K) spectroscopy. The lime-coloured block indicates the period of irradiation. After the irradiation ceased, no change in the ratio linear:cyclic was observed over the course of the experiment.

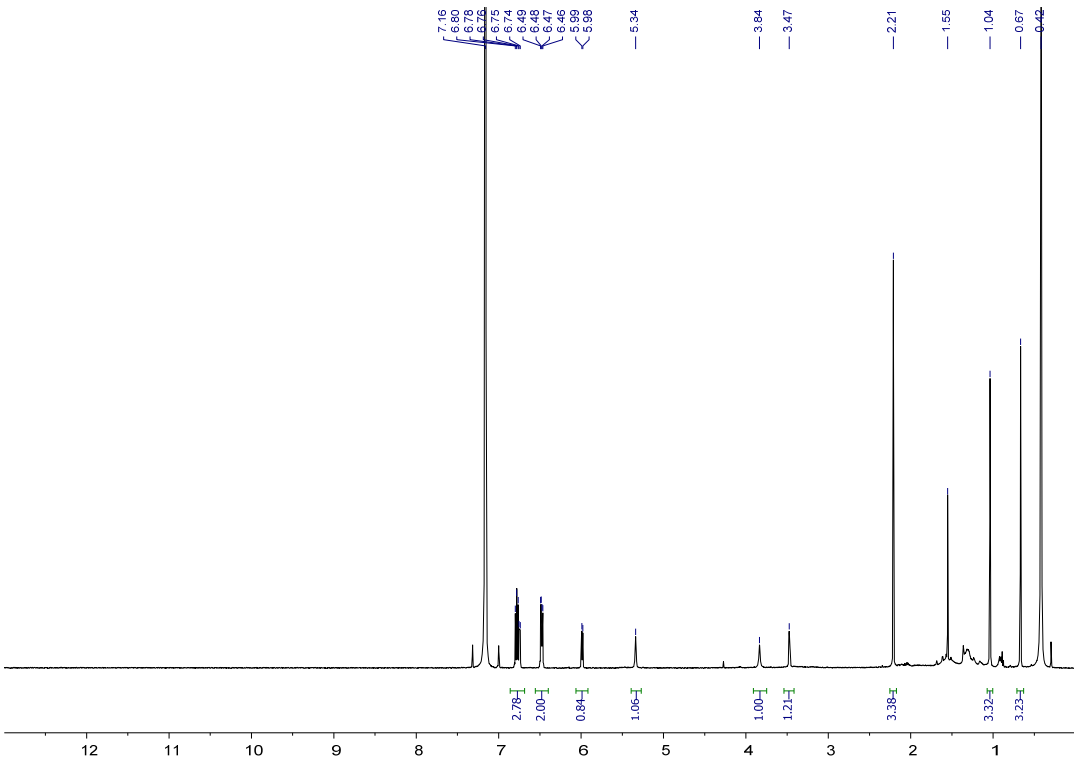

Figure S67. ^{1}H NMR (500 MHz, C_6D_6, 298 K) spectrum of **6a**/**6b** after continuous irradiation for 5 min.

Table S6. Apparent half-life times of compounds **3-6** measured by NMR spectroscopy at 298 K.

Compound	$t_{½}$ [min] CD_3CN	$t_{½}$ [min] $CDCl_3$	$t_{½}$ [min] C_6D_6
3	n.d.[a]	4.7±0.2[b]	17.3±0.1
4	9.9±0.1	11.7±0.1	194.2±6.7
5	5.8±0.2	21.4±0.3	n.d.[c]
6	5.8±0.3	56.5±2.3	n.d.[c]

n.d., Not determined. [a] No significant changes in equilibrium could be observed by NMR spectroscopy. [b] All errors were calculated by the error on the exponential fit. [c] During thermal relaxation, no significant changes in ratio were observed during the course of the experiment.

Table S7. First order rate constants for thermal isomerization of compounds **3-6** measured by NMR spectroscopy at 298 K.

Compound	CD_3CN			$CDCl_3$			C_6D_6		
	k_1[a] [10^{-4} s^{-1}]	k_{-1}[b] [10^{-4} s^{-1}]	K	k_1[a] [10^{-4} s^{-1}]	k_{-1}[b] [10^{-4} s^{-1}]	K	k_1[a] [10^{-4} s^{-1}]	k_{-1}[b] [10^{-4} s^{-1}]	K
3	n.d.[c]	n.d.[c]	n.d.[c]	4.45	20.0	0.22	2.42	4.25	0.57
4	8.76	2.91	3.01	4.81	5.07	0.95	0.42	0.17	2.43
5	18.1	1.77	10.2	4.11	1.28	3.20	n.d.[d]	n.d.[d]	n.d.[d]
6	18.4	1.43	12.8	1.74	0.31	5.66	n.d.[d]	n.d.[d]	n.d.[d]

[a] 1st order rate constant for the conversion of linear to cyclic in the dark. [b] 1st order rate constant for the conversion of cyclic to linear in the dark. n.d., not determined. [c] No significant changes in the equilibrium could be observed by NMR spectroscopy. [d] During thermal relaxation, no significant changes in ratio were observed during the course of the experiment.

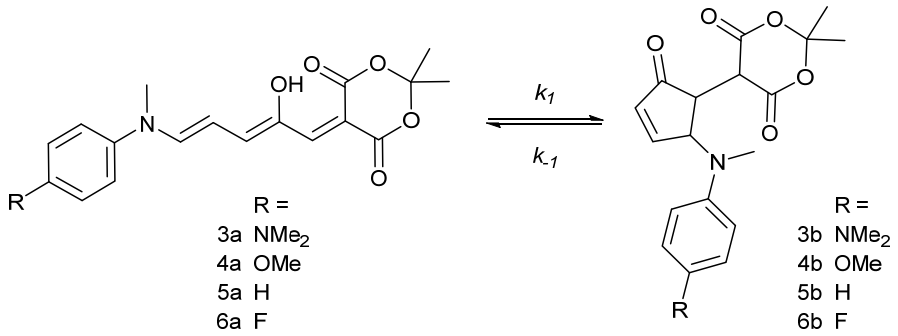

Scheme S3. Kinetic model of thermal isomerization

Table S8. Comparison of the ratio linear:cyclic (**a**:**b**) of compounds **3-6** in various solvents, determined by integration and from the rate constants obtained in the switching experiments

Compound	CD_3CN		$CDCl_3$		C_6D_6	
	Integrated[a]	Derived from K[b]	Integrated[a]	Derived from K[b]	Integrated[a]	Derived from K[b]
3	66:34	n.d.[c]	83:17	82:18	65:36	64:36
4	26:74	25:75	54:46	51:49	32:68	29:71
5	4:96	9:91	17:83	24:76	12:88	n.d. [d]
6	4:96	7:93	14:86	15:85	6:94	n.d. [d]

[a] See Section S10 for spectra. [b] Equilibria constants are listed in Table S7. n.d., Not determined. [b] No significant changes in equilibrium could be observed by NMR spectroscopy. [d] During thermal relaxation, no significant changes in ratio were observed during the course of the experiment.

19 Thermal equilibration of 5a/5b upon dissolving in CD_3CN

Since compounds **3-6** exist as a mixture of two isomers in solution, kinetic data can be measured on the change of ratio between the linear and cyclic isomers upon dissolving. Since the product is isolated as primarily linear isomer, linear to cyclic isomerization will take place after dissolving the compounds. This process was followed by ^{1}H NMR spectroscopy, where a sample of **5** was dissolved in CD_3CN.

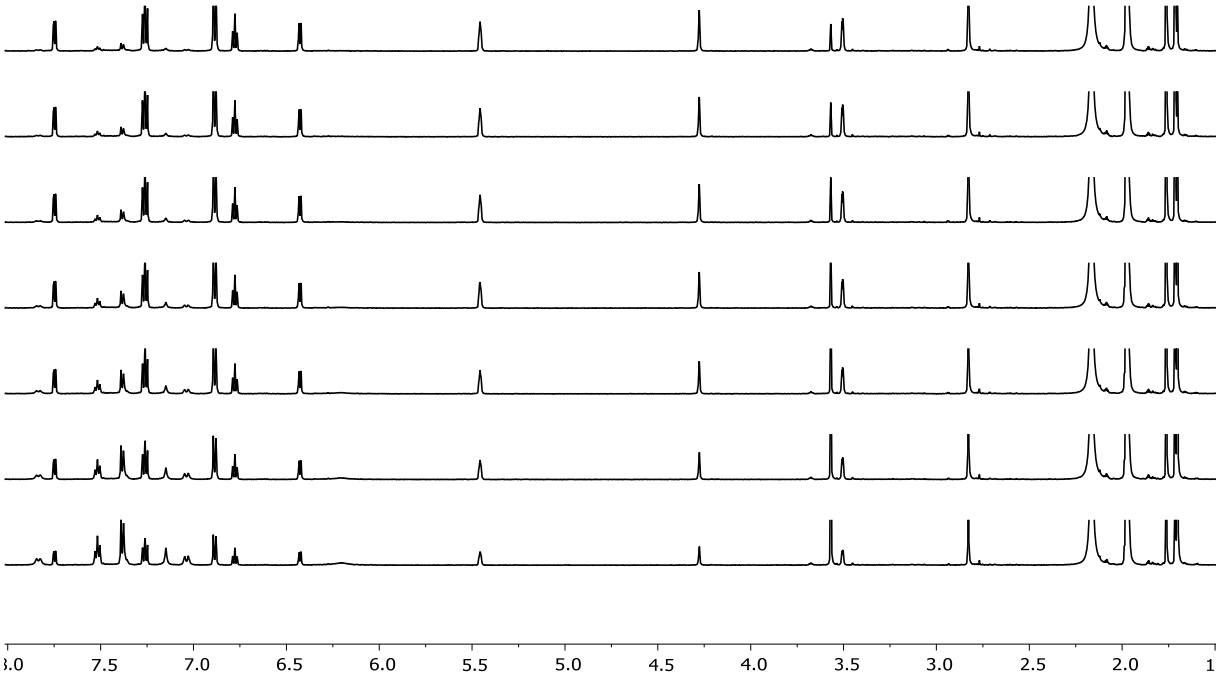

Figure S68. Stacked ^{1}H NMR (600 MHz, CD_3CN, 298 K) spectra of **5a**/**5b**, equilibrating to the dark equilibrium after dissolving (bottom to top, decimated in steps of 3).

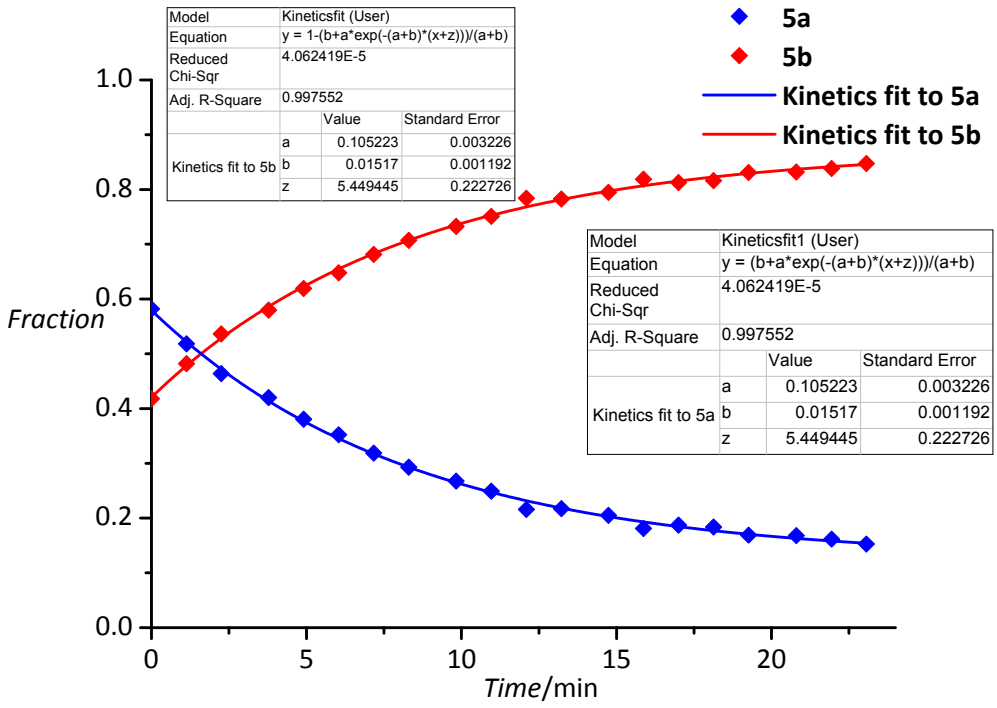

Figure S69. Fractions **5a**/**5b** upon dissolving, measured by 1H NMR (600 MHz, CD_3CN, 298 K) spectroscopy (Figure S68). Exponential curves were fitted to determine the apparent rate constants of isomerization.

Table S9. Rate constants for the isomerization of **5a**/**5b** in CD_3CN, measured by ^1H NMR spectroscopy after dissolving and after photoisomerization, measured at 298 K.

	k_1 [10^{-4} s^{-1}][a]	k_{-1} [10^{-4} s^{-1}][b]	K
Rates upon dissolving[c]	17.5	2.53	6.94
Rates after photoisomerization[d]	18.1	1.77	10.2

[a] 1st order rate constant for the conversion of linear to cyclic in the dark. [b] 1st order rate constant for the conversion of cyclic to linear in the dark. [c] Rate constants were measured after dissolving **5**, which is isolated as mainly **5a**, in CD_3CN, see Figure S69. [d] Rate constants were measured upon thermal relaxation after a photostationary state of 100% **5b** was obtained, see Figure S42

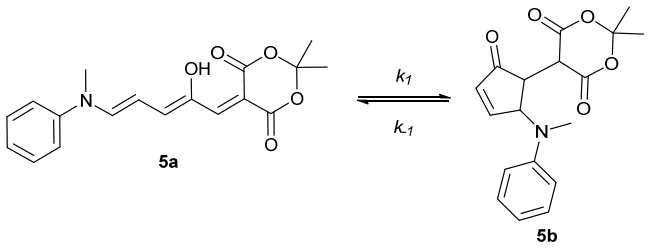

Scheme S4. Kinetic model of isomerization of **5a**/**5b** in CD_3CN.

20 Fatigue resistance of photoswitching monitored by NMR

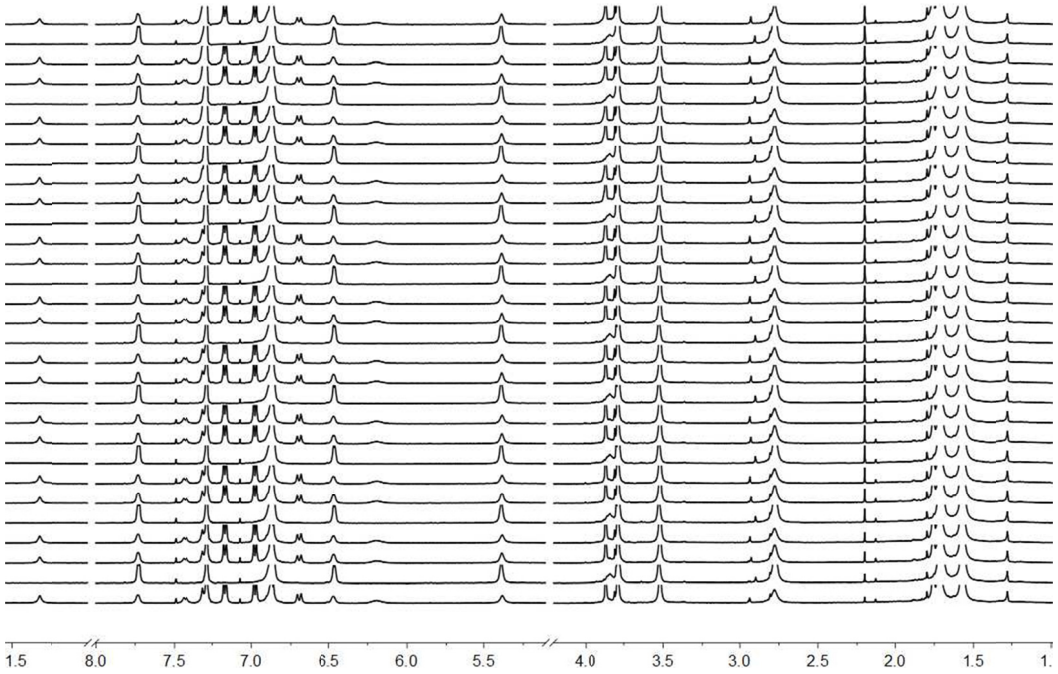

Figure S70. Stacked ^{1}H NMR (500 MHz, $CDCl_3$, 298 K) spectra of **4**, decimated in steps of 30 (bottom to top). The sample was irradiated with 567 nm light for 15 minutes, followed by 75 minutes of darkness to allow thermal reversion, repeated over 10 cycles. Figure 3 in the article shows the ratio linear:cyclic over time derived from this data.

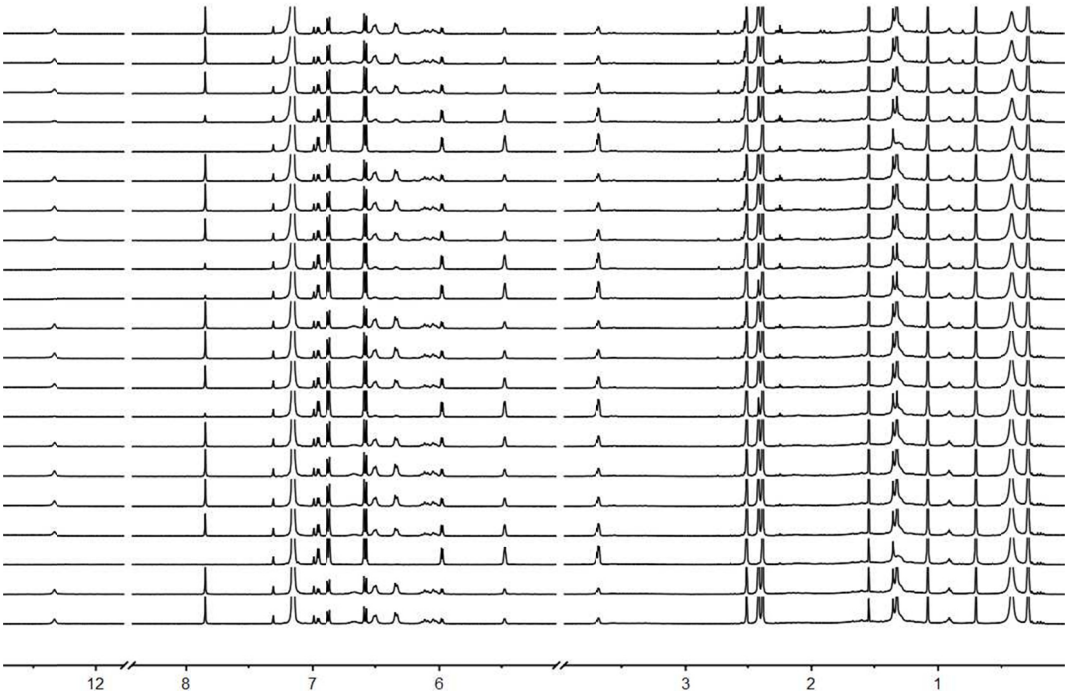

Figure S71. Stacked ^{1}H NMR (500 MHz, C_6D_6, 298 K) spectra of **3**, decimated in steps of 40 (bottom to top). The sample was irradiated with 567 nm light for 45 minutes, followed by 150 minutes of darkness to allow thermal reversion, repeated over 4 cycles. Figure S72 shows a graph of the linear and cyclic fractions over time derived from the NMR experiment.

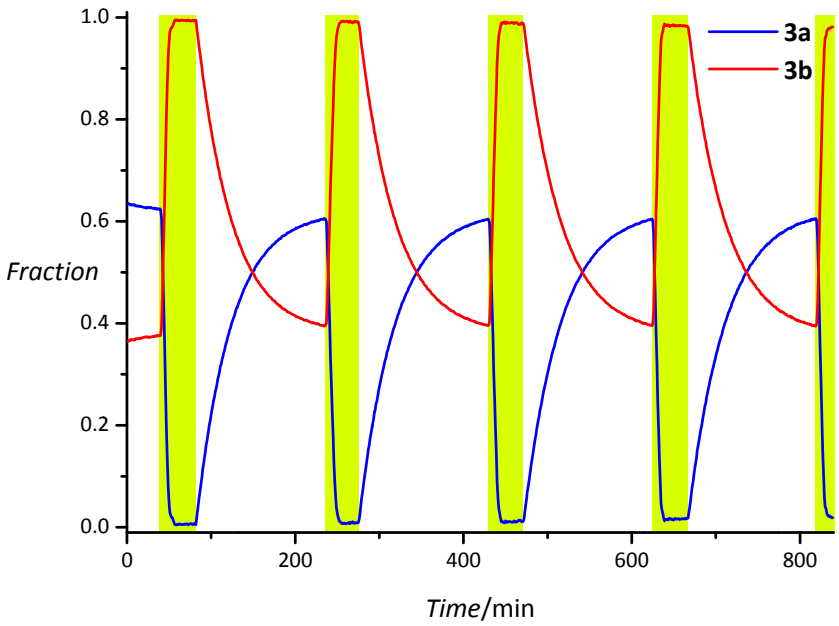

Figure S72. Reversible switching of compound **3a**/**3b** in benzene-d_6. The isomerization was monitored by ^{1}H NMR (500 MHz, 298 K, 1.7 mM) spectroscopy and the relative ratio was determined by the average integrals. The coloured blocks indicate periods of photo irradiation (567 nm).

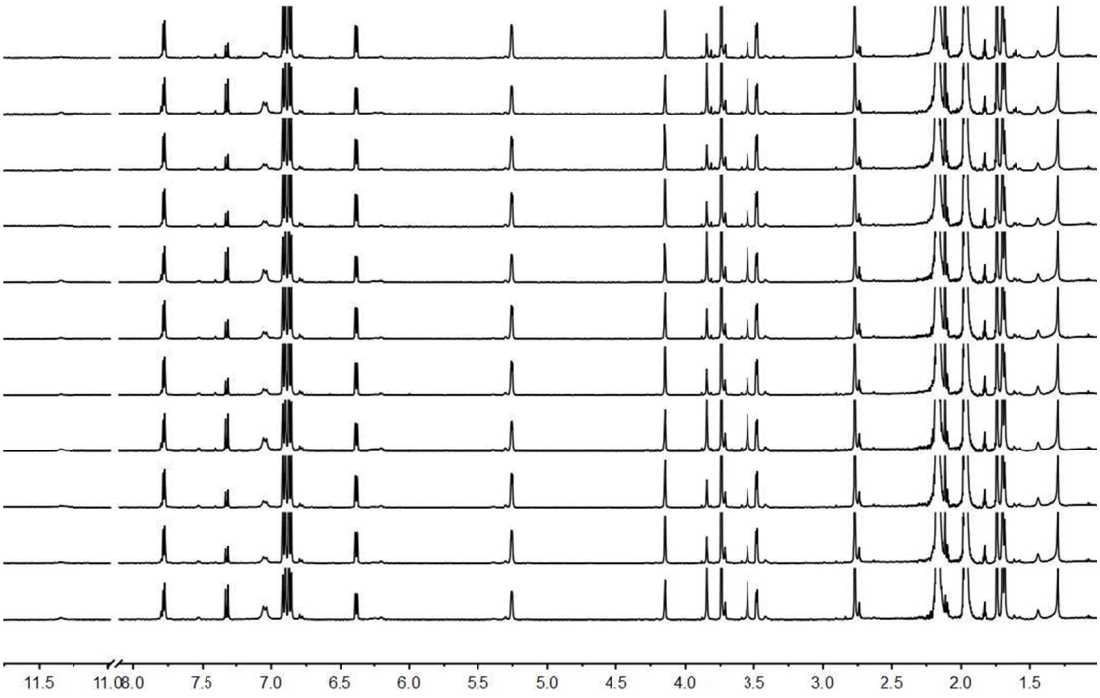

Figure S73. Stacked ^{1}H NMR (500 MHz, CD_3CN, 298 K) spectra of **4**, decimated in steps of 40 (bottom to top). The sample was irradiated with 567 nm light for 60 minutes, followed by 60 minutes of darkness to allow thermal reversion, repeated over 3.5 cycles. Figure S74 shows a graph of the linear and cyclic relative proportions over time derived from the NMR experiment.

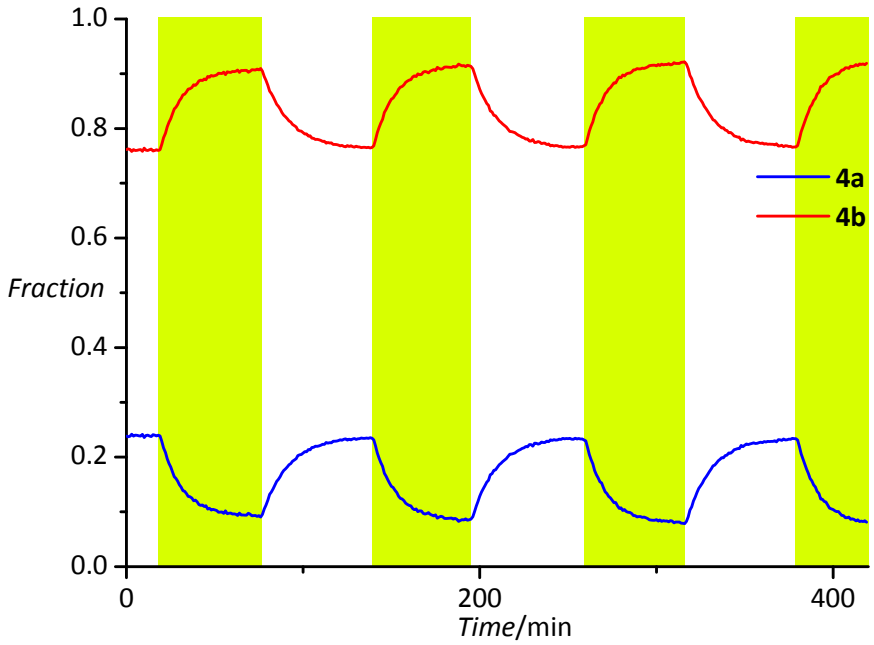

Figure S74. Reversible switching of **4a**/**4b** in CD_3CN. The isomerization was monitored by ^1H NMR (500 MHz, 298 K, 1.7 mM) spectroscopy and the relative ratio was determined by the average integrals. The coloured blocks indicate periods of photo irradiation (567 nm).

21 Variable temperature study

Variable temperature studies were performed to determine if the equilibrium and rate of switching are affected by temperature.

21.1 Variable temperature UV-vis spectroscopy

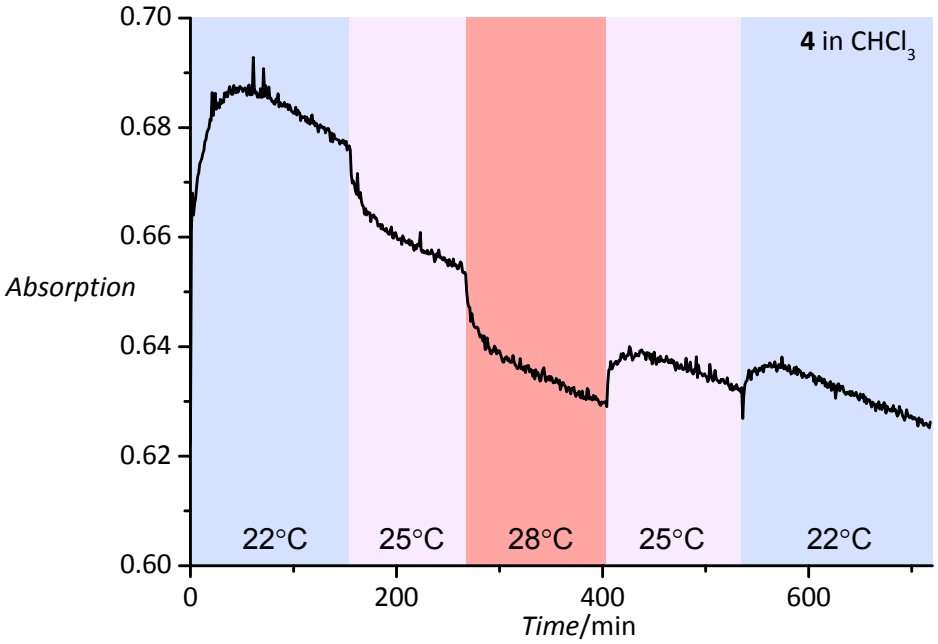

Figure S75. Variable-temperature UV-vis measurement of **4a**/**4b** in $CHCl_3$, measured at λ_{max}. The equilibrium between the two isomers shows sensitivity towards small changes in temperature, which is reversible. The loss in absorption over time corresponds to decomposition of the linear form.

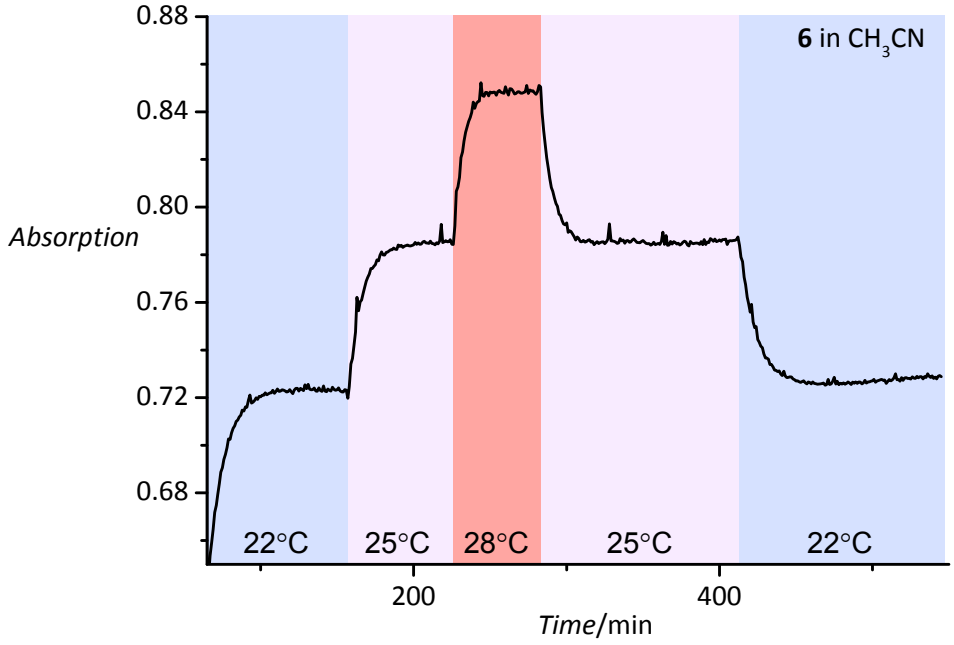

Figure S76. Variable-temperature UV-vis measurement of compound **6a**/**6b** in acetonitrile, measured at λ_{max}. Small changes in temperature result in large changes in absorption, indicating the shifting of the linear:cyclic equilibrium. Upon heating and cooling the same absorption is obtained, showing reversibility of the system.

21.2 Temperature dependent NMR of 4 in $CDCl_3$

The investigated DASA compounds show sensitivity towards temperature, where small changes in temperature have a significant influence in both the dark equilibrium and cyclic-to-linear thermal reversion rates. A 3.44 mM solution of **4** in $CDCl_3$ was investigated by NMR spectroscopy at 27 °C, in contrast to previous experiments performed at 25 °C.

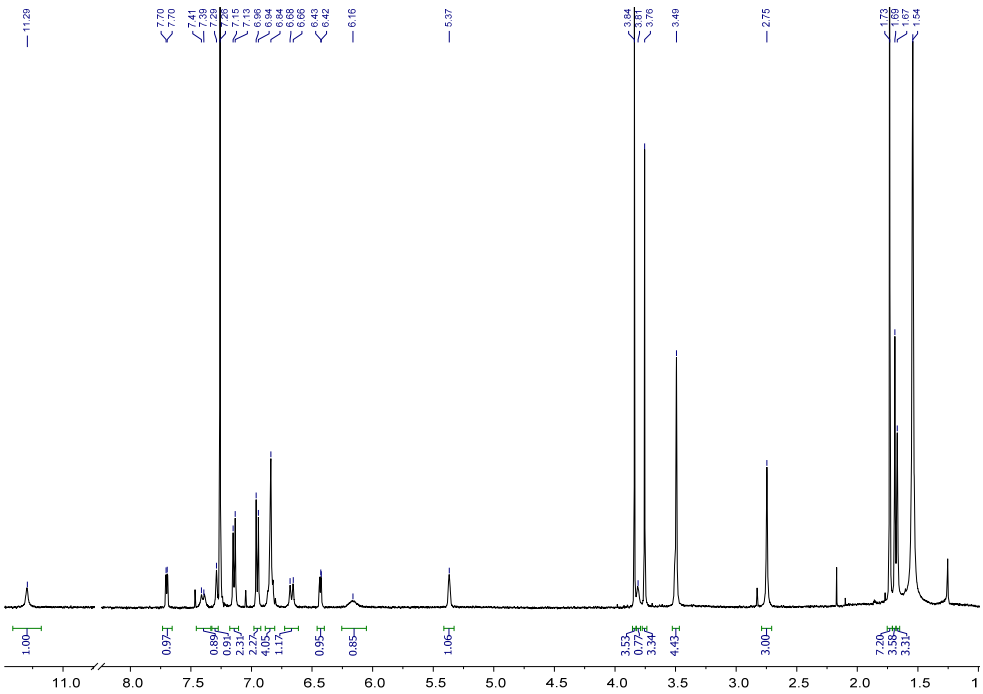

Figure S77. ^{1}H NMR (500 MHz, $CDCl_3$, 300 K) spectrum of **4a/4b**. The ratio linear:cyclic of 50:50 was determined by the average integral of all non-overlapping signals.

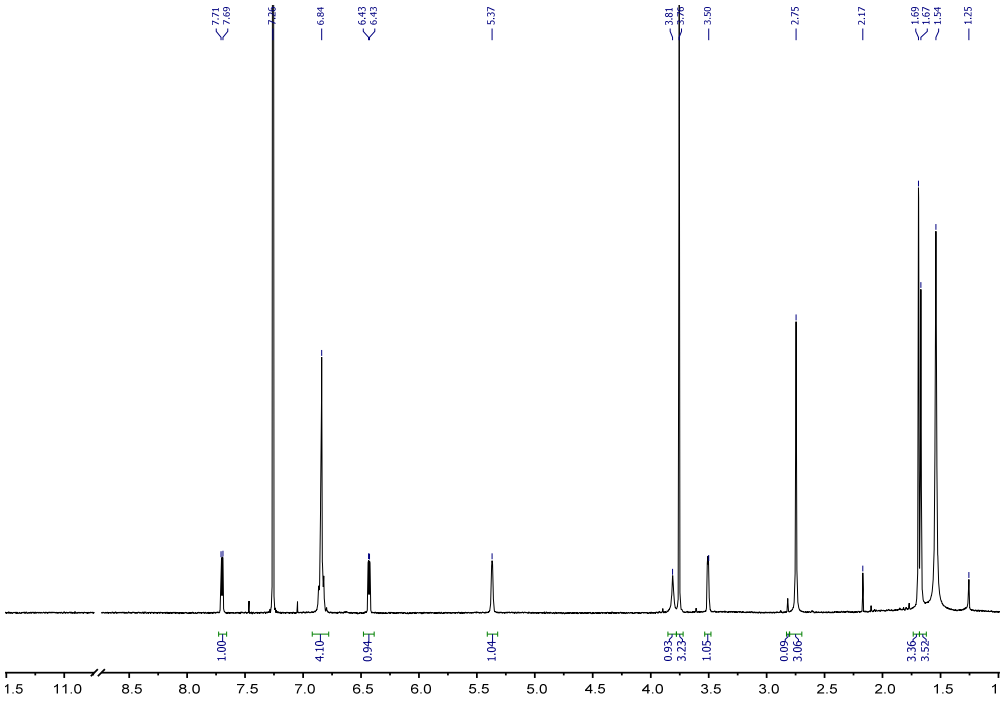

Figure S78. ^{1}H NMR (500 MHz, $CDCl_3$, 300 K) spectrum of compound **4a**/**4b** after 20 minutes of irradiation (567 nm).

A pseudo-2D NMR experiment, as described in 18.1, was performed to follow the isomerization by photo irradiation and thermal reversion. Integration of all non-overlapping signals was used to determine the ratio between the two isomers.

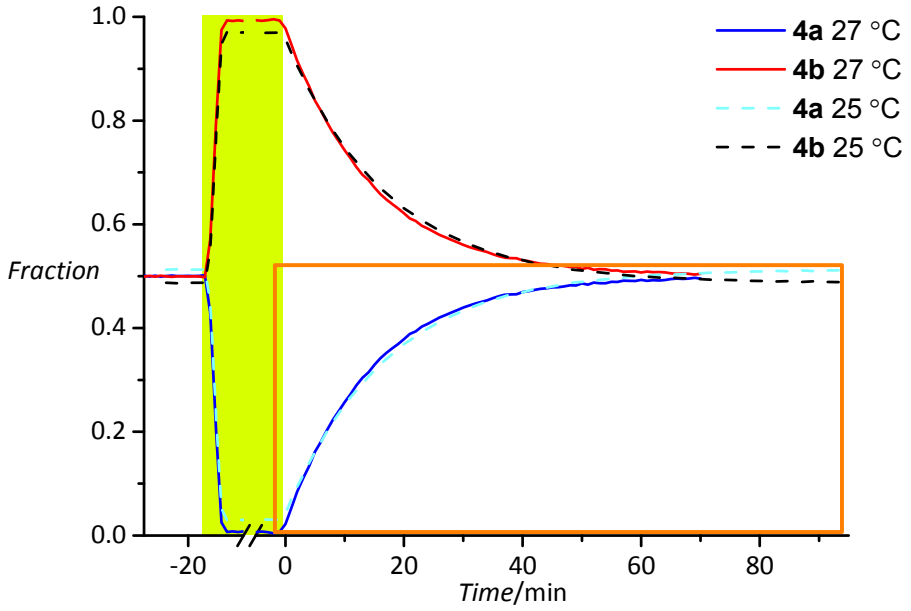

Figure S79. Optical switching of **4a**/**4b** at 27 °C and 25 °C, measured by ^{1}H NMR (500 MHz, $CDCl_3$) spectroscopy. The coloured block indicates the period of irradiation (567 nm), and the orange box highlights the phase of thermal relaxation used to calculate the apparent half-life times and rate constants. The deviation in the PSS at the different temperatures is caused by poor signal-to-noise of the linear compound under irradiation. At 25 °C, the dark equilibrium ratio linear:cyclic is 54:46, while at 27 °C the dark equilibrium is 50:50.

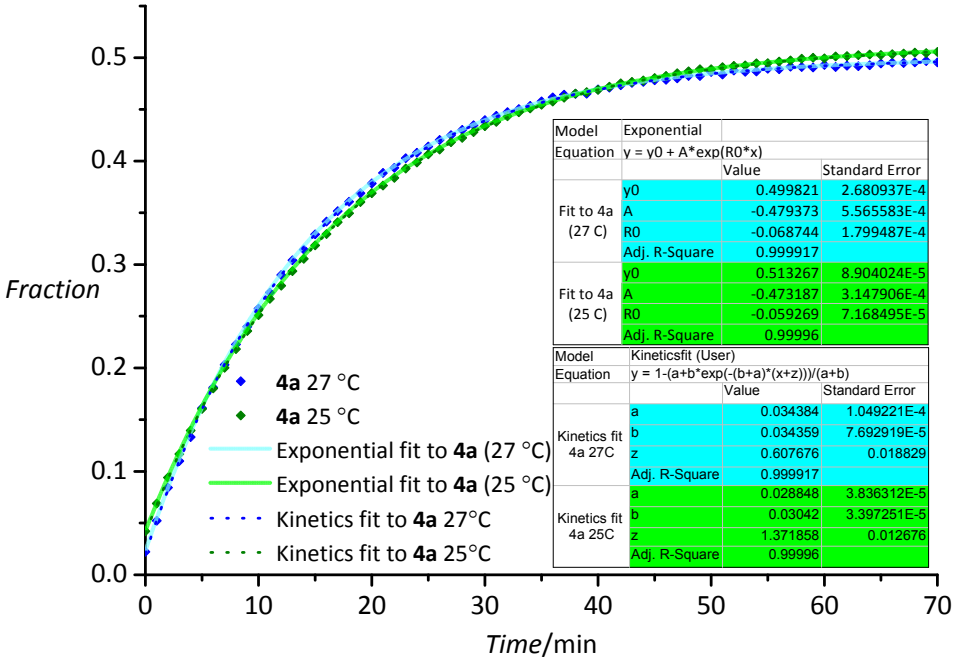

Model	Exponential		
Equation	y = y0 + A*exp(R0*x)		
		Value	Standard Error
Fit to 4a (27 C)	y0	0.499821	2.680937E-4
	A	-0.479373	5.565583E-4
	R0	-0.068744	1.799487E-4
	Adj. R-Square	0.999917	
Fit to 4a (25 C)	y0	0.513267	8.904024E-5
	A	-0.473187	3.147906E-4
	R0	-0.059269	7.168495E-5
	Adj. R-Square	0.99996	

Model	Kineticsfit (User)		
Equation	y = 1-(a+b*exp(-(b+a)*(x+z)))/(a+b)		
		Value	Standard Error
Kinetics fit 4a 27C	a	0.034384	1.049221E-4
	b	0.034359	7.692919E-5
	z	0.607676	0.018829
	Adj. R-Square	0.999917	
Kinetics fit 4a 25C	a	0.028848	3.836312E-5
	b	0.03042	3.397251E-5
	z	1.371858	0.012676
	Adj. R-Square	0.99996	

Figure S80. Thermal reversion of **4b** to **4a** at 27 °C (blue) compared to thermal reversion at 25 °C (green), followed by ^{1}H NMR (500 MHz, $CDCl_3$) spectroscopy. Exponential curves were fitted to determine the apparent half-life time and rate constants, as described in 18.

Table S10. Temperature dependence of compound **4** in $CDCl_3$, calculated by integrals of ^1H signals as displayed in Figure S79 and Figure S80. Apparent half-life times $t_{1/2}$ and rate constants k_1 and k_{-1} were obtained through exponential regression analysis as described in 18.

	a:**b** equilibrium	PSS	$t_{½}$ [min]	k_1 [10^{-4} s^{-1}][a]	k_{-1} [10^{-4} s^{-1}][b]	K
4a/**4b** 27 °C	50:50	0:100	10.1±0.1	5.73	5.73	1.00
4a/**4b** 25 °C	54:46	0:100	11.7±0.1	4.81	5.07	0.95

[a] 1st order rate constant for the conversion of linear to cyclic in the dark. [b] 1st order rate constant for the conversion of cyclic to linear in the dark.

22 *Z-E* isomerization upon irradiation

In situ optical switching of compounds **4-6** generally completes within 5 seconds, as followed by UV-vis experiments. Using standard UV-visible spectroscopy, the *Z-E* isomerization proposed by Feringa[4] (Scheme S5) cannot be observed due to this short time scale. Using a photodiode array spectrophotometer, complete spectra could be obtained with half-second resolution, enabling the observation of the *E*-linear DASA cyclisation intermediate.

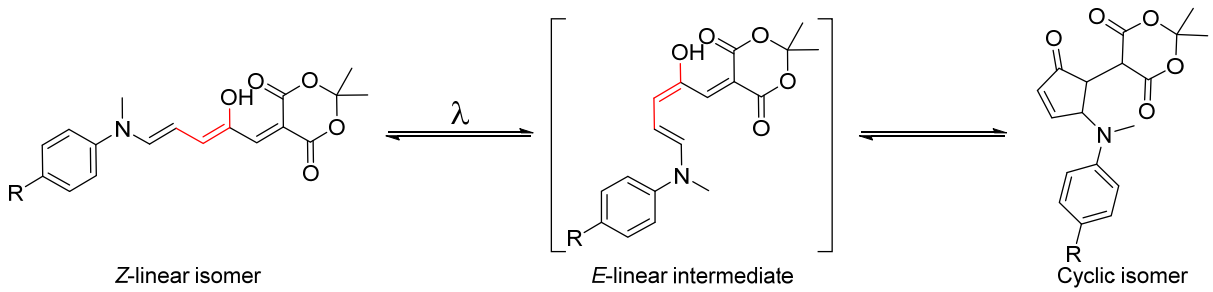

Scheme S5. The proposed mechanism of isomerization. Upon irradiation, a Z-E isomerization generates a short lived intermediate which undergoes ring-closing to form the cyclic isomer.

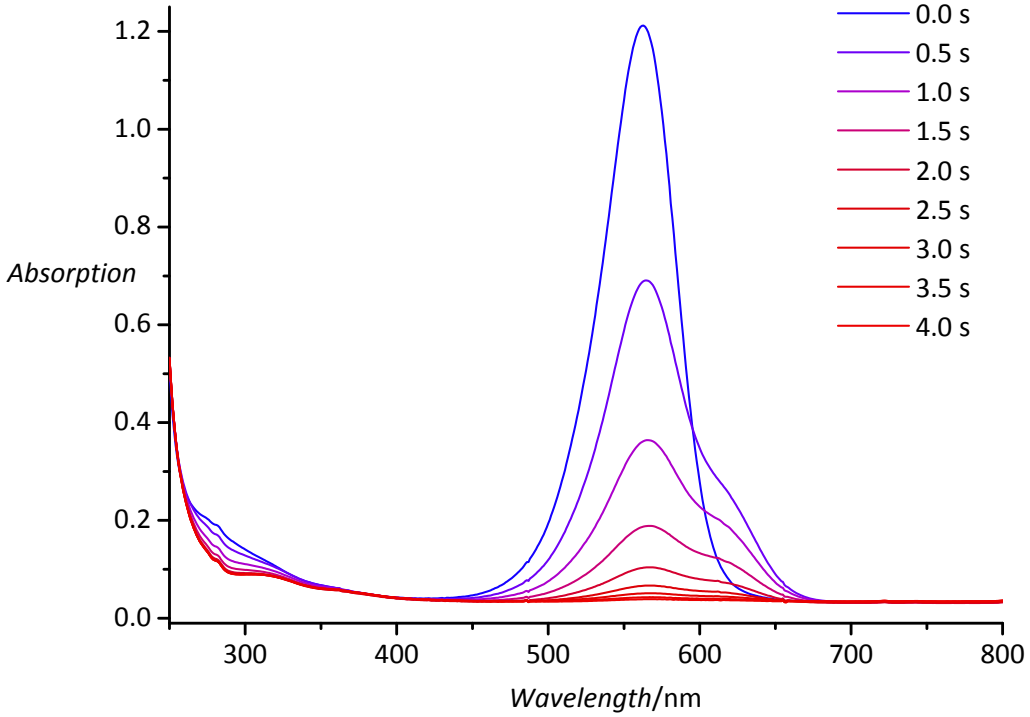

Figure S81. Optical switching of compound **4a** to **4b** ($CHCl_3$, 298 K). Irradiation of the sample results in the decrease of absorption at λ_{max} of 563 nm, indicating isomerization to the cyclic form. During irradiation a redshifted signal consistent with the formation of the *E*-linear isomer, as identified by Feringa for **2**,[4] appears at ~623 nm.

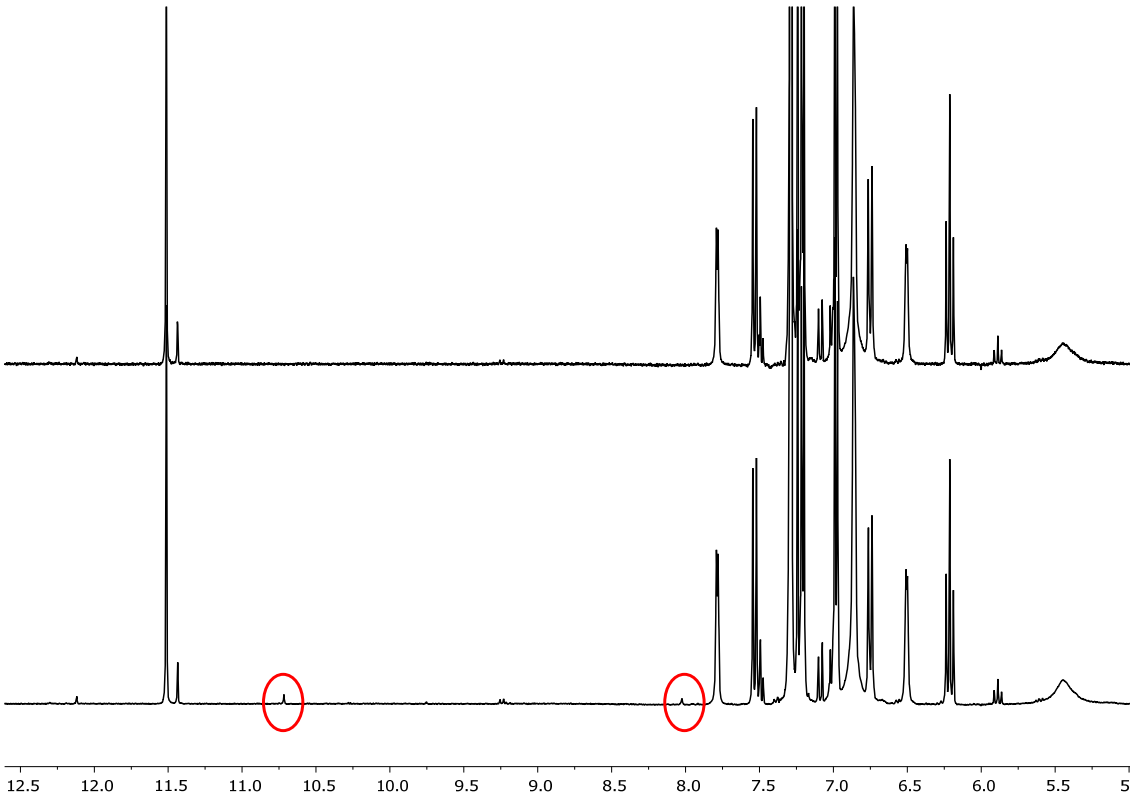

Figure S82. Low temperature ^{1}H NMR (500 MHz, CDCl3, 233 K) before (top) and during (bottom) irradiation (567 nm) show the appearance of new signals upon irradiation (highlighted with red circles), presumably of the *E*-isomer proposed by Feringa.[4] The new signals disappear once irradiation is ceased. NB: At this low temperature, signals for linear compound **4a** are resolved into the two conformers discussed in 12.

23 X-ray crystal structures

23.1 General X-ray experimental

Single crystals of **3a**, **4a**, **4b** and **5a** were measured by Bruker kappa-II CCD diffractometer at 150 K using IμS Incoatec Microfocus Source with Mo-Kα radiation (λ = 0.710723 Å). The single crystal, mounted on the goniometer using a cryo loop for intensity measurements, was coated with immersion oil type NVH and then quickly transferred to the cold nitrogen stream generated by an Oxford Cryostream 700 series. Symmetry related absorption corrections using the program SADABS[6] were applied and the data were corrected for Lorentz and polarization effects using Bruker APEX2 software. The structure was solved by Direct methods and the full-matrix least-square refinements were carried out using SHELXL-2014.[7] The non-hydrogen atoms were refined anisotropically.

Single crystal of **6b** was collected at synchrotron X-ray radiation (λ = 0.71023 Å) (MX2 Beamline at Australian Synchrotron). Data collection was carried out using BluIce[8] software and unit cell refinement, data reduction and processing was carried out with program XDS.[9] The structure was solved using dual space methods with SHELXT.[10] The least-squares refinement was carried out SHELXL-2014.[7]

CCDC depository numbers: 1500303 – 1500307.

23.2 Single crystal X-ray structure of 3a

3a $C_{20}H_{24}N_2O_5$, M= 372.41, violet block, triclinic, space group P-1, a= 8.9003(13), b= 9.3364(14), c= 11.3581(15) Å, α=83.515(6), β=76.869(5), γ=82.053(6)°, U=907.1(2) Å^3, Z= 2, D_c= 1.364 g/cm^3,μ(MoK α)= 0.098 mm^{-1}, T= 150 K, 12987 reflections collected. Refinement of 250 parameters using 4309 independent reflections against F^2 converged at final R_1= 0.0539 (R_1 all data= 0.1297), wR_2= 0.1105 (wR_2 all data= 0.1450), GOF= 0.970.

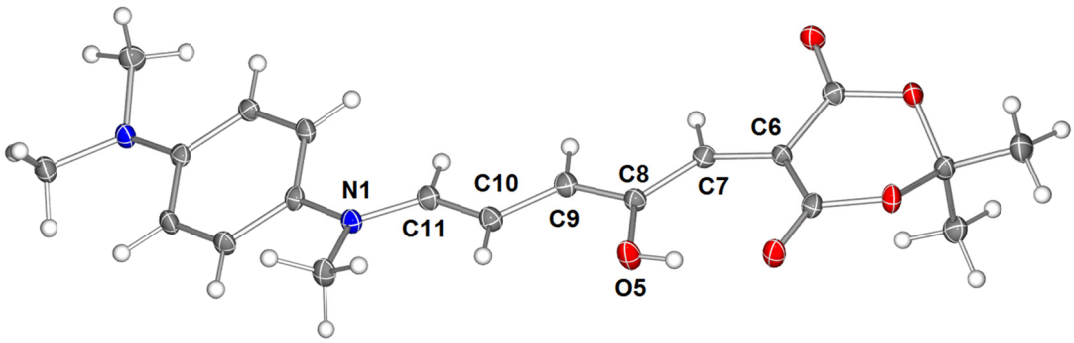

Figure S83. An ORTEP representation of the X-ray crystal structure of **3a**. Thermal ellipsoids are drawn at 50% probability. C: grey; N: blue; O: red and H: white.

23.3 Single crystal X-ray structure of 4a

4a $C_{19}H_{21}NO_6$, M= 359.37, dark violet block, triclinic, space group P-1, a= 7.787(9), b= 9.080(12), c= 12.994(16) Å, α=106.14(7), β=91.08(7), γ=94.96(7)°, U=878.3(19) Å^3, Z= 2, D_c= 1.359 g/cm^3, μ(MoK α)= 0.102 mm^{-1}, T= 150 K, 12675 reflections collected. Refinement of 240 parameters using 3094 independent reflections against F^2 converged at final R_1= 0.0598 (R_1 all data= 0.1091), wR_2= 0.1305 (wR_2 all data= 0.1527), GOF= 0.981.

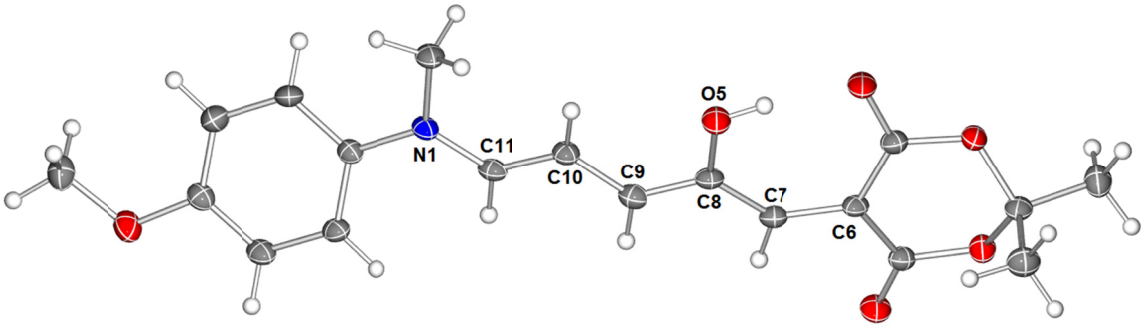

Figure S84. An ORTEP representation of the X-ray crystal structure of **4a**. Thermal ellipsoids are drawn at 50% probability. C: grey; N: blue; O: red and H: white.

23.4 Single crystal X-ray structure of 4b

4b $C_{19}H_{21}NO_6$, M= 359.37, Colourless plate, orthorhombic, space group $Pca2_1$, a= 10.200(3), b= 12.903(3), c= 14.787(3) Å, α=90, β=90, γ=90°, U=1946(17) Å^3, Z= 4, D_c= 1.227 g/cm^3, μ(MoK α)= 0.092 mm^{-1}, T= 150 K, 9527 reflections collected. Refinement of 239 parameters using 3750 independent reflections against F^2 converged at final R_1= 0.0843 (R_1 all data= 0.2424), wR_2= 0.1451 (wR_2 all data= 0.2131), GOF= 0.921.

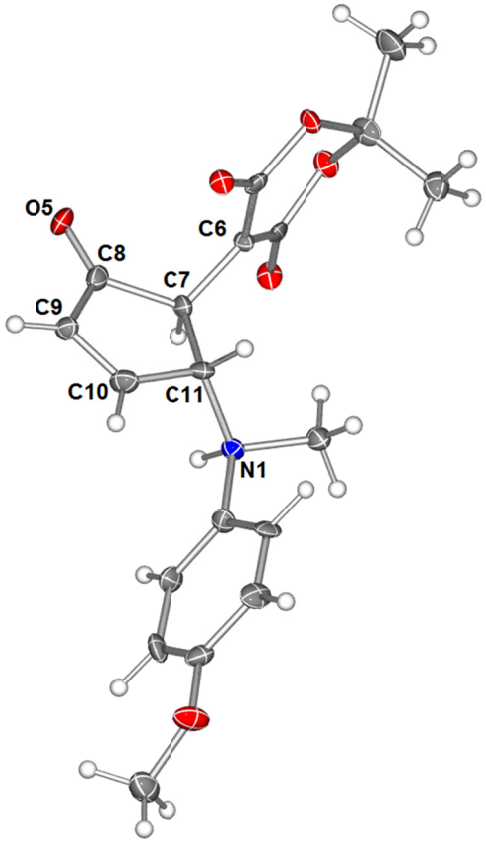

Figure S85. An ORTEP representation of the X-ray crystal structure of **4b**. Thermal ellipsoids are drawn at 50% probability. C: grey; N: blue; O: red and H: white.

23.5 Single crystal X-ray structure of 5a

5a $C_{18}H_{19}NO_5$, M= 329.34, greenish blue block, monoclinic, space group $P2_1/c$, a= 7.3465(6), b= 12.3261(10), c= 18.1727(12) Å, α=90, β=95.772(2), γ=90°, U=1637.3(2) Å^3, Z= 4, D_c= 1.336 g/cm^3, μ(MoK α)= 0.098 mm^{-1}, T= 150 K, 14387 reflections collected. Refinement of 221 parameters using 3579 independent reflections against F^2 converged at final R_1= 0.0374 (R_1 all data= 0.0428), wR_2= 0.0946 (wR_2 all data= 0.0983), GOF= 1.054.

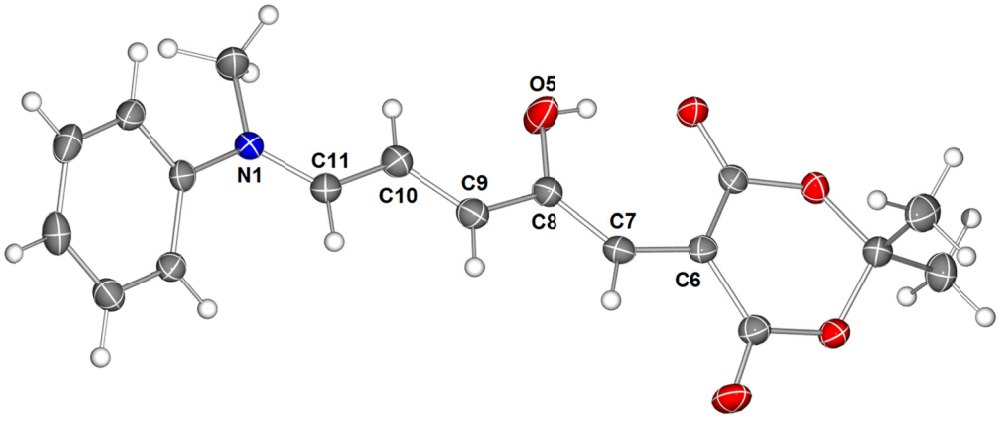

Figure S86. An ORTEP representation of the X-ray crystal structure of **5a**. Thermal ellipsoids are drawn at 50% probability. C: grey; N: blue; O: red and H: white.

23.6 Single crystal X-ray structure of 6b

6b $C_{18}H_{18}FNO_5$, M= 347.33, colourless needle, monoclinic, space group $P2_1/c$, a= 18.990(4), b= 5.4180(11), c= 17.320(4) Å, α=90, β=113.90(3), γ=90°, U=1629.2(7) Å^3, Z= 4, D_c= 1.416 g/cm^3, μ(MoK α)= 0.111 mm^{-1}, T= 100 K, 23383 reflections collected. Refinement of 229 parameters using 3558 independent reflections against F^2 converged at final R_1= 0.0432 (R_1 all data= 0.0491), wR_2= 0.1098 (wR_2 all data= 0.1140), GOF= 1.061.

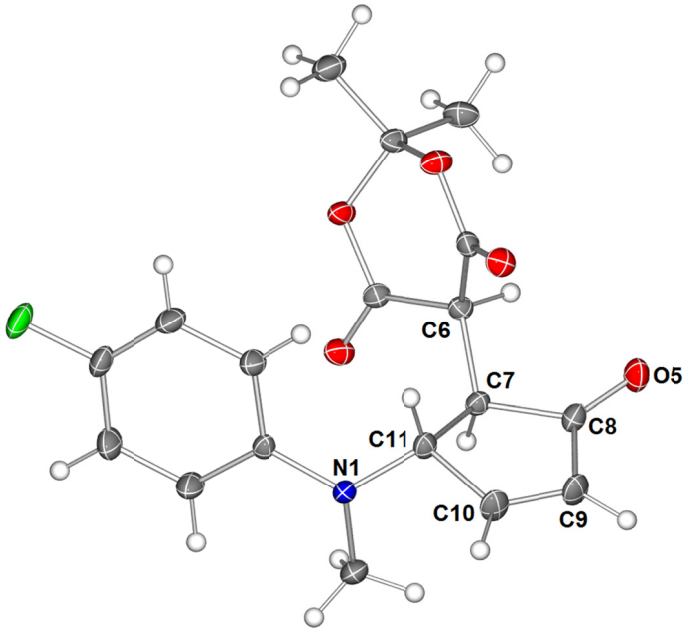

Figure S87. An ORTEP representation of the X-ray crystal structure of **6b**. Thermal ellipsoids are drawn at 50% probability. C: grey; N: blue; O: red; F: green and H: white.

24 Comparison of bond lengths within the conjugated polyene systems of linear isomers

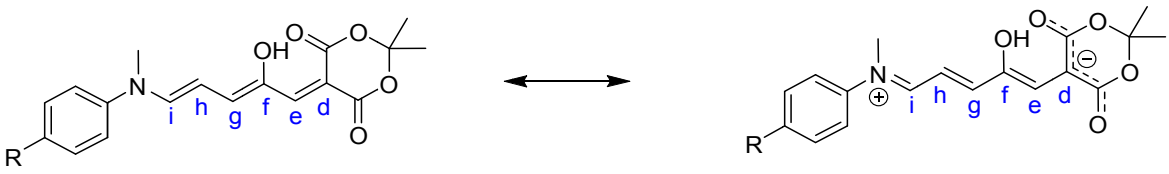

Figure S88. Resonance structures of linear DASA compounds. Analysis of bond lengths within the conjugated triene system suggests that the charge-separated zwitterion is a better representation of the solid-state structure.

While the conjugated triene system within the linear DASA compounds is generally drawn to show a neutral molecule, it can also be depicted as a zwitterion as shown in Figure S88. Figure S89 shows bond lengths across the conjugated system for the three linear DASA compounds that crystal structures were obtained for, along with those for known compound **2a**.[1] The bond length alternation between the shorter C=C double bonds and longer C-C single bonds within the conjugated systems of the linear DASA compounds appear to support the second zwitterionic form. This interpretation is supported by the significantly different ^{15}N chemical shifts observed for the two anilinic nitrogen environments (see p. 33) which show that the nitrogen within the triene system is significantly deshielded in comparison to the *N,N*-dimethylaniline nitrogen.

Normal C-C and C=C bond lengths within a conjugated triene system are respectively 1.44 Å and 1.35 Å.[11] The similarity between the single and double bond lengths observed here indicates that bonding across the polyene system in the aromatic DASAs is significantly delocalized.

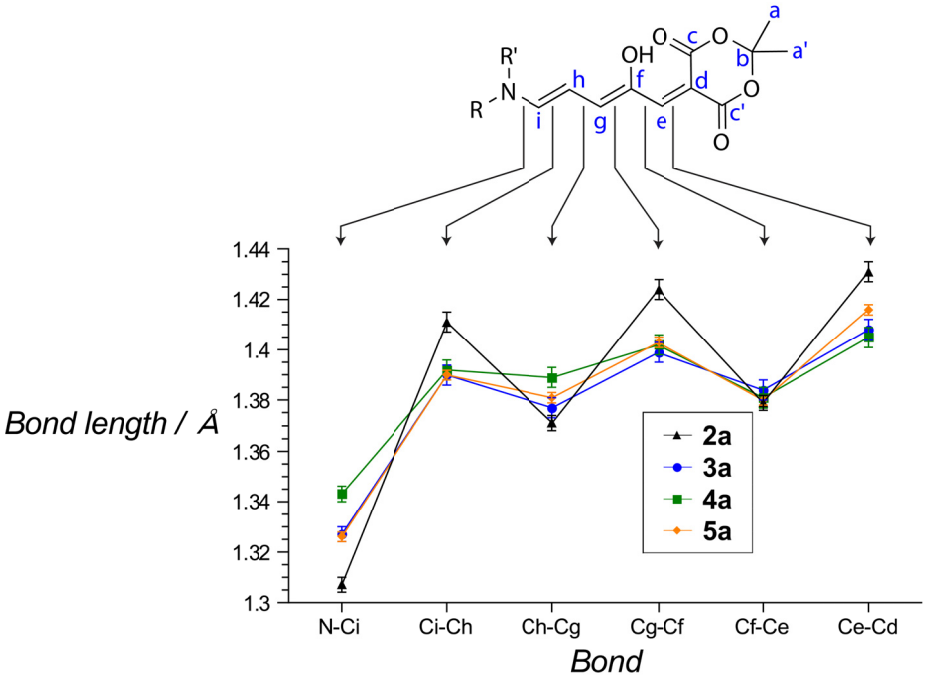

Figure S89. Bond lengths within the conjugated triene system suggest that the zwitterionic form shown in Figure S88 is a more accurate representation of conjugated bonding than the neutral form usually depicted**.**

Table S11. Bond lengths within the conjugated polyene system for linear DASA compounds, as determined from single crystal X-ray structures.

Compound	N-C^i	C^i-C^h	C^h-C^g	C^g-C^f	C^f-C^e	C^e-C^d
2a[a]	1.307(3)	1.411(4)	1.371(3)	1.424(4)	1.379(3)	1.431(4)
3a	1.327(3)	1.390(4)	1.377(4)	1.399(4)	1.384(4)	1.408(4)
4a	1.343(3)	1.392(4)	1.389(4)	1.402(4)	1.381(4)	1.405(4)
5a	1.326(2)	1.390(2)	1.381(2)	1.403(2)	1.380(2)	1.416(2)

[a] Data for compound **2a** was reported by Helmy *et. al.*[1]

25 Comparison of bond lengths within the Meldrum's acid adduct of cyclic isomers

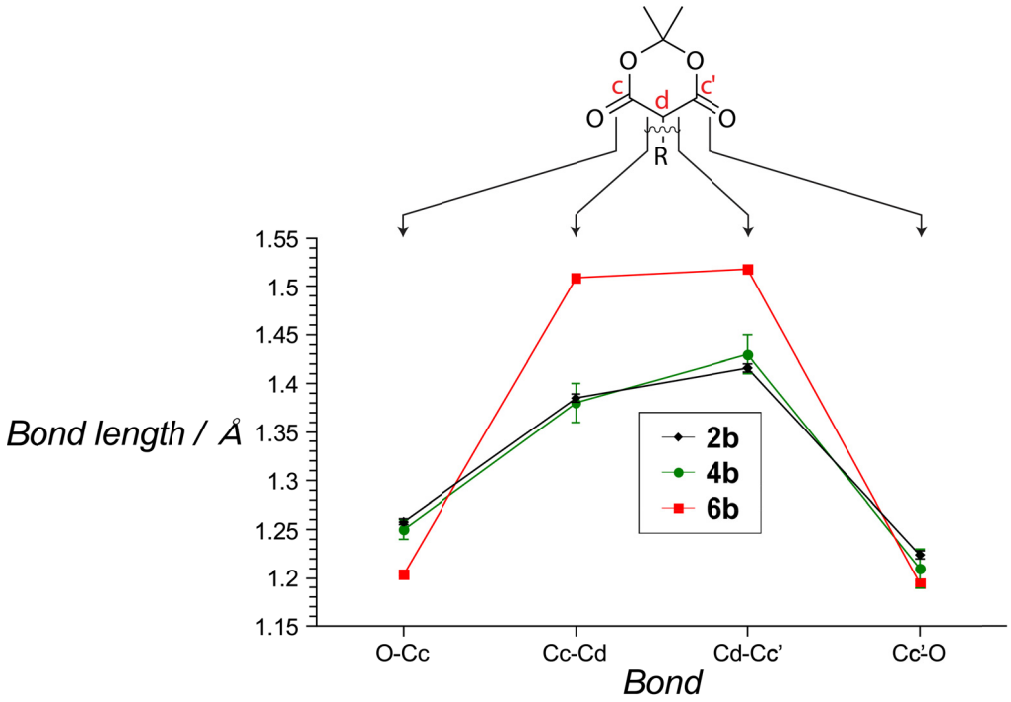

Figure S90. Bond lengths within the dicarbonyl system of cyclic-form DASA compounds **2b**, **4b** and **6b**. Compounds **2b** and **4b** exist as enolic zwitterions in the solid state, while compound **6b** shows bond lengths consistent with the neutral di-*keto* tautomer.

Single crystal X-ray structures of cyclic compounds **4b** and **6b** and previously reported compound **2b**[1] were used to compare the O-C-C-C-O bond lengths across the Meldrum's acid dicarbonyl system (Table S12, Figure S90). The crystal structure of cyclic compound **4b** shows C-O bonds (and both C-C bonds) of unequal lengths across the Meldrum's acid dicarbonyl system, consistent with the zwitterionic enolate form previously reported for *N,N*-diethyl DASA compound **2b**. As NMR experiments previously found **4b** to exist as a neutral species in solution (see p. 28), this supports the hypothesis that the neutral and zwitterionic forms of the aromatic DASAs are relatively equal in energies. In contrast, the crystal structure of fluorinated compound **6b** shows both C=O bonds (and both C-C bonds) are equal lengths, which is consistent with the neutral diketone *keto* tautomer observed in solution state experiments.

Table S12. Bond lengths across the Meldrum's acid dicarbonyl system of DASA compounds in the cyclic form (see Figure S90).

Compound	O-C^c	C^c-C^d	C^d-$C^{c'}$	$C^{c'}$-O
2b[a]	1.258(3)	1.385(4)	1.416(4)	1.224(4)
4b	1.25(1)	1.38(2)	1.43(2)	1.21(2)
6b	1.195(2)	1.518(2)	1.509(2)	1.204(2)

[a] Data for compound **2a** was reported by Helmy *et. al.*[1]

26 References

1. S. Helmy, S. Oh, F. A. Leibfarth, C. J. Hawker and J. Read de Alaniz, *J Org Chem*, 2014, **79**, 11316-11329.
2. H. Taneda, K. Inamoto and Y. Kondo, *Chem. Commun.*, 2014, **50**, 6523-6525.
3. S. Helmy, F. A. Leibfarth, S. Oh, J. E. Poelma, C. J. Hawker and J. Read de Alaniz, *J. Am. Chem. Soc.*, 2014, **136**, 8169-8172.
4. M. M. Lerch, S. J. Wezenberg, W. Szymanski and B. L. Feringa, *J. Am. Chem. Soc.*, 2016, **138**, 6344-6347.
5. C. Feldmeier, H. Bartling, E. Riedle and R. M. Gschwind, *J. Magn. Reson.*, 2013, **232**, 39-44.
6. W. Kabsch, *J. Appl. Crystallogr.*, 1993, **26**, 795-800.
7. G. Sheldrick, *Acta Crystallograph. Sect. C*, 2015, **71**, 3-8.
8. T. M. McPhillips, S. E. McPhillips, H.-J. Chiu, A. E. Cohen, A. M. Deacon, P. J. Ellis, E. Garman, A. Gonzalez, N. K. Sauter, R. P. Phizackerley, S. M. Soltis and P. Kuhn, *J. Synchrotron Rad.*, 2002, **9**, 401-406.
9. W. Kabsch, *Acta Crystallograph. Sect. D*, 2010, **66**, 125-132.
10. G. M. Sheldrick, *Acta Crystallograph. Sect. A*, 2015, **71**, 3-8.
11. W. M. Haynes, *CRC Handbook of Chemistry and Physics*, CRC Press, Boca Raton, Florida, 96. edition. edn., 2015.